2011

Biorenewable polymeric materials from vegetable oils

Ying Xia
Iowa State University

Biorenewable polymeric materials from vegetable oils

by

Ying Xia

A dissertation submitted to the graduate faculty

in partial fulfillment of the requirements for the degree of

DOCTOR OF PHILOSOPHY

Major: Chemistry

Program of Study Committee:
Richard C. Larock, Co-Major Professor
Michael R. Kessler, Co-Major Professor
Malika Jeffries-EL
Klaus Schmidt-Rohr
Yan Zhao

Iowa State University

Ames, Iowa

2011

To Nan and my parents for everything

TABLE OF CONTENTS

LIST OF ABBREVIATIONS

ADMET	acyclic diene metathesis polymerization
APTES	(3-aminopropyl)triethoxysilane
ATMET	acyclic triene metathesis polymerization
BFE	boron trifluoride diethyl etherate
CP	cyclopentene
DBTDL	dibutyltin dilaurate
DCPD	dicyclopentadiene
Dil	Dilulin
DMA	dynamic mechanical analysis
DMPA	dimethylol propionic acid
DSC	differential scanning calorimetry
DVB	divinylbenzene
HAP	hazardous air pollutant
HDI	hexamethylene diisocyanate
HESA	*N, N-bis*(2-hydroxyethyl)soybean amide
HS	hard segment
IPDI	isophorone diisocyanate
ISO	*D*-isosorbide
IV	iodine value
LAH	lithium aluminum hydride
MDEA	*N*-methyl diethanolamine
MEK	methyl ethyl ketone

MSOL	methoxylated soybean oil polyol
MTES	methyltriethoxysilane
NB	norbornene
NCA	norbornenyl-functionalized castor oil alcohol
NCO	norbornenyl-functionalized castor oil
NFO	Norway fish oil
NMCA	norbornenyl-modified castor alcohol
NMDA	norbornenyl-modified Dilulin alcohol
NMMA	norbornenyl-modified ML189 alcohol
NMR	nuclear magnetic resonance
NMSA	norbornenyl-modified soybean alcohol
PU	polyurethane
PUD	polyurethane dispersion
PUU	polyurethane-urea
PUUD	polyurethane-urea dispersion
ROMP	ring-opening metathesis polymerization
ST	styrene
TEA	triethylamine
TEM	transmission electron microscope
TGA	thermogravimetric analysis
THF	tetrahydrofuran
VOC	volatile organic chemical
ε	elongation at break

σ	tensile strength
υ_e	crosslink density
E	Young's modulus
E'	storage modulus
G'	storage shear modulus
G''	loss shear modulus
ΔC_p	heat capacity change
T_g	glass transition temperature
T_p	peak temperature
T_5	temperature at 5% weight loss
T_{10}	temperature at 10% weight loss
T_{50}	temperature at 50% weight loss
T_{max}	temperature at maximum degradation

CHAPTER 1. GENERAL INTRODUCTION

A portion of this introduction was taken from a critical review published in
Green Chemistry, 12, 1893-1909.

Ying Xia and Richard C. Larock*

Department of Chemistry, Iowa State University, Ames, Iowa 50011

Polymeric materials play a prominent role in everyday life and have been essential to a variety of industries. Nowadays, most commercially available polymers are derived from non-renewable resources and account for approximately 7% of worldwide oil and gas use.[1] Considering the continuous depletion of fossil feedstocks, dramatic fluctuations in the oil price, and environmental issues, academic and industrial researchers are devoting increasing attention and efforts to the utilization of renewable resources as raw materials for the production of polymeric materials.[2-5]

The most widely used renewable raw materials include polysaccharides (mainly cellulose and starch), wood, proteins, and plant oils.[6] Among these, vegetable oils are the most widely used renewable resources due to their low toxicity, inherent biodegradability, ready availability, and relatively low price.[5] In the chemical industry, vegetable oils have found a wide range of applications, including soaps, drying agents, coatings, hydraulic fluids, lubricants, monomers (*e.g.* polyols and dimer acids), and polymers.[5] In recent years, biorenewable fuels, mainly biodiesel, have also been prepared from vegetable oils.[7] Scheme 1 shows the representative structure of vegetable oils, which consist of mainly triglycerides formed between glycerol and various fatty acids.

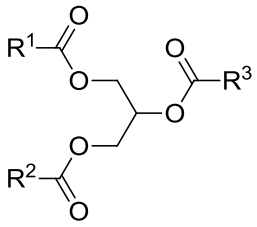

Scheme 1. Triglyceride structure of vegetable oils (R^1, R^2, R^3 represent fatty acid chains).

Table 1 summarizes the most common fatty acids present in vegetable oils. As can be seen from the table, most fatty acids are long straight-chain compounds with an even number of carbons and the double bond in most of these unsaturated fatty acids possesses a *cis* configuration. Some fatty acid chains, like those in ricinoleic and vernolic acids, bear functional groups, hydroxyl and epoxy groups respectively. Different vegetable oils

Table 1. Formulas and structures of the most important fatty acids.[8]

Fatty Acid	Formula	Structure
Palmitic	$C_{16}H_{32}O_2$	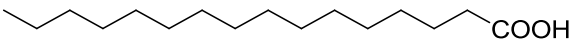
Palmitoleic	$C_{16}H_{30}O_2$	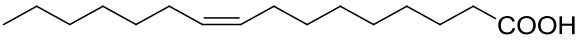
Stearic	$C_{18}H_{36}O_2$	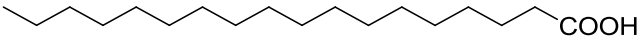
Oleic	$C_{18}H_{34}O_2$	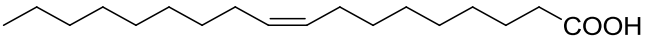
Linoleic	$C_{18}H_{32}O_2$	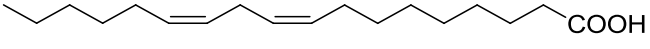
Linolenic	$C_{18}H_{30}O_2$	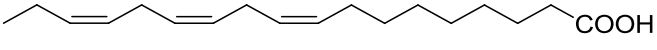
α-Eleostearic	$C_{18}H_{30}O_2$	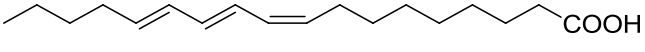
Ricinoleic	$C_{18}H_{34}O_3$	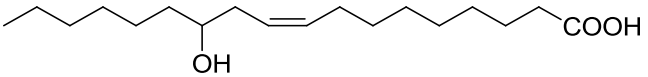
Vernolic	$C_{18}H_{32}O_3$	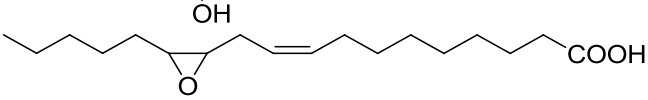

contain different compositions of fatty acids depending on the plant and the growing conditions. The fatty acid compositions of the most common vegetable oils are summarized in Table 2. The chemical and physical properties of the vegetable oils depend heavily on the degree of unsaturation, which can be determined by measuring the iodine value (IV). The IV value represents the amount of iodine (mg) that reacts with the carbon-carbon double bonds in 100 g of the vegetable oil; the larger IV value indicates more carbon-carbon double bonds per vegetable oil triglyceride. Thus, vegetable oils can be classified as drying oils (IV > 130), semi-drying oils (100 < IV < 130), and non-drying oils (IV < 100). The IV values of common vegetable oils are summarized in Table 2 as well.

Table 2. Properties and fatty acid compositions of the most common vegetable oils.[6]

Vegetable oil	Double bonds[a]	Iodine value[b] (mg/100g)	Fatty acids (%)				
			Palmitic	Stearic	Oleic	Linoleic	Linolenic
Palm	1.7	44-58	42.8	4.2	40.5	10.1	-
Olive	2.8	75-94	13.7	2.5	71.1	10.0	0.6
Groundnut	3.4	80-106	11.4	2.4	48.3	31.9	-
Rapeseed	3.8	94-120	4.0	2.0	56.0	26.0	10.0
Sesame	3.9	103-116	9.0	6.0	41.0	43.0	1.0
Cottonseed	3.9	90-119	21.6	2.6	18.6	54.4	0.7
Corn	4.5	102-130	10.9	2.0	25.4	59.6	1.2
Soybean	4.6	117-143	11.0	4.0	23.4	53.3	7.8
Sunflower	4.7	110-143	5.2	2.7	37.2	53.8	1.0
Linseed	6.6	168-204	5.5	3.5	19.1	15.3	56.6

a) Average number of double bonds per triglyceride.
b) The amount of iodine (mg) that reacts with the double bonds in 100g of vegetable oil.

During the last decade, a variety of vegetable oil-based polymeric systems have been developed.[9] Unmodified vegetable oils have been used to prepare biorenewable polymers by thermal[10] or cationic[11] polymerization methods, taking advantage of the carbon-carbon double bonds in the fatty acid chains. Modified vegetable oils with acrylic double bonds

exhibit higher reactivities and can undergo free radical polymerization to afford thermosets with good thermal and mechanical properties.[12] Recently, relatively new polymerization methods, acyclic diene metathesis polymerization (ADMET)[13] and ring-opening metathesis polymerization (ROMP),[14-15] have been employed to synthesize vegetable oil-based polymers as well. Vegetable oil-based polyols are another promising monomer, which can react with diisocyanates to afford polyurethane elastomers,[16] as well as waterborne polyurethane dispersions,[17] which have various applications in foams, coatings, and adhesives.

Dissertation Organization

This dissertation is divided into eight chapters. This first chapter simply explains the overall organization of the thesis. Chapter two discusses the synthesis and characterization of novel thermosets prepared from the cationic copolymerization of modified linseed oils (Dilulin and ML189) and dicyclopentadiene. The third and fourth chapters cover vegetable oil-based thermosets synthesized by ring-opening metathesis polymerization (ROMP). The fifth, sixth and seventh chapters focus on vegetable oil-based polyurethane dispersions (PUDs). Chapter five reports the incorporation of isosorbide into PUDs. Chapter six covers the post-cure of PUDs with an aziridine-based crosslinker, and Chapter seven discusses the reinforcement of castor oil-based polyurethane coatings by preparing polyurethane-silica nanocomposite dispersions. Chapter eight makes some general conclusions.

References

1. C. K. Williams and M. A. Hillmyer, *Polym. Rev.*, 2008, **48**, 1-10.
2. J. J. Bozell, *Science*, 2010, **329**, 522-523.
3. Y. Xia and R. C. Larock, *Green Chem.*, 2010, **12**, 1893-1909.
4. D. P. Pfister, Y. Xia and R. C. Larock, *ChemSusChem*, 2011, **4**, 703-717.
5. Y. S. Lu and R. C. Larock, *ChemSusChem*, 2009, **2**, 136-147.

6. M. N. Belgacem and A. Gandini, in *Monomers, Polymers and Composites from Renewable Resources*, eds. M. N. Belgacem and A. Gandini, Elsevier, Amsterdam, 2008, pp. 39-66.
7. A. Demirbas, *Energy Sources, Part A: Recovery, Util. Environ. Eff.*, 2010, **32**, 628-636.
8. R. Verhé, in *Renewable Bioresources: Scope and Modification for Non-food Applications*, eds. C. V. Stevens and R. Verhé, Wiley, West Sussex, 2004, pp. 208-250.
9. M. Galia, L. M. de Espinosa, J. C. Ronda, G. Lligadas and V. Cadiz, *Eur. J. Lipid Sci. Technol.*, 2010, **112**, 87-96.
10. F. K. Li and R. C. Larock, *Biomacromolecules*, 2003, **4**, 1018-1025.
11. F. Li and R. C. Larock, in *Natural Fibers, Biopolymers and Biocomposites*, eds. A. K. Mohanty, M. Misra and L. T. Drzal, CRC Press, Boca Raton, FL, 2005, pp. 727-750.
12. S. N. Khot, J. J. Lascala, E. Can, S. S. Morye, G. I. Williams, G. R. Palmese, S. H. Kusefoglu and R. P. Wool, *J. Appl. Polym. Sci.*, 2001, **82**, 703-723.
13. A. Rybak, P. A. Fokou and M. A. R. Meier, *Eur. J. Lipid Sci. Technol.*, 2008, **110**, 797-804.
14. Y. Xia, Y. Lu and R. C. Larock, *Polymer*, 2010, **51**, 53-61.
15. Y. Xia and R. C. Larock, *Polymer*, 2010, **51**, 2508-2514.
16. Z. S. Petrovic, *Polym. Rev.*, 2008, **48**, 109-155.
17. Y. S. Lu and R. C. Larock, *Biomacromolecules*, 2008, **9**, 3332-3340.

CHAPTER 2. NOVEL THERMOSETS FROM THE CATIONIC COPOLYMERIZATION OF MODIFIED LINSEED OILS AND DICYCLOPENTADIENE

A Paper published in Macromolecular Materials and Engineering, 294, 590-598.

Ying Xia, Phillip H. Henna, Richard C. Larock*

Department of Chemistry, Iowa State University, Ames, Iowa 50011

Abstract

A series of soft to tough copolymers have been prepared by the cationic copolymerization of the modified linseed oils Dilulin (Dil) or ML189 with dicyclopentadiene (DCPD) initiated by boron trifluoride diethyl etherate (BFE). The yields of the bulk copolymers are essentially quantitative, while the yields of the crosslinked copolymers remaining after Soxhlet extraction with methylene chloride range from 84% to 90% and depend on the amount of DCPD used. Soxhlet extraction and solid-state ^{13}C NMR spectra indicate that the bulk copolymers consist of a crosslinked oil-DCPD network interpenetrated with certain amounts of soluble components, such as the free oil, oil-DCPD oligomers and some low molecular weight oil fragments. The T_gs of the resulting Dil-DCPD and ML189-DCPD copolymers range from 15-83 ^oC and 8-77 ^oC, respectively, and have a linear relationship with the amount of DCPD used. Moreover, the T_gs of the Dil-DCPD copolymers are higher than the ML189-DCPD copolymers. DMA analysis reveals that the tan δ values for both copolymers are in the range 0.7-1.1. The room temperature storage moduli increase with an increase in the amount of DCPD and range from 4.43×10^6 Pa to 1.52×10^9 Pa for the

Dil-DCPD copolymers and 3.72×10^6 Pa to 1.44×10^9 Pa for the ML189-DCPD copolymers, respectively. Thermogravimetric analysis (TGA) indicates that these biocopolymers are thermally stable up to 150 ^oC, with 10% and 50% weight loss temperatures ranging from 304-334 ^oC and 459-468 ^oC, respectively.

Introduction

Biorenewable materials are attracting more and more attention because of the shortage and unstable price of crude petroleum.[1] One major initiative has been the synthesis and application of a wide range of bio-based materials from sustainable and environmentally friendly starting materials, such as starch, cellulose, vegetable oils and proteins.[2-5] These materials offer the advantages of low cost, being readily available from renewable natural resources, and often possessing comparable or better properties than those of widely used industrial polymers. As such, they might replace petroleum-based polymers.

Recently, much work on bio-based polymers prepared from natural and functionalized natural oils has been reported. Wool *et al.* prepared rigid thermosets from maleic anhydride-modified soybean and castor oils[6] or soybean oil monoglyceride maleates[7-8] copolymerized free radically with styrene. Petrovic and co-workers have converted the C=C bonds of soybean oil into polyols, which were then reacted with isocyanates to produce polyurethane thermosets.[9-12] Our group has successfully prepared a wide range of industrially-promising biopolymers by taking advantage of the C=C bonds of natural oils, such as soybean oil,[13] corn oil,[14] linseed oil,[15,16] tung oil,[17] fish oil,[18] and a number of other natural oils,[19] via cationic,[13,14,18,19] free radical,[15] and thermal polymerizations.[16,17] However, the large difference in reactivity between vegetable oils and petroleum-based comonomers, such as divinylbenzene (DVB), results in heterogeneous

copolymers consisting of an oil-rich phase and a DVB-rich phase. It was found that Norway fish oil (NFO) could be used to modify initiating systems to produce homogeneous copolymers,[20] since NFO is completely miscible with both vegetable oils and DVB.

Linseed oil, which is widely used as a drying oil for surface coatings,[21] is a triglyceride oil composed of 4% steric (C18:0), 19% oleic (C18:1), 24% linoleic (C18:2), and 47% linolenic (C18:3) acids with approximately six C=C bonds per triglyceride.[19] The high number of double bonds per triglyceride makes linseed oil particularly susceptible to cationic polymerization. Several chemically-modified linseed oils are commercially available. For example, Dilulin is a commercially available vegetable oil-based monomer with approximately one norbornene ring per triglyceride prepared by a Diels-Alder reaction between dicyclopentadiene (DCPD) and linseed oil.[22] ML189, another commercially available modified linseed oil with cyclopentene rings attached to the triglyceride chains, is also prepared by reacting linseed oil with dicyclopentadiene.[23] Herein, we wish to report the synthesis and characterization of a range of novel biopolymers prepared from the cationic copolymerization of Dilulin and ML189 with DCPD. The norbornene ring of the Dilulin and the cyclopentene ring of the ML189 enhance their reactivities towards DCPD, thus affording homogeneous copolymers without acquiring NFO as modified catalyst.

Experimental

Materials. Dilulin was obtained from Cargill (Chicago, IL). ML189 was supplied by Northern Sun, a division of Archer Daniels Midland Company (Red Wing, MN). Dicyclopentadiene (DCPD) (> 95%) was purchased from Alfa Aesar (Ward Hill, MA). Boron trifluoride diethyl etherate (BFE) (distilled grade) was purchased from Sigma-Aldrich

(Milwaukee, WI). Unless otherwise stated, all reagents were used as received without further purification.

Cationic Copolymerization and Nomenclature. Pre-weighed amounts of oils (Dilulin or ML189) and DCPD were mixed in a beaker and stirred vigorously in an ice water bath until a homogeneous solution was obtained (total = 97 wt %). During this time, 3 wt % of BFE catalyst was added slowly to the mixture of the oil and DCPD. The reaction mixture was stirred vigorously until it became homogeneous, and then poured into a glass mold and cured for 12 h at 60 ℃ and then 24 h at 110 ℃. The resulting polymers were obtained in essentially quantitative yields. The nomenclature adopted in this paper for the polymer samples is as follows: a polymer sample prepared from 77 wt % Dilulin, 20 wt % DCPD, 3 wt % BFE is designated as Dil77-DCPD20-BFE3.

Soxhlet Extractions. A 3-4 g sample of the bulk polymer was extracted with 100 mL of refluxing methylene chloride for 24 h using a Soxhlet extractor. Following extraction, the resulting solution was concentrated under reduced pressure and dried in a vacuum oven at 60 ℃ overnight. The recovered insoluble portion was also dried under a vacuum prior to weighing.

Characterization. ^{1}H NMR spectroscopic analysis of the oil and the soluble substances extracted from the biopolymers by methylene chloride were recorded in $CDCl_3$ using a Varian spectrometer (Palo Alto, CA) at 400 MHz. Cross-polarization with total spinning sideband suppression (CPTOSS) ^{13}C NMR spectral analysis of the insoluble materials remaining after Soxhlet extraction of the bulk polymers was performed using a Bruker AVANCE 600 spectrometer (Bruker America, Billerica). Dynamic mechanical analysis (DMA) was recorded on a TA Instruments (New Castle, DE) Q800 dynamic mechanical

analyzer using a three-point bending mode. Rectangular samples 1.5 mm thick and 10 mm wide were used for the analysis. Samples were cooled and held isothermally for 3 minutes at -80 ℃ before the temperature was increased at 3 ℃/min to 200 ℃. Thermogravimetric analysis (TGA) of the specimens was carried out on a TA Instruments (New Castle, DE) Q50. Samples were scanned from 50 ℃ to 650 ℃ in air with a heating rate of 20 ^{o}C/min.

Results and Discussion

Dilulin, ML189 and DCPD as Cationic Monomers. Both Dilulin and ML189 are commercially available oils prepared from linseed oil. Dilulin is synthesized by a Diels-Alder reaction between cyclopentadiene and the double bonds of linseed oil (Scheme 1a). However, the Diels-Alder reaction can also happen between cyclopentadienes, resulting in a mixture of Dilulin and DCPD, as well as DCPD oligomers. Purification of Dilulin was carried out on a

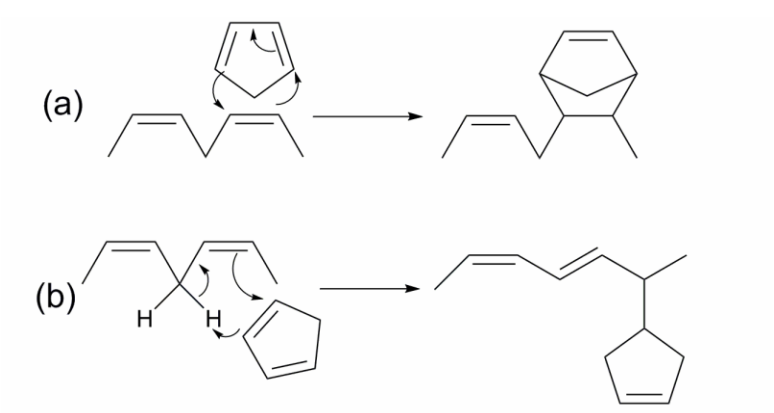

Scheme 1. (a) Diels-Alder reaction between linseed oil and cyclopentadiene, (b) ene reaction between cyclopentadiene and the bis-allylic hydrogens in linseed oil.

flash silica gel column with hexanes and ethyl acetate used to elute the column following the procedure we reported before.[24] It was found that the commercially available Dilulin consists of approximately 95 wt % of "pure" Dilulin and about 5 wt % DCPD oligomers. ^{1}H

NMR spectral analysis of commercial Dilulin (Figure 1c) and "pure" Dilulin (Figure 1a) provided essentially identical results; therefore, only characterization of the non-purified Dilulin will be discussed. Figure 1b shows the DCPD oligomers, the peaks from 5.9 ppm to 6.1 ppm are due to the norbornene ring in the DCPD oligomers; the peaks at 5.4 ppm and 5.6 ppm are due to the cyclopentene ring in the DCPD oligomers.

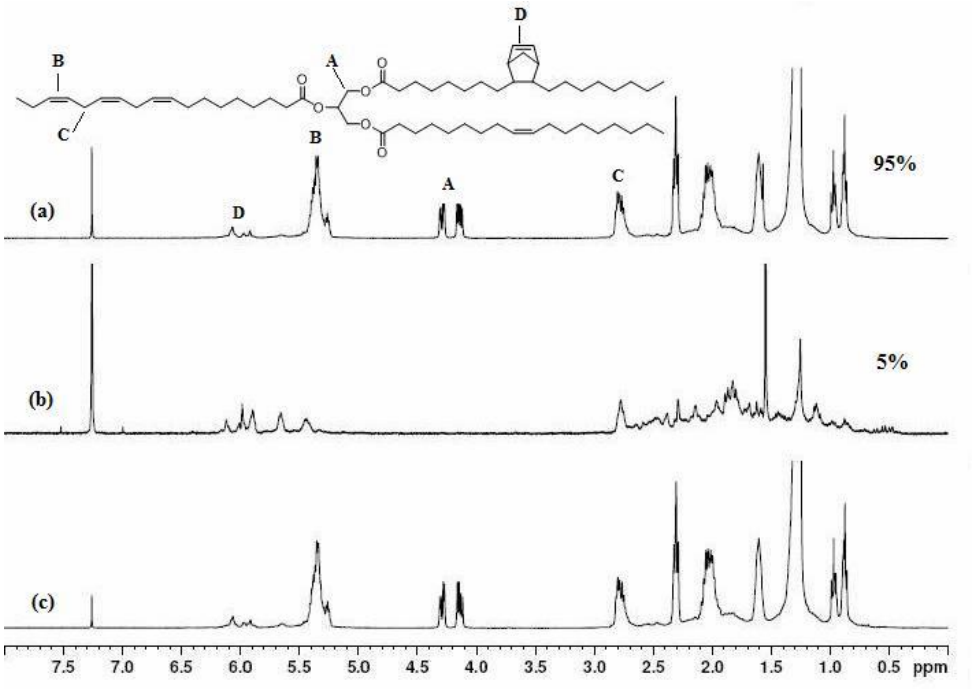

Figure 1. ^{1}H NMR spectra of (a) purified Dilulin, (b) DCPD oligomers, and (c) commercial Dilulin.

ML189 is obtained by an ene reaction between cyclopentadiene and the bis-allylic hydrogens in linseed oil as shown in Scheme 1b. Purification using a flash silica gel column indicates that ML189 contains approximately 80 wt % "pure" ML189 and 20 wt % "oil with more than one cyclopentene ring per triglyceride". ^{1}H NMR spectral analysis of commercial

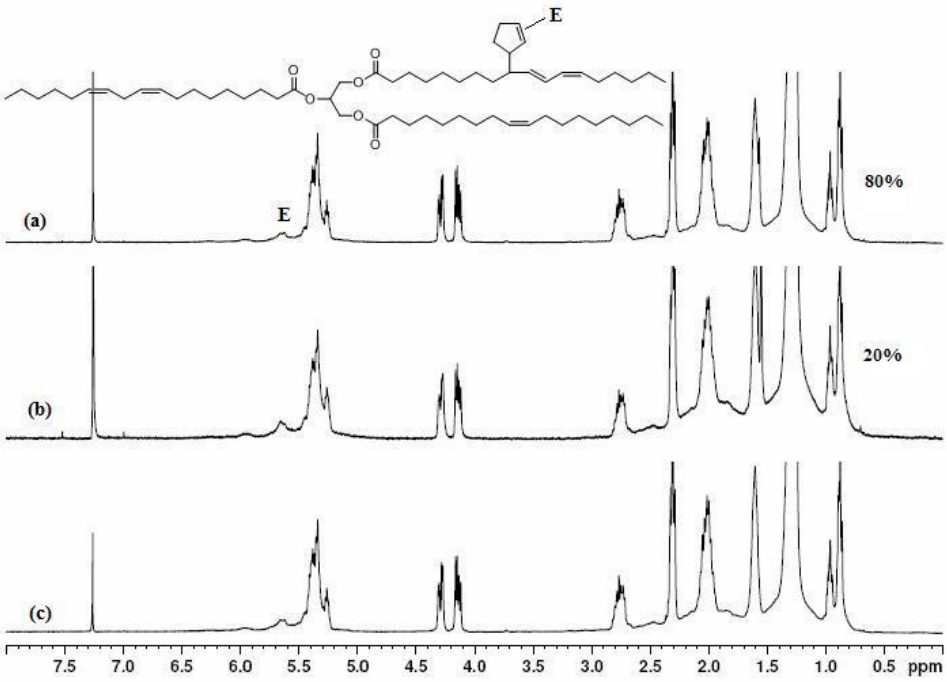

Figure 2. ^{1}H NMR spectra of (a) purified ML189, (b) oil containing more than on CP ring, and (c) commercial ML189.

ML189 (Figure 2c) and purified ML189 (Figure 2a) indicates that the two materials have similar structures; the only difference is the number of cyclopentene rings per triglyceride. These two materials have essentially identical chemical properties, so only characterization of the non-purified ML189 will be discussed.

Dilulin contains approximately one norbornene ring per linseed oil-based triglyceride, whereas ML189 contains about one cyclopentene ring per linseed oil triglyceride. The strained norbornene and cyclopentene rings are more reactive than the original double bonds of the fatty acid chains, so both Dilulin and ML189 are more reactive than regular linseed oil. Because of the high reactivity of the strained rings and the high degree of unsaturation of

Dilulin and ML189, these oils afford interesting highly crosslinked polymer networks upon cationic copolymerization with DCPD.

DCPD is a well known Diels-Alder product of cyclopentadiene, and forms rapidly at room temperature. DCPD contains two polymerizable double bonds, one norbornene-like (NB) and one cyclopentene-like (CP) double bond. Different structural units are generated in the polyDCPD backbone upon homopolymerization of DCPD, since the NB C=C bond of DCPD is more reactive than the CP C=C bond and skeletal rearrangements are known to occur.[25] For instance, Corner *et al.*[26] used $PdCl_2(PhCN)_2$ and BFE to polymerize DCPD and found that the polymerization occurred through the NB double bonds. The resulting polymer chains contain both an endo-unit (1) and an exo-unit (2) through either direct addition or cationic rearrangement (Scheme 2). It is also important to mention that the exo-unit (2) is more stable than the endo unit (1).[20] Peng *et al.*[27] have polymerized DCPD by various cationic initiating systems in toluene, *n*-hexane or dichloromethane and found that under specific conditions, besides units (1) and (2), structures derived from direct addition to a CP unit (3) and a transannular unit (4) were also present (Scheme 3).

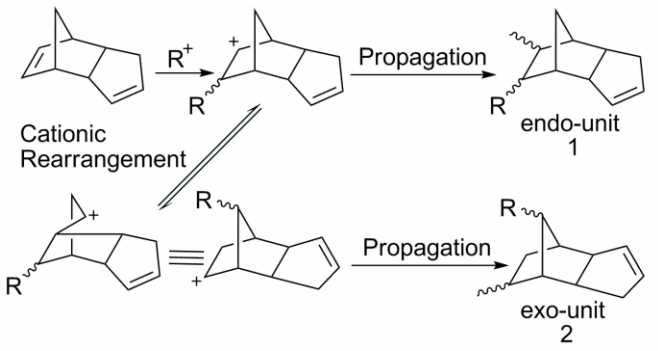

Scheme 2. Formation of polyDCPD via polymerization of NB-like double bonds.

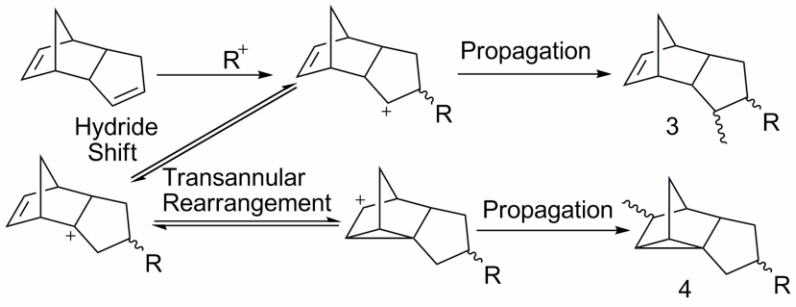

Scheme 3. Formation of polyDCPD via polymerization of CP-like double bonds.

Structure of the Dil-DCPD and ML189-DCPD copolymers. The presence of multiple double bonds in Dilulin and ML189 makes them suitable for cationic polymerization to generate solid polymeric materials. To increase the physical properties of the samples, copolymerization with the rigid monomer DCPD is effected using BFE as catalyst. Previously, soybean oil has been cationically copolymerized with DCPD by us.[20] However, BFE modifiers, such as NFO, needed to be added to produce homogeneous copolymers, because the reactivity of DCPD is higher than that of soybean oil. Here in this work, the NB rings of the Dilulin and the CP rings of the ML189 better homogenize the copolymer with the DCPD monomer to obtain homogeneous polymer samples. DCPD is a diene with a rigid bicyclic structure; it can act as a crosslinker in the cationic copolymerization to enhance the properties of the copolymers.

Scheme 4 illustrates the formation and growth of the crosslinked Dil-DCPD copolymer network during copolymerization due to the presence of multiple double bonds in both the Dilulin oil and the DCPD. The polymerization process appears to produce both exo and endo DCPD units in the polymer backbone (according to Scheme 2), and DCPD acts as a crosslinker. Fully cured Dil-DCPD and ML189-DCPD copolymers have been obtained in essentially quantitative yields. All of the copolymers are dark brown materials at room

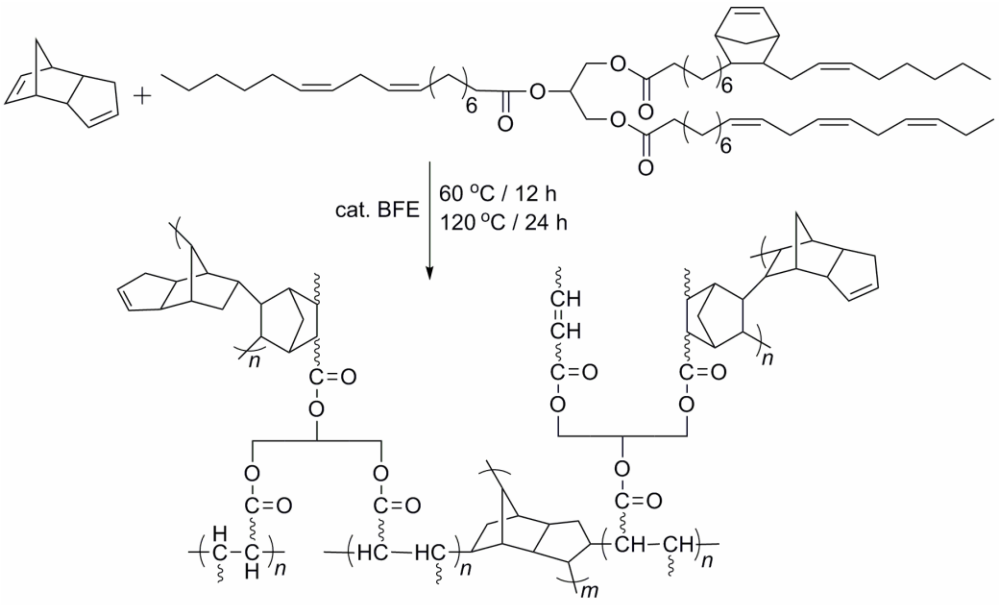

Scheme 4. Cationic copolymerization of Dilulin and DCPD.

temperature, and range from soft and rubbery to hard and strong as the amount of DCPD increases. The data from Soxhlet extraction of these copolymers using methylene chloride as the refluxing solvent are summarized in Table 1. Typically, after 24 hours of extraction, about 84-90 and 85-88 wt % of insoluble materials (crosslinked polymer) are obtained for the

Table 1: Soxhlet extraction data for all copolymers

Copolymer	Soluble %	Insoluble %
Dil97DCPD0BFE3	10	90
Dil87DCPD10BFE3	11	89
Dil77DCPD20BFE3	13	87
Dil67DCPD30BFE3	12	88
Dil57DCPD40BFE3	16	84
ML189-97DCPD0BFE3	13	87
ML189-87DCPD10BFE3	12	88
ML189-77DCPD20BFE3	12	88
ML189-67DCPD30BFE3	13	87
ML189-57DCPD40BFE3	15	85

Dil-DCPD and ML189-DCPD bulk materials, respectively. Interestingly, all of the extraction data are fairly similar as the amount of DCPD increases from 0 to 40 wt %. For instance, an increase in DCPD content from 0 to 30 wt % in the Dil-DCPD copolymer only lowers the yield of the insoluble crosslinked polymer about 2 wt %, whereas an increase in the DCPD content from 0 to 30 wt % in the ML189-DCPD mixture does not lower the yield of crosslinked polymer at all. However, when the amount of DCPD in both the Dil-DCPD and ML189-DCPD mixtures is increased to 40 wt %, the yield of the insoluble crosslinked polymers decreases 4 and 2 wt % compared to Dil-DCPD30 and ML189-DCPD30, respectively. We believe that these results are a direct consequence of the similar reactivities between the Dilulin or ML189 oils and DCPD. Also the oils can crosslink very well without DCPD, because of the multiple double bonds in the oils. DPCD in the mixture seems to increase the rigidity of the copolymers, rather than the crosslinking density (discussed later). When the amount of DCPD was increased to 40 wt %, the rigid DCPD segment may restrain the movement of the natural oil chains and affect the polymerization of the oils, leading to the slight increase in the soluble portion. Solid state ^{13}C NMR spectral analysis of the insoluble components remaining after Soxhlet extraction confirms the incorporation of both Dilulin and DCPD units into the crosslinked network (Figure 3). This is evidenced by the presence of both C=O and C=C signals at 170 and 130 ppm, respectively.

It has also been noted that the incorporation of Dilulin or ML189 in the crosslinked copolymer increases with increasing amounts of oil in the initial composition for all of the Dil-DCPD and ML189-DCPD copolymers. Provided that the soluble components consist solely of unreacted natural oils and oil oligomers, then the oil incorporated in the crosslinked material is equal to the initial wt % of oil minus the wt % of the soluble material. In this way,

an almost linear relationship exists between the amounts of oil incorporated in the crosslinked material and the amount of the initial oil as shown in Figure 4. This is most likely due to the similar reactivities of the Dilulin or ML189 oils and DCPD. Similar results have also been reported for soybean oil-DCPD copolymers.[20]

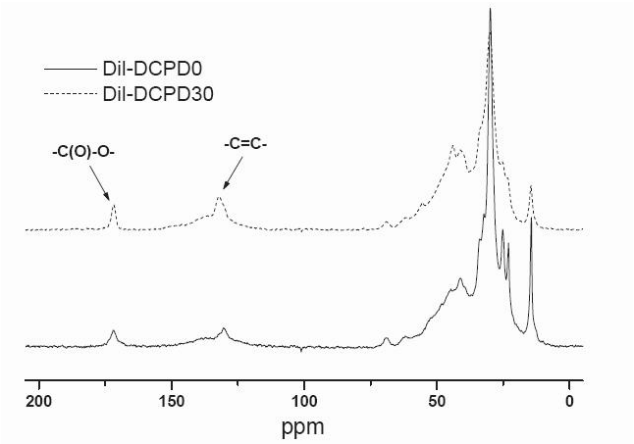

Figure 3. Solid-state ^{13}C NMR spectra of the insoluble materials remaining after Soxhlet extraction of the Dil-DCPD0 and Dil-DCPD30 bulk polymers.

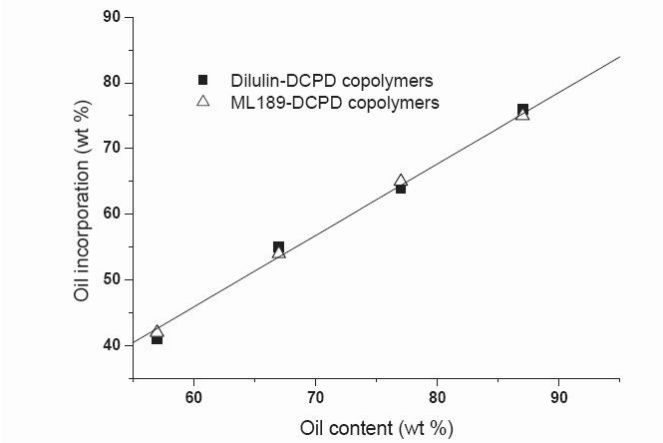

Figure 4. Dependence of oil incorporation in the crosslinked material on the wt % of oils in the initial composition.

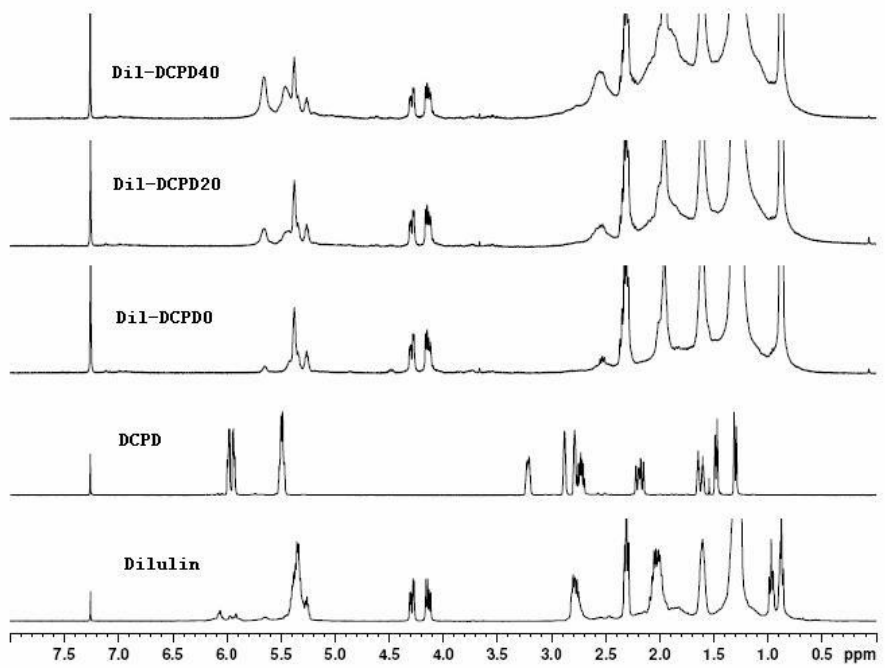

Figure 5. ^{1}H NMR spectra of the extracts from the Dil-DCPD copolymers in CH_2Cl_2.

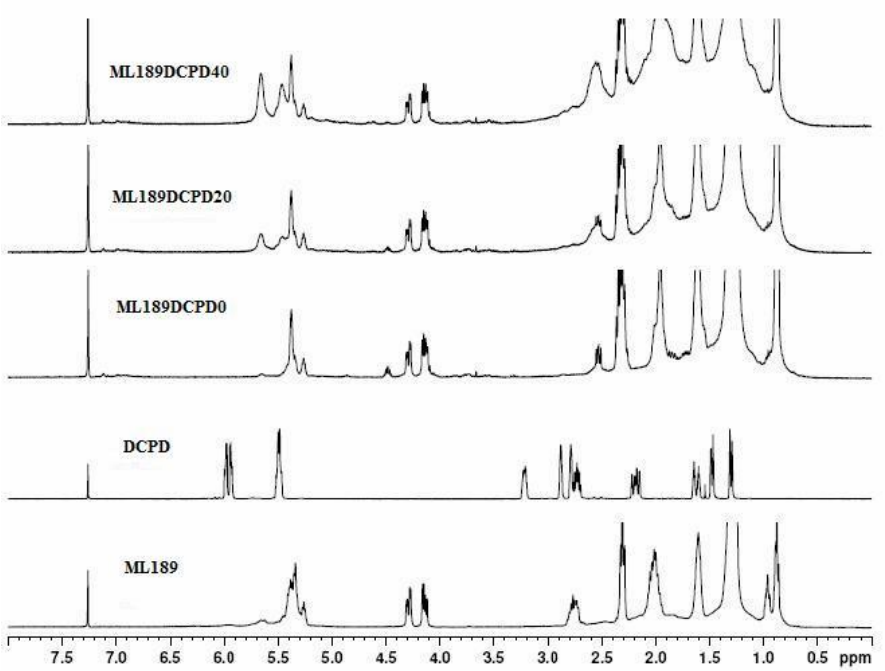

Figure 6. ^{1}H NMR spectra of the extracts from the ML189-DCPD copolymers in CH_2Cl_2.

Both the Dil-DCPD and ML189-DCPD bulk materials consist of a large amount of insoluble crosslinked materials interpenetrated with a certain amount of soluble components. ^{1}H NMR spectral analysis of these soluble materials confirms the presence of both oils and DCPD units, as evidenced by signals at 4.1-4.4 ppm and 5.5-5.6 ppm, respectively (Figures 5 and 6). The peaks at 4.1-4.4 ppm correspond to the hydrogen atoms of the glycerol unit in the Dilulin and ML189,[19] while the peaks at 5.45 ppm and 5.5-5.6 ppm correspond to the olefinic hydrogens on the endo-unit (1) and the exo-unit (2) (Scheme 2) of the DCPD.[28] Additional proof that these two peaks (5.45 ppm and 5.5-5.6 ppm) correspond to DCPD has been acquired through comparative ^{1}H NMR spectral analysis. Figures 5 and 6 show a series of ^{1}H NMR spectra of the monomers and the soluble extracts of the Dil-DCPD and ML189-DCPD copolymers. The results indicate that the intensities of the above mentioned signals (5.45 ppm and 5.5-5.6 ppm) increase with increasing amounts of DCPD in the initial composition, meaning that they are DCPD related. Moreover, the absence of the signal at 5.9-6.1 ppm clearly indicates that all of the NB C=C bonds have reacted. The CP C=C bonds that do react during the cationic copolymerization, along with the NB C=C bonds, form effective crosslinks in the bulk materials.[25]

Thermal Properties. Table 2 summarizes the glass transition temperatures (T_gs), crosslink densities, tan δ values, and TGA data for all of the Dil-DCPD and ML189-DCPD copolymers. The T_gs of the copolymers have been calculated from the maximum of the tan δ peaks. The crosslink densities have been calculated from the storage moduli at T_g + 100 ^{o}C based on rubber elasticity theory, which has been described in our previous work.[19] Thermogravimetric data includes 10% and 50% weight loss temperatures (T_{10} and T_{50}) and the temperatures of maximum thermal degradation (T_{max}).

Table 2. DMA, TGA, and extraction analysis for all copolymers

Copolymer	T_g (°C)[a]	υ_e (mol/m^3)[b]	Tan δ	E' at 25 °C (Pa)	TGA data (°C)		
					T_{10}[c]	T_{50}[d]	T_{max}[e]
Dil97DCPD0BFE3	14.6	249	0.99	4.43×10^6	304	462	466
Dil87DCPD10BFE3	32.8	194	0.81	6.38×10^7	305	462	464
Dil77DCPD20BFE3	47.0	228	0.78	4.25×10^8	317	464	465
Dil67DCPD30BFE3	64.3	517	0.75	1.09×10^9	320	466	464
Dil57DCPD40BFE3	83.2	365	0.70	1.52×10^9	334	468	465
ML189-97DCPD0BFE3	7.5	379	1.10	3.72×10^6	305	459	468
ML189-87DCPD10BFE3	20.8	260	0.93	1.43×10^7	310	462	465
ML189-77DCPD20BFE3	38.3	210	0.78	1.52×10^8	308	464	465
ML189-67DCPD30BFE3	55.7	441	0.77	7.14×10^8	328	468	465
ML189-57DCPD40BFE3	76.9	333	0.75	1.44×10^9	329	467	463

a) Glass transition temperatures represent the maxima of the tan δ curves obtained by DMA analysis.
b) Crosslink densities have been calculated at temperatures 100 °C above the *T*g.
c) 10% Weight loss temperature.
d) 50% Weight loss temperature.
e) Temperature of maximum thermal degradation.

The T_gs of the Dil-DCPD and ML189-DCPD copolymers range from 15 to 83 °C and 8 to 77 °C, respectively. The T_gs of all copolymers increase linearly with increasing amounts of DCPD as shown in Figure 7. Similar results have been reported by Wool[29] and Lu,[30] and the T_gs increase linearly relative to the crosslink densities in their results. However, there is no correlation between the crosslink densities and the amount of DCPD (Table 2) in this work, and the linear relationship between T_gs and the amount of DCPD is mainly due to the incorporation of rigid DCPD molecules into the crosslinked copolymer which reduces the mobility of the polymer chains. Figure 7 also indicates that the copolymers prepared from ML189 have lower T_gs than those from Dilulin. This is in good agreement with Dilulin having a more rigid norbornene ring than ML189 with a cyclopentene ring. As discussed earlier, the crosslink densities of all copolymers show no dependence on the amount of DCPD in the initial composition. However, the highest crosslink densities have been

observed when the DCPD amount is 30 wt % in both the Dilulin and ML189 copolymers. This is probably because this is an optimal concentration for copolymerization of the Dilulin or ML189 and DCPD to produce the highest crosslink densities.

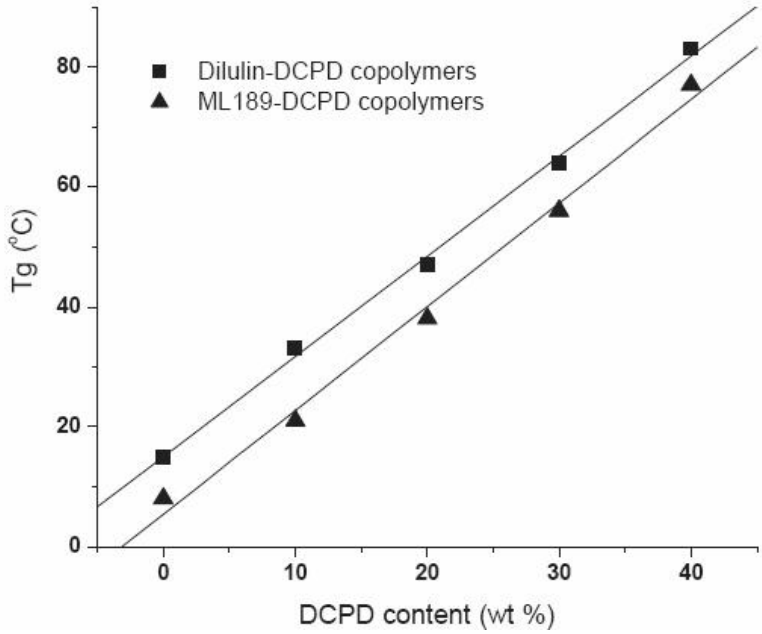

Figure 7. Dependence of T_g on the wt % of DCPD.

Also shown in Table 2 are the tan δ values for all of the copolymers. It can be seen that an increase in the DCPD amount results in a decrease in the tan δ values. This is expected, since rigid DCPD units in the copolymer restrain the movement of the polymer chains. All copolymers exhibit only one tan δ peak, as shown in Figure 8, indicating there is no phase separation of the resulting copolymers. However, the tan δ peak broadens with increasing amounts of DCPD, indicating that the copolymers are less homogeneous with more DCPD in the initial composition. Figure 9 shows the temperature dependence of the storage moduli of the Dil-DCPD and ML189-DCPD copolymers. All copolymers behave as

typical thermosets as evidenced by the presence of rubbery plateaus in their DMA curves. The presence of the rubbery plateau in the DMA curves is evidence for the existence of a crosslinked network as discussed previously. As expected, the room temperature storage modulus (E') (Table 2) increases with an increase in the DCPD content, due to reinforcement by the rigid DCPD.

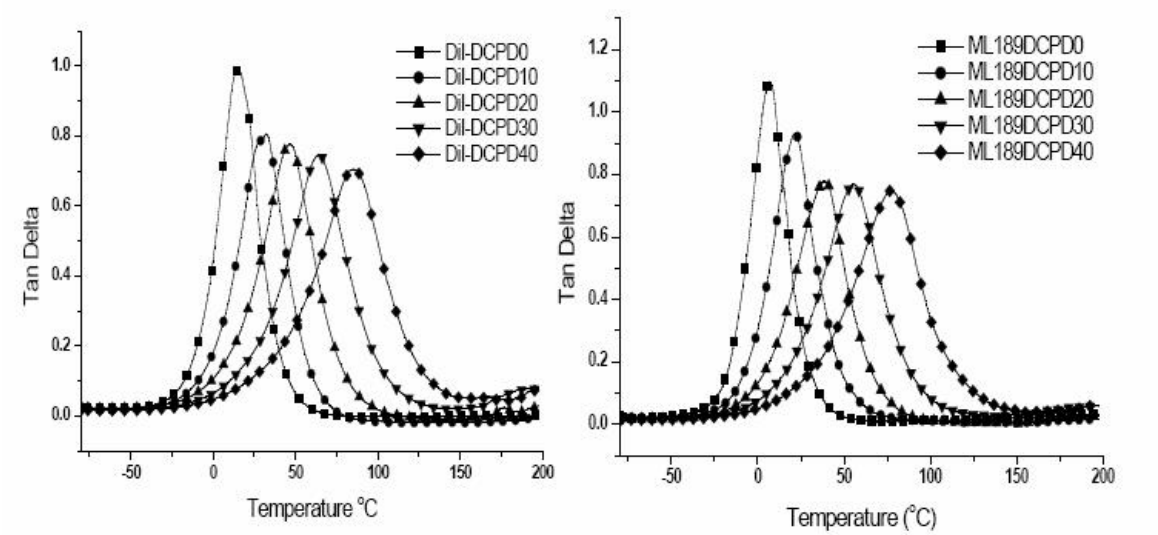

Figure 8. Tan δ curves obtained by DMA for the Dil-DCPD and ML189-DCPD copolymers.

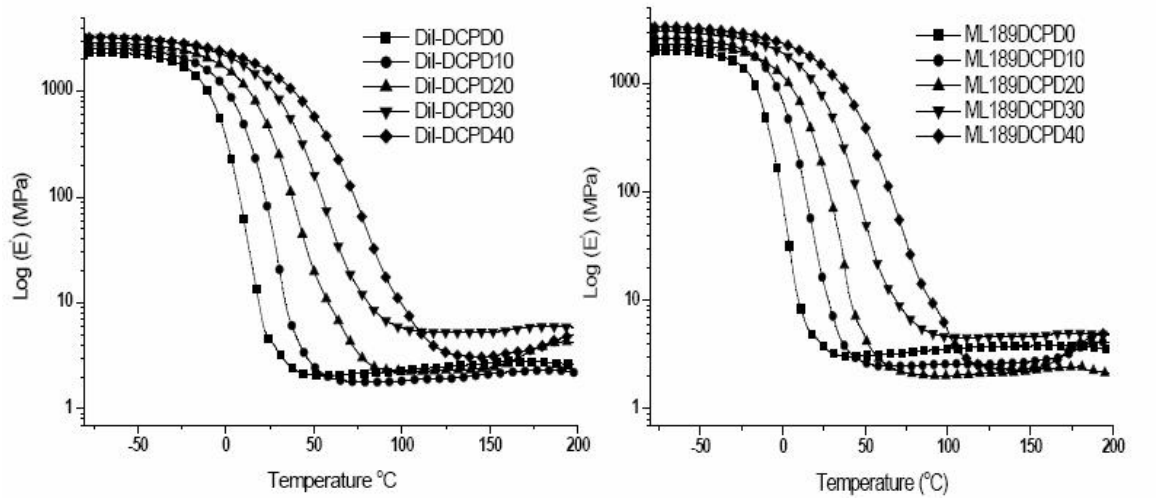

Figure 9. Storage moduli obtained by DMA for the Dil-DCPD and ML189-DCPD copolymers.

Table 2 and Figure 10 show the TGA data obtained from the oils, and the Dil-DCPD and ML189-DCPD copolymers. It is found that all of the copolymers are thermally stable up to 150 ^{o}C and exhibit a three-stage thermal degradation above this temperature. The first stage represents the evaporation and decomposition of some of the soluble components and is evident from 150 to 420 ^{o}C. The second stage, which appears in the region from 420 to 500 ^{o}C, is the fastest degradation stage and corresponds to degradation and char formation of the crosslinked polymer structure. The third stage (500-650 ^{o}C) corresponds to gradual oxidation of the char residue.[20] It can be seen from Figure 10 that Dilulin starts to degrade at about 200 ^{o}C, while ML189 degrades at about 300 ^{o}C, which is in good agreement with the fact that the norbornene ring in Dilulin has more strain and is less stable than the cyclopentene ring in ML189. The T_{10} values of the Dil-DCPD and ML189-DCPD copolymers (Table 2) range from 304 to 334 and 305 to 329 ^{o}C, respectively, and increase gradually with an increase in the amount of DCPD. The reason for this is that more oil in the initial composition causes more oil-related and easy-vaporized substances, resulting in lower T_{10} values.[20]

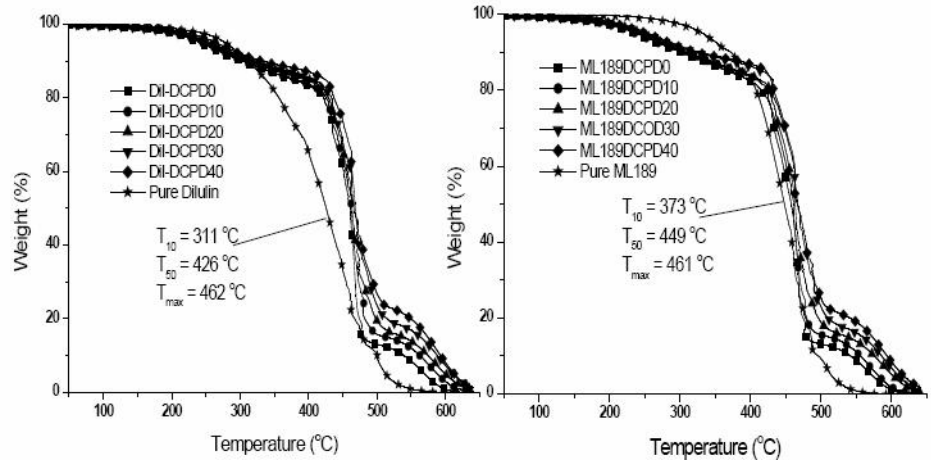

Figure 10. Thermal degradation of the Dil-DCPD and ML189-DCPD copolymers, and the pure oils.

The T_{50} values for the Dil-DCPD and ML189-DCPD copolymers are in the range of 462-468 and 459-468 ^{o}C, respectively. The T_{50} values correspond to the second thermal degradation stage, which corresponds to degradation of the crosslinked polymer structure. It can be seen that the incorporation of rigid bicyclic DCPD units into the copolymer structures does not effectively increase their thermal stability, due to the fact that an increase in DCPD in the initial composition does not significantly increase the crosslink densities, because oils with more than 6 double bonds per triglyceride can self-crosslink very well. Besides the T_{50} values, the second-stage degradation is also characterized by the T_{max} values, which are in the range of 464-466 and 463-468 ^{o}C for the Dil-DCPD and ML189-DCPD copolymers, respectively. All of the Dil-DCPD and ML189-DCPD copolymers exhibit similar T_{50} and T_{max} values. This is in agreement with the fact that Dilulin, ML189 and DCPD have similar reactivities.

Conclusions

A series of soft to tough thermosets containing 57-97 wt % biorenewable materials have been prepared by the cationic copolymerization of Dilulin or ML189 and DCPD initiated by a BFE catalyst. All monomers used in this study exhibit similar reactivities, resulting in homogeneous copolymers.

All copolymers are dark brown in color and consist of a crosslinked oil-DCPD network interpenetrated with certain amounts of soluble components, which appear to include free oil, oil-DCPD oligomers and some low molecular weight oil fragments, such as mono- and diglycerides or fatty acids. The T_gs of the Dil-DCPD and ML189-DCPD copolymers range from 15-83 ^{o}C and 8-77 ^{o}C, respectively, and increase linearly with the amount of DCPD. Moreover, the room temperature storage moduli increase with an increase

in the amount of DCPD. Due to the similar reactivities of Dilulin, ML189 and DCPD, similar thermal stabilities have been observed for samples of Dil-DCPD and ML189-DCPD copolymers with similar compositions. All oil-DCPD copolymers are thermally stable up to 150 ^{o}C in air. T_{10} and T_{50} values are in the range 304-334 ^{o}C and 459-468 ^{o}C, respectively. These properties suggest that these materials may prove useful alternatives for current petroleum-based plastics and find widespread utility.

Acknowledgments

This project was supported by the Center for Crops Utilization Research (CCUR) at Iowa State University. We are thankful to Dr. Michael Kessler from the Department of Materials Science and Engineering at Iowa State University for his thermal analysis equipment. In addition, we also thank Dr. Yongshang Lu from the Chemistry Department at Iowa State University for his thoughtful insights into this work.

References

1. "Feedstocks for the Future: Renewables for the Production of Chemicals and Materials", ACS Symposium Series 921; J. J. Bozell, M. K. Patel, Eds., American Chemical Society, Washington, DC, 2006.
2. I. Y. Qudsieh, A. F. I-Razi, N. A. Kabbashi, M. E. S. Mirghani, K. G. Fandi, M. Z. Alam, S. A. Muyibi, M. M. Nasef, *J. Appl. Polym. Sci.* **2008**, *109*, 3140-3147.
3. H. Qi, C. Chang, L. Zhang, *Green Chem*. **2009**, *11*, 177-184.
4. L. Candy, C. Vaca-Garcia, E. Borredon, *J. Am. Oil Chem. Soc.* **2005**, *82*, 271-277.
5. W. Liu, M. Misra, P. Askeland, L. T. Drzal, A. K. Mohanty, *Polymer* **2005**, *46*, 2710-2721.
6. E. Can, R. P. Wool, S. Küsefoğlu, *J. Appl. Polym. Sci.* **2006**, *102*, 1497-1504.
7. E. Can, S. Küsefoğlu, R. P. Wool, *J. Appl. Polym. Sci.* **2001**, *81*, 69-77.
8. E. Can, S. Küsefoğlu, R. P. Wool, *J. Appl. Polym. Sci.* **2002**, *83*, 972-980.
9. Z. S. Petrovic, W. Zhang, I. Javni, *Biomacromolecules* **2005**, *6*, 713-719.
10. M. Ionescu, Z. S. Petrovic, X. Wan, *J. Polym. Environ.* **2007**, *15*, 237-243.
11. Z. S. Petrovic, L. Yang, A. Zlatanic, W. Zhang, I. Javni, *J. Appl. Polym. Sci.* **2007**, *105*, 2717-2727.
12. Z. S. Petrovic, A. Guo, I. Javni, I. Cvetkonic, D. P. Hong, *Polym. Int.* **2008**, *57*, 275-281.

13. F. Li, M. V. Hanson, R. C. Larock, *Polymer* **2001**, *42*, 1567-1579.
14. F. Li, J. Hasjim, R. C. Larock, *J. Appl. Polym. Sci.* **2003**, *90*, 1830-1838.
15. P. H. Henna, D. D. Andjelkovic, P. P. Kundu, R. C. Larock, *J. Appl. Polym. Sci.* **2007**, *104*, 979-985.
16. P. P. Kundu, R. C. Larock, *Biomacromolecules* **2005**, *6*, 797-806.
17. F. Li, R. C. Larock, *Biomacromolecules* **2003**, *4*, 1018-1025.
18. F. Li, R. C. Larock, J. U. Otaigbe, *Polymer* **2000**, *41*, 4849-4862.
19. D. D. Andjelkovic, M. Valverde, P. Henna, F. Li, R. C. Larock, *Polymer* **2005**, *46*, 9674-9685.
20. D. D. Andjelkovic, R. C. Larock, *Biomacromolecules* **2006**, *7*, 927-936.
21. D. K. Salunkhe, J. K. Chavan, R. N. Adsule, S. S. Kadam, World Oilseeds: Chemistry, Technology, and Utilization.; Van Nostrand Reinhold: New York, 1991.
22. D. R. Kodali, U.S. Patent 6,420,322, 2002.
23. http://www.adm.com/en-us/Products/_layouts/ProductDetails.aspx?productid= 1160
24. P. Henna, R. C. Larock, *J. Appl. Polym. Sci.* **2009**, *112*, 1788-1797.
25. Y. Peng, J. Liu, L. Cun, *J. Polym. Sci.: Part A: Polym. Chem.* **1996**, *34*, 3527-3530.
26. T. Corner, R. G. Foster, P. Hepworth, *Polymer* **1969**, *10*, 393-397.
27. Y. Peng, J. Liu, L. Cun, *Acta Chim. Sin.* **1997**, *55*, 710-715.
28. Y. Peng, H. Dai, L. Cun, *J. Appl. Polym. Sci.* **1997**, *64*, 1719-1723.
29. J. La Scala, R. P. Wool, *Polymer* **2005**, *46*, 61-69.
30. Y. Lu, R. C. Larock, *Biomacromolecules* **2008**, *9*, 3332-3340.

CHAPTER 3. RING-OPENING METATHESIS POLYMERIZATION (ROMP) OF NORBORNENYL-FUNCTIONALIZED FATTY ALCOHOLS

A Paper published in Polymer, 51, 53-61.

Ying Xia, Yongshang Lu, Richard C. Larock*

Department of Chemistry, Iowa State University, Ames, Iowa 50011

Abstract

Novel biorenewable-based thermosets have been successfully synthesized by the ring-opening metathesis polymerization (ROMP) of norbornenyl-functionalized fatty alcohols derived from soybean oil (NMSA), Dilulin (NMDA), ML189 (NMMA) and castor oil (NMCA). The effects of the monomer structure on the polymerization process, and the thermal and mechanical properties of the resulting thermosets have been extensively investigated. The number of ROMP-reactive rings appended to the fatty acid chain and the viscosity play an important role in controlling the initiation and propagation processes of the polymerization and the final properties of the thermosets obtained. The thermosets have been characterized by Soxhlet extraction, DMA, TGA, and tensile tests. It has been found that polyNMDA and polyNMMA have best thermo-mechanical properties. Compared with polyNMSA, the polyNMDA and polyNMMA thermosets exhibit lower soluble fractions, and higher thermal stabilities and mechanical properties, because of more effective crosslinking; whereas, polyNMCA exhibits a higher soluble fraction, and lower thermal stability, resulting from incomplete polymerization of the more viscous NMCA monomer.

Introduction

Bio-based materials have attracted much attention because of their sustainability and environmental concerns.[1] Recently, renewable materials synthesized from plant products have shown great promise as a replacement for petroleum-based materials.[2] Thermosetting resins,[3] biodegradable polymers,[4] biocomposites[5] and polyurethane dispersions[6,7] from acrylated epoxidized soybean oil, soy protein and vegetable oil-based polyols have been successfully synthesized by free radical, ring-opening and addition polymerizations. In our previous work, we have taken advantage of the carbon-carbon double bonds in soybean,[8] linseed,[9] tung,[10] corn[11] and fish[12] oils to develop a variety of new polymeric materials by cationic or thermal copolymerization of these natural oils with styrene (ST) and divinylbenzene (DVB). The resulting thermosetting polymers can be varied from elastomers to tough and rigid plastics by simply changing the stoichiometry, and the nature of the oil and alkene comonomers. These new polymers exhibit thermophysical and mechanical properties that are comparable to those of commercially available elastomers and conventional plastics and may serve as replacements for petroleum-based polymers in many applications.

Olefin metathesis has also been employed in the synthesis of vegetable oil-based polymers, primarily through acyclic diene (triene) metathesis polymerization (ADMET/ATMET)[13,14] and ring-opening metathesis polymerization (ROMP).[15,16] Recently, Meier *et al.* investigated the ADMET and ATMET bulk polymerizations of vegetable oil-based undecyl undecenoate and glyceryl triundec-10-enoate, respectively, using Grubbs' and Hoveyda–Grubbs' ruthenium catalysts, leading to high-molecular-weight triblock and branched polyesters.[13,14] Moreover, the molecular weight of the resulting polyesters can be controlled by adjusting the ratio of the monomer and the chain stopper in a one-step, one-pot

procedure.

Scheme 1. A general example of ROMP.

In our previous work, we reported the synthesis of vegetable oil-based polymers by ROMP, which is a powerful tool to convert cyclic olefins to various polymeric materials (see Scheme 1 for an example).[17] In our work, two kinds of vegetable oil-based ROMP thermosetting polymers have been obtained successfully by the copolymerization of Dilulin, a commercially available norbornene-modified linseed oil,[18] with dicyclopentadiene (DCPD)[15] and a norbornene-functionalized castor oil (BCO) with cyclooctene[16] using Grubbs 2nd generation catalyst. Their good thermal and mechanical properties indicate great promise for these environmentally-friendly, vegetable oil-based materials as a new class of plastics. However, phase separations were observed in both the Dilulin/DCPD and BCO/cyclooctene thermosets, because of the large difference in reactivity between the vegetable oil-based monomers and the petroleum-based comonomers. The relatively low reactivity of the vegetable oil-based monomers can be attributed to their high viscosity and the free fatty acid chains, which may hinder coordination between the catalyst and the norbornene moiety present in the Dilulin and BCO. Similar results have also been observed in the vegetable oil-based thermosets from Dilulin and norbornene-based crosslinkers.[19]

To address the phase separation, which occurred in the vegetable oil-based ROMP systems, while maintaining the good thermophysical and mechanical properties of the resulting polymers, in this work, four novel norbornenyl-functionalized fatty alcohols with

different side chain structures have been successfully synthesized from soybean oil, Dilulin, ML189 and castor oil by first reducing the vegetable oil triglycerides to fatty alcohols, which were then reacted with 5-norbornene-2,3-dicarboxylate anhydride (see Scheme 2 for an example). These norbornenyl-functionalized biorenewable monomers can easily undergo ring-opening metathesis homopolymerization under Grubbs 2nd generation catalyst, leading to vegetable oil-based thermosets with good thermophysical and mechanical properties with no apparent phase separation.

Experimental

Materials. Soybean oil was purchased at the local supermarket. Dilulin was supplied by Cargill (Chicago, IL). ML189 was obtained from Northern Sun, a division of Archer Daniels Midland (ADM) Company (Red Wing, MN). Castor oil, 5-norbornene-2,3-dicarboxylate anhydride (endo) and the 2nd generation Grubbs catalyst were purchased from Sigma-Aldrich (Milwaukee, WI). Lithium aluminum hydride (LAH) was purchased from Acros (Geel, Belgium). Benzene, ethyl acetate, methylene chloride and hydrochloric acid were obtained from Fisher (Fair Lawn, NJ). Tetrahydrofuran (THF) was distilled over sodium/benzophenone under N_2. Unless otherwise stated, all reagents were used as received without further purification.

Synthesis of Norbornenyl-Functionalized Fatty Alcohols. The synthesis of the norbornenyl-modified soybean alcohol (NMSA) is shown in Scheme 2. LAH (15.7 g, 0.41 mol) was dissolved in 100 mL of THF and stirred in a 500 mL two-neck round bottom flask. Soybean oil (120 g, 0.14 mol) was dissolved in THF (150 mL) and then added dropwise to the LAH solution. The reaction was carried out at 0 ^{o}C overnight. The reaction mixture was poured into ice water, followed by the addition of 1 M HCl, until the solution was clear. Then,

300 mL of ethyl acetate was added, resulting in two layers. The organic layer was washed with water to remove the glycerol, and then dried over $MgSO_4$ and filtered. Finally, the clear soybean alcohol was obtained after removal of the organic solvent under vacuum.

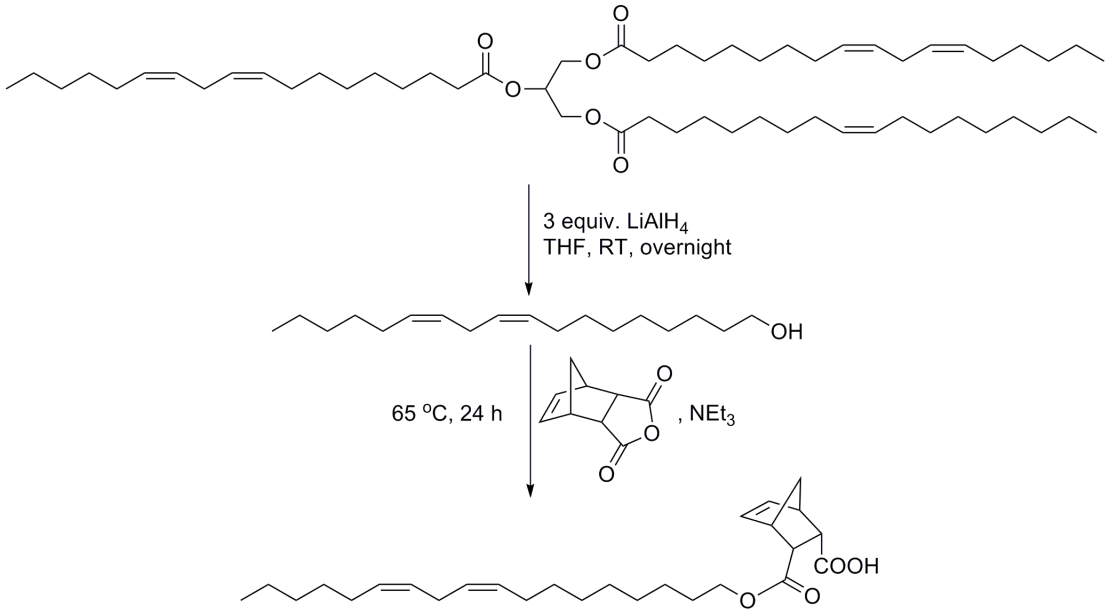

Scheme 2. Synthesis of norbornenyl-modified soybean alcohol (NMSA).

The soybean alcohol (50 g, 0.19 mol) was added to a 250 mL round bottom flask, and then 34.2 g (0.21 mol) of 5-norbornene-2,3-dicarboxylate anhydride (endo) was added, followed by 21.04 g (0.21 mol) of triethylamine. The mixture was stirred at 65 ^oC for 24 h and then diluted by the addition of 100 mL of ethyl acetate. The mixture was poured into a 1M aqueous HCl (400 mL) solution and stirred overnight to convert excess 5-norbornene-2,3-dicarboxylate anhydride to water soluble 5-norbornene-2,3-dicarboxylic acid. Then the mixture was extracted by ethyl acetate, washed by 1 M HCl and brine, and dried over $MgSO_4$. After evaporating the solvent under vacuum, a near quantitative yield of endo-norbornenyl-

modified soybean alcohol (NMSA) was obtained (see later for peak assignments and integration in ^{1}H NMR).

The other vegetable oil-based monomers, norbornenyl-modified Dilulin alcohol (NMDA), norbornenyl-modified ML189 alcohol (NMMA) and norbornenyl-modified castor alcohol (NMCA) were synthesized and purified using the same method as that mentioned above.

Freeze-drying of the Grubbs Catalyst. To improve the solubility of the Grubbs catalyst in the monomers, freeze-drying of the catalyst was carried out according to a literature procedure.[20] The 2nd generation Grubbs catalyst (250 mg) was dissolved in 5 mL of benzene and the solution was frozen in a liquid nitrogen bath. The frozen sample was then placed in a vacuum oven at room temperature for 5 h to sublime the benzene. This process provided catalyst with larger surface areas.

Polymerization. Ten grams of monomer was weighed into a PTFE-coated 20 mL vial. Freeze-dried Grubbs 2nd generation catalyst (50 mg, 0.5 wt %) was mixed with the monomer using a spatula until all of the catalyst was dissolved and a homogeneous solution was obtained. The mixture was heated at 65 ^{o}C for 1 h and 150 ^{o}C for 3 h. The resulting thermosets were slightly transparent and retain the oil's original color.

Soxhlet Extractions. A 2-3 g sample of the bulk polymer was extracted with 100 mL of refluxing methylene chloride for 24 h using a Soxhlet extractor. Following extraction, the resulting solution was concentrated under reduced pressure and dried in a vacuum oven at 60 ℃ overnight.

Characterization. ^{1}H NMR spectroscopic analysis of the monomers and the soluble substances extracted from the thermosets by methylene chloride were recorded in $CDCl_3$

using a Varian spectrometer (Palo Alto, CA) at 300 MHz.

The viscosities of the monomers were measured with a cone (1^{o}, 40 mm diameter) and detachable sample plate on an AR2000ex (TA Instruments, New Castle, DE) at 25 ℃, while the shear rate was increased from 0 to 500 s^{-1}. The gelation time was also determined on the AR2000ex by applying an oscillating strain to the sample and measuring the response stress. All experiments were performed at 65 ^{o}C, using stress control mode at 1 Hz, with 25-mm diameter disposable parallel plates and a 0.5 mm gap.

Differential scanning calorimetry (DSC) cure analyses of the monomers were recorded on a TA Instruments Q20. Monomers were mixed with the Grubbs 2^{nd} generation catalyst, and then the mixtures were transferred to an aluminum DSC pan and loaded into the DSC chamber immediately. The samples were scanned from -50 ℃ to 240 ℃ at a heating rate of 10 ℃/min.

The dynamic mechanical analyses (DMA) was recorded on a TA Instruments Q800 dynamic mechanical analyzer using a three-point bending mode at 1 Hz. Rectangular samples 1.5 mm thick and 10 mm wide were used for the analysis. Samples were cooled and held isothermally for 3 min at -80 ℃ before the temperature was increased at 3 ℃/min to 200 ℃.

Thermogravimetric analysis (TGA) of the specimens was carried out on a TA Instruments (New Castle, DE) Q50. Samples were scanned from 50 ℃ to 650 ℃ in air with a heating rate of 20 ^{o}C/min.

The mechanical properties of the thermosets were determined using an Instron universal testing machine (model 4502) with a crosshead speed of 50 mm/min. Rectangle specimens of 70 × 10 × 3 mm^3 (length × width × thickness) were used. An average value of

five replicates of each sample was taken. The toughness of the polymer, which is the fracture energy per unit volume of the sample, was obtained from the area under the corresponding tensile stress-strain curves.

Results and Discussion

Monomer Characterization. Structures representative of the commercially available vegetable oils employed in this study are shown in Scheme 3. Soybean oil is a triglyceride structure consisting of mainly unsaturated oleic, linoleic and linolenic fatty acids.[21] Dilulin and ML189 are linseed oil-based commercial industrial oils with complex components, which have been characterized before.[22] Dilulin with approximately one norbornene ring per triglyceride is prepared by the Diels-Alder reaction between linseed oil and cyclopentadiene under high temperature and pressure,[18] while ML189 is also a dicyclopentadiene-modified linseed oil,[23] which appears to contain approximately one cyclopentene ring per triglyceride. The ROMP of Dilulin or ML189 results in soft, but weak, polymers, which indicates that the rings appended onto the fatty acid chains can be ring opened to form polymers. Castor oil, consisting of approximately ninety percent ricinoleic acid, has about 2.7 hydroxyl groups per triglyceride.[16] The variety of fatty acid chains present in these oils makes it possible to vary the nature of the monomer and examine the properties of the resulting thermosets.

Figure 1 shows the detailed ^{1}H NMR spectra of NMSA with integrations. The signals at 6.1-6.4 ppm (b) correspond to the norbornene protons, and the vinylic hydrogens of the fatty acid chains (c) are typically found at 5.2-5.5 ppm. The peaks centered at about 4.0 ppm (d) are attributed to the methylene protons close to the ester group of the monomer. Figure 2 illustrates the ^{1}H NMR spectra for the four monomers and the new peaks not present in NMSA are assigned. Compared to NMSA, peaks at 5.9-6.1 (p) and 5.6 ppm (s) are observed

in NMDA and NMMA, which are attributed to the norbornene and cyclopentene rings

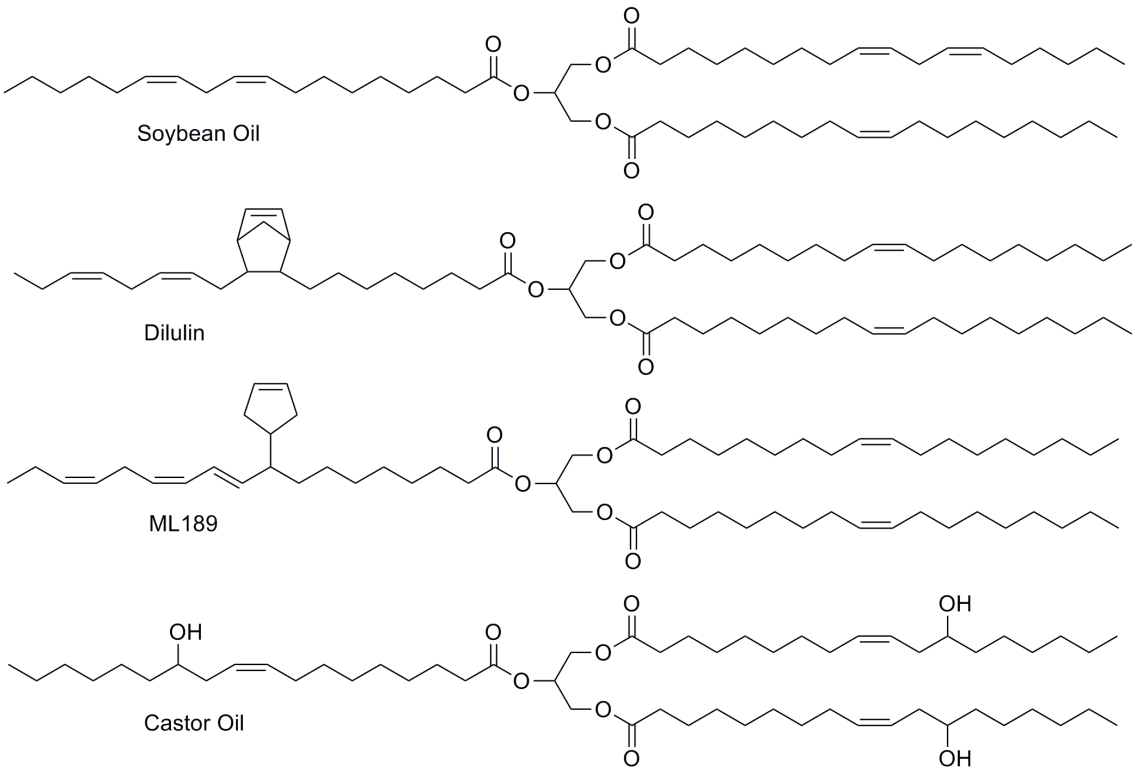

Scheme 3. Representative chemical structures of soybean oil, Dilulin, ML189 and castor oil.

attached to the fatty acid chains in NMDA and NMMA, respectively. For the monomer NMCA, the tertiary hydrogen on the fatty acid chain is observed around 4.8 ppm (t) and a new methylene peak is seen at 2.2 ppm (u). These norbornenyl-modified fatty alcohols are suitable for ring-opening metathesis polymerization, due to the strained norbornene ring present in the monomer. For NMDA and NMMA, approximately one third of the fatty acid side chains are appended with a norbornene ring or a cyclopentene ring (calculated from the integration of the ^{1}H NMR spectra), which leads to crosslinking in the resulting thermosets. Compared with the other three monomers, 90% of NMCA has two norbornene rings, which should result in an even higher crosslink density.

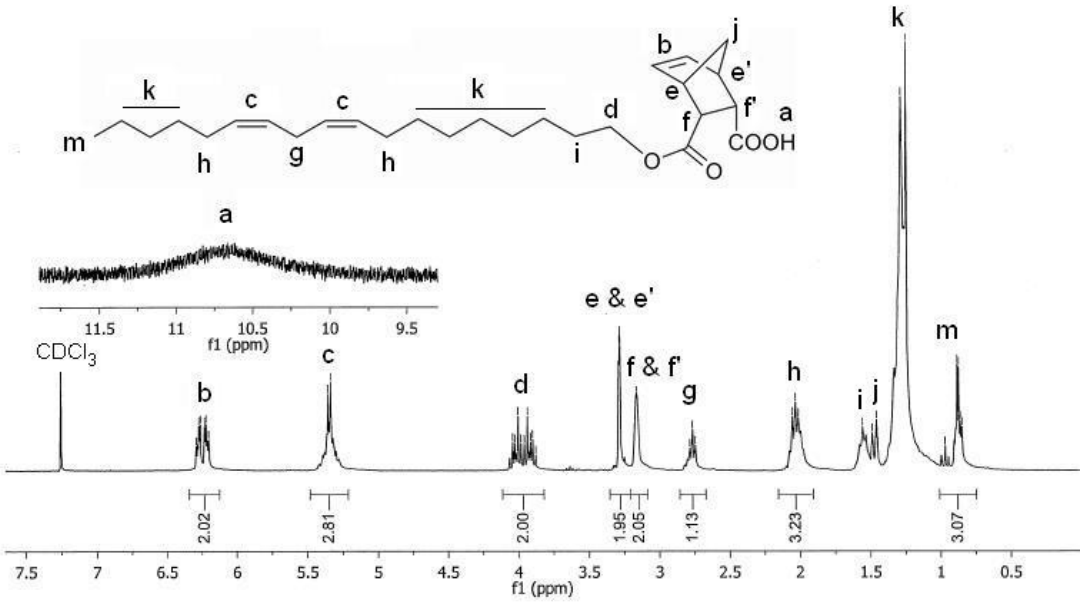

Figure 1. [1]H NMR spectra of NMSA.

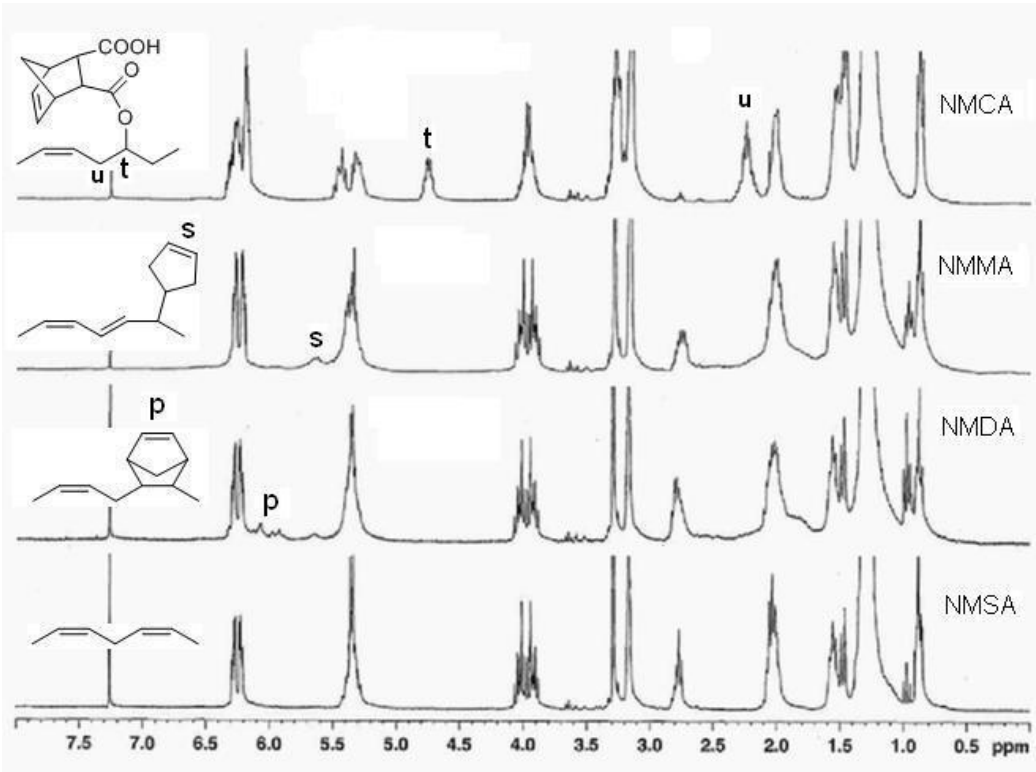

Figure 2. [1]H NMR spectra of NMSA, NMDA, NMMA and NMCA.

ROMP of the Monomers. In the ROMP initiation process using the 2nd generation Grubbs catalyst, the phosphine ligand first dissociates, then the olefin in the monomer coordinates to the reactive ruthenium center to initiate the polymerization process.[24] However, if the bulk monomer is too viscous, it may be more difficult to coordinate with the metal center, resulting in a slow initiation process and propagation of the polymerization[16]. Figure 3 illustrates the viscosities of the four monomers. NMCA has a much higher viscosity than the other three monomers due to the stronger hydrogen bonding through the extra carboxylic acid groups. The relatively high viscosity of NMCA presumably prevents the movement of the monomer and this affects the initiation process and propagation of the polymerization process. Similar results have been reported previously.[16]

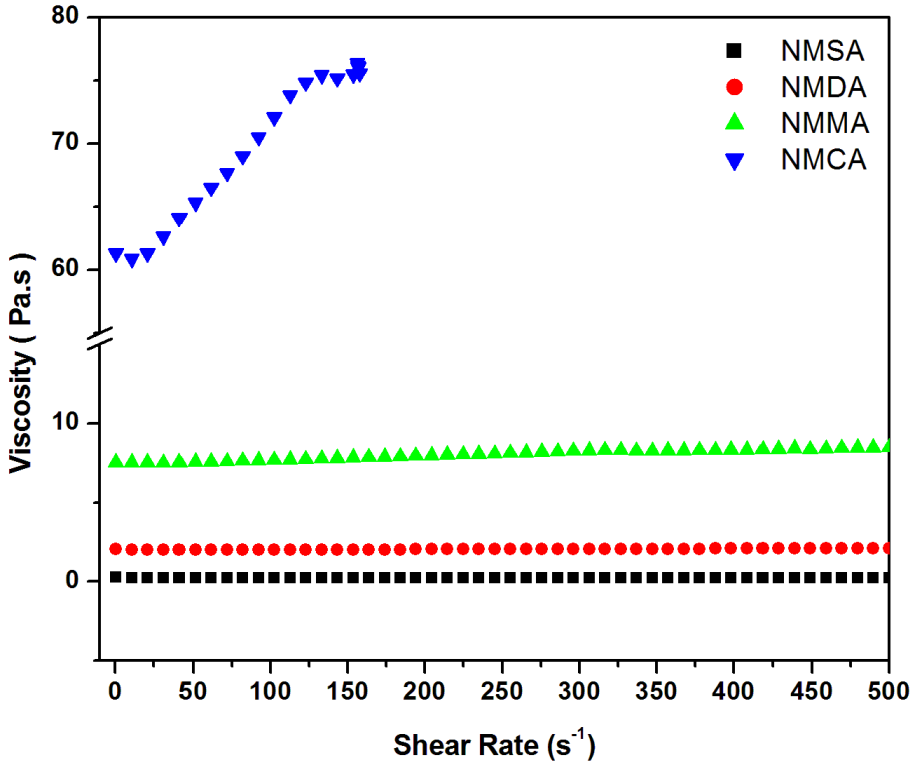

Figure 3. Viscosities of the monomers.

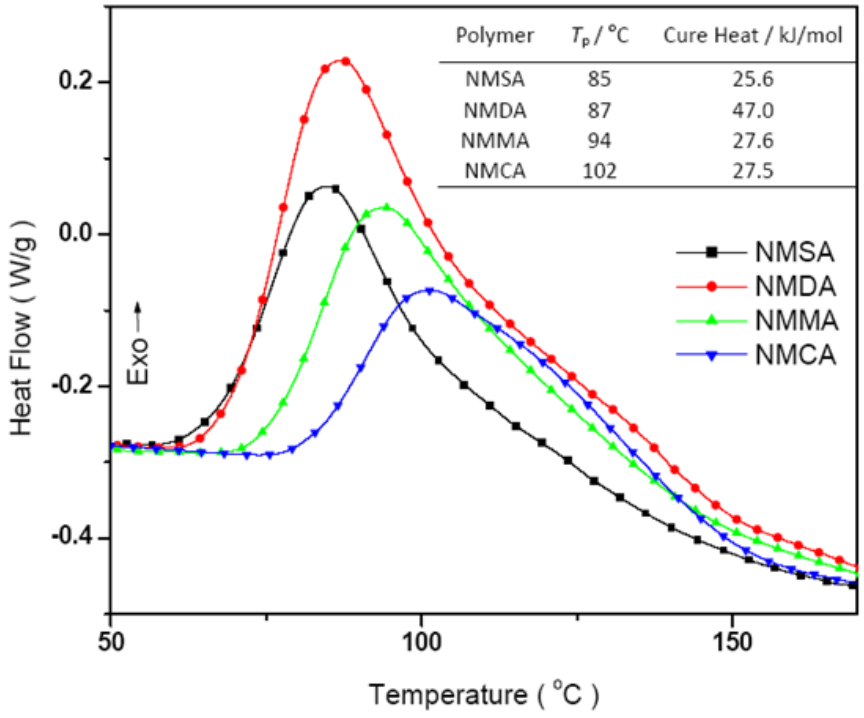

Figure 4. Curing kinetic curves for the monomers.

Figure 4 illustrates the peak temperatures (T_p) and cure heat for the curing kinetic curves of all four monomers. The T_ps increase as the viscosities of the monomers increase, which is in good agreement with the fact that the olefin in the monomer can coordinate to the ruthenium center more easily and thus initiate polymerization with the less viscous monomers. The exothermic peaks are due to the heat release from the strained rings present in the monomer and the cure heat was calculated based on the data obtained from DSC and molecular weight of the monomer. NMDA exhibits the largest cure heat of 47.0 kJ/mol which results from the additional norbornene ring in the monomer. However, NMMA containing an extra cyclopentene ring shows only a slightly higher cure heat than NMSA. This can be explained by the fact that the cyclopentene rings present in the side chains of NMMA are less strained than the norbornene rings present in the side chains of NMDA. In addition, NMCA

with nearly two norbornene rings exhibited lowest cure heat, probably due to incomplete polymerization of the NMCA monomers within the DSC scan time. More specifically, NMCA monomers having a much higher viscosity were constrained by strong hydrogen bonding between monomers, which significantly restricts the mobility of the monomer.

The gelation time for the four monomers was determined rheologically using a reported procedure.[25] Generally, the viscosity of the system increases dramatically when gelation occurs. A parallel plate oscillatory rheometer was used to measure the time dependence of the storage shear modulus, G', and the loss shear modulus, G'', for the monomer/catalyst mixture. As shown in Figure 5, both G' and G'' increase gradually with time, the build-up rate of G' was much higher than that of G'' due to the formation of elastic polymers from chemical crosslinking. The differential in rates leads to a crossover of G' and G'', which is defined as the gel time, indicating the transition of the system from liquid phase dominated to a solid phase dominated viscoelastic behavior, also suggesting three-dimensional (3-D) network formation.[26] Table 1 summarizes the gelation time of the monomer/catalyst mixtures at 65 ^{o}C. As seen from the table, the monomer gelation times follow the order: NMDA < NMMA < NMCA $\approx$ NMSA, indicating that the gelation time is not only determined by the monomer structure, but also the viscosities of the monomers. Thus, the low viscosity NMDA with a more reactive norbornene ring present in the side chain exhibits the shortest gelation time, while the highly viscous NMCA with an extra norbornenyl ring present in the side chain shows a much longer gelation time than the other three monomers.

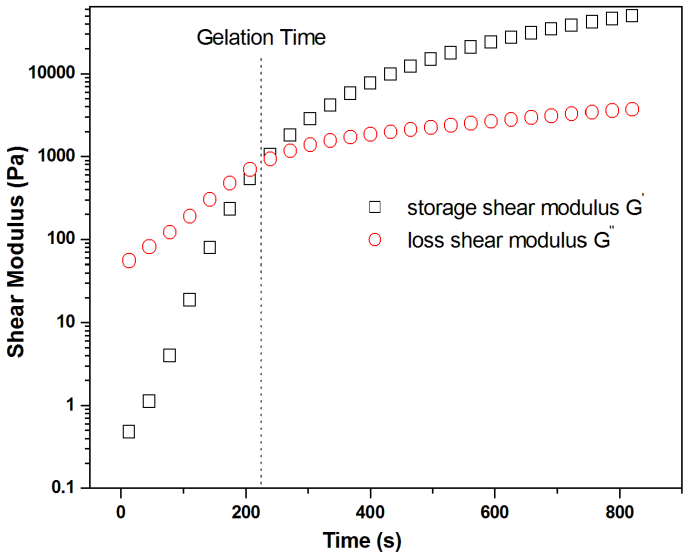

Figure 5. Evolution of shear moduli during the reaction of the monomer/catalyst blend. Shown here is the NMDA/catalyst mixture curing at 65 ^{o}C.

As shown in Figure 6, all polymer samples are fairly transparent and exhibit essentially the same color as the original oils. Both polyNMDA and polyNMMA exhibit smooth surfaces due to the fact that the extra reactive rings present in the side chain of the oil and the appropriate viscosities of the monomers afford the best incorporation of the polymer chains. However, polyNMSA and polyNMCA exhibit coarse surfaces and lower transparencies, which is probably due to their relatively low crosslink densities and incomplete polymerization of the monomers as discussed later.

Figure 6. Sample pictures for the polymers (from left to right: polyNMSA, polyNMDA, polyNMMA, and polyNMCA).

Table 1. Gel time, extraction data and DMA data for the polymers.

Polymer	Gel Time/s[a]	Soluble (wt %)	E' at 25 °C (Pa)	T_g (°C)[b]	υ_e (mol/m^3)[c]
polyNMSA	1495	13	1.6×10^8	50.0	159
polyNMDA	220	5	5.9×10^8	66.5	307
polyNMMA	889	5	5.5×10^8	70.3	267
polyNMCA	1456	18	7.3×10^8	68.2	331

[a] Gel time was determined at 65 °C. [b] Glass transition temperatures represent the maxima of the tan δ curves obtained by DMA analysis. [c] Crosslink densities have been calculated at temperatures 50 °C above the T_g.

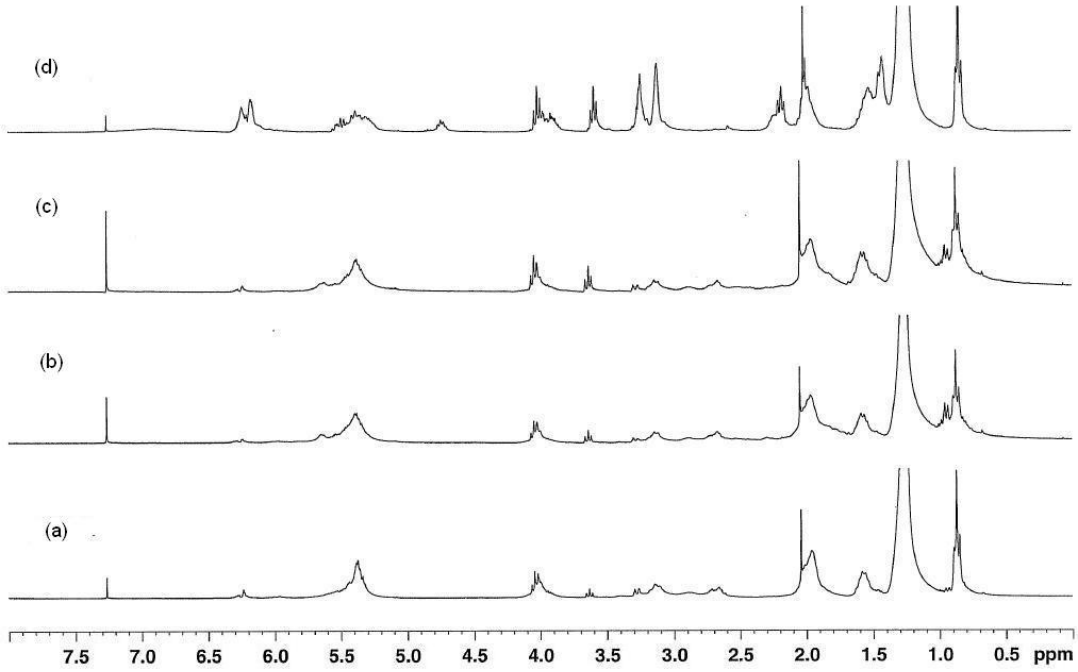

Figure 7. ^{1}H NMR spectra for the extracted materials from (a) polyNMSA, (b) polyNMDA, (c) polyNMMA, and (d) polyNMCA.

To investigate how the polymer structure is affected by the chemical structure of the monomer, all polymer samples have been subjected to Soxhlet extraction to extract the soluble materials present in the final polymers. As shown in Table 1, about 13 wt % of polyNMSA was soluble; while both polyNMDA and polyNMMA afforded only 5 wt % of soluble materials, indicating that the extra norbornene or cyclopentene rings play an

important role in increasing the crosslink densities of the resulting thermosets. However, about 18 wt % of polyNMCA was extracted, presumably due to incomplete polymerization of the NMCA. Figure 7 illustrates the ^{1}H NMR spectra of the soluble materials extracted from the four polymers. Compared to Figure 2, the peaks between 0.5 and 2 ppm indicated that the soluble fractions mainly consist of the oil fractions. The intensity of the characteristic peaks assigned to the norbornene ring is dramatically decreased in the soluble fractions obtained from polyNMSA, polyNMDA and polyNMMA indicating that almost all of the norbornene rings were ring-opened. However, a significant portion of the norbornene rings remain unreactive in the resulting polyNMCA soluble fraction apparently because the propagation process is hindered by the high viscosity of the monomers.

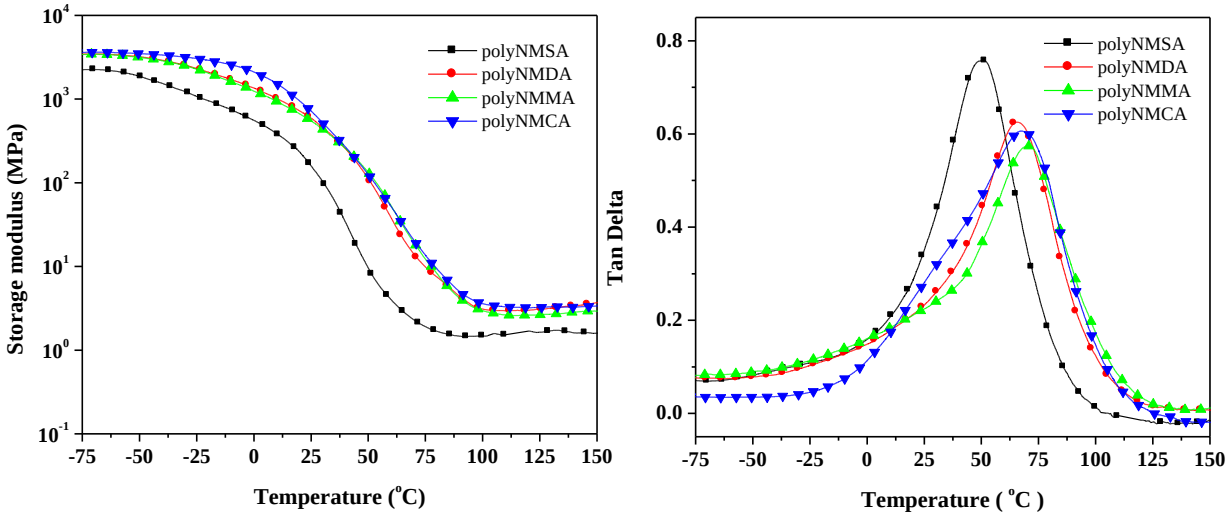

Figure 8. Tan δ and storage modulus curves for all polymers.

Thermal and Mechanical Properties. Figure 8 shows the storage modulus (*E′*) and loss factor (tan δ) curves as a function of temperature for the four polymers. All polymers exist in the glassy state at a very low temperature, and the modulus deceases slightly with increasing

temperature. Then, a sharp decrease in the E' value is observed in the temperature range from 0 to 100 ^{o}C. This corresponds to the primary relaxation process (α) of the resulting thermosets, where a maximum is observed in the loss factor curve, which is taken as the T_g. The polymer polyNMSA shows a relatively low storage modulus, and its loss factor shows a very sharp relaxation process centered at about 50 ℃. When compared with polyNMSA, the E' values of polyNMDA, polyNMMA and polyNMCA were significantly increased over the entire temperature range, due to incorporation of the extra reactive rings present in the side chains. For instance, the E' values for polyNMDA, polyNMMA and polyNMCA at room temperature (Table 1) are approximately 3.7, 3.4 and 4.6 times higher, respectively, than that of polyNMSA. The rubbery plateau modulus can be explained by qualitative consideration of the crosslinking density (ν_e) of the thermosets, according to rubber elasticity theory, using the following equation:[27, 28]

$$E' = 3\nu_e RT$$

where E' is the storage modulus at T_g + 50 ^{o}C in the rubbery plateau, R is the gas constant, and T is the absolute temperature. As seen in Table 1, the thermosets from the monomers with reactive rings in the side chains exhibit much higher crosslink densities then polyNMSA and are typically in the range of 2.6 $\times 10^2$ – 3.3 $\times 10^2$ mol/m^3. This indicates that the extra reactive rings in the side chains of the monomers are effectively incorporated into the polymer networks, resulting in higher crosslinked vegetable oil-based thermosets with a resulting enhancement in the rubbery modulus. As molecular motions became more restricted due to the crosslinking, the amount of energy that can be dissipated throughout the polymer specimen decreases dramatically. Therefore, a shift of the loss factor peak to higher

temperature is observed for polyNMDA, polyNMMA and polyNMCA as shown in the tan δ - *T* curves when compared with polyNMSA. The tan δ intensities also diminish. Meanwhile, a significant broadening of the α-relaxation is observed. For the sample polyNMCA, a shoulder peak around 30 ^{o}C is observed in the α-relaxation process, which might be attributed to the relaxation of NMCA oligomer-rich phases, because of incomplete polymerization of the viscous NMCA monomers.

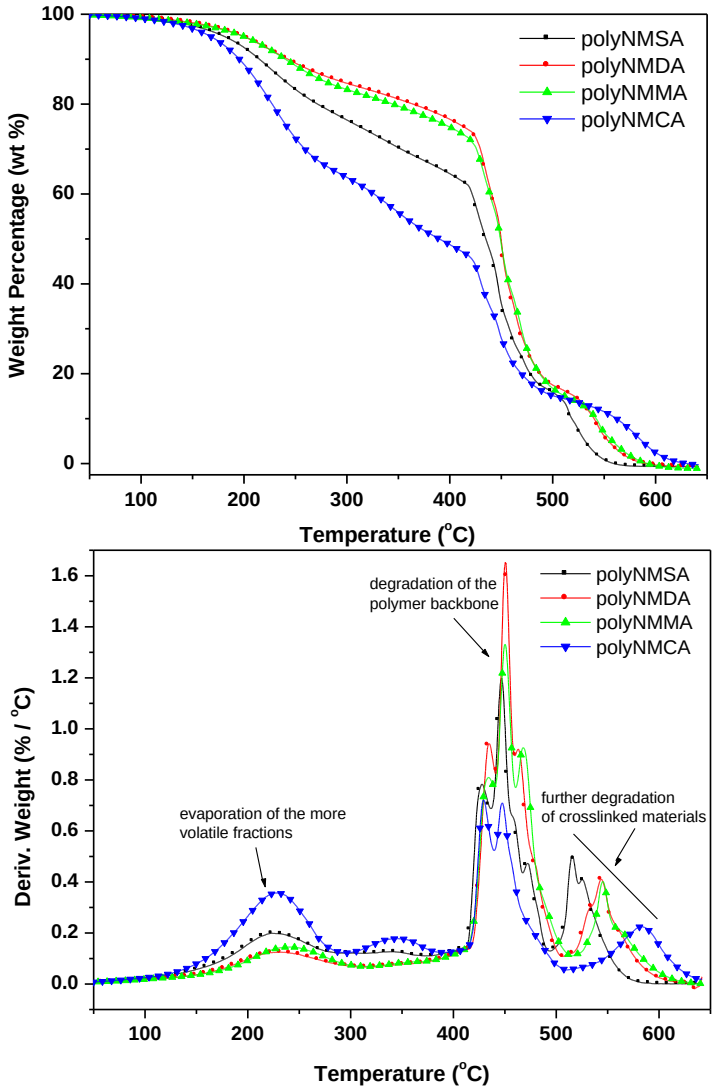

Figure 9. TGA curves and their derivative curves for all polymers.

Table 2. TGA data and mechanical properties for the polymers.

Polymer	TGA data (°C)			Mechanical Properties[d]			
	T_{10}[a]	T_{50}[b]	T_{max}[c]	E (MPa)	σ_b (MPa)	ε_b (%)	Toughness (MPa)
polyNMSA	215	435	447	-	-	-	-
polyNMDA	243	450	451	311.4 ±16.7	15.4 ±0.5	34.5 ±4.7	4.1 ±0.6
polyNMMA	240	449	450	154.8 ±1.1	9.9 ±0.3	41.0 ±4.2	2.9 ±0.3
polyNMCA	196	390	429	-	-	-	-

[a] 10% Weight loss temperature. [b] 50% Weight loss temperature. [c] Temperature of maximum thermal degradation.
[d] E = Young's modulus, σ_b = tensile strength, and ε_b = elongation at break.

Figure 9 shows the TGA analysis of the resulting thermosets and the corresponding data are summarized in Table 2. As seen in Figure 9, the polymers are stable up to 150 °C in air and undergo three major thermal degradation processes. The weight loss of the first degradation process from 180 °C to 250 °C approximately equals the soluble fraction as shown in Table 1 and can be attributed to evaporation of any unreacted monomers and oil fragments. In this stage, more than 20 % of the overall weight was lost for polyNMCA, because of incomplete polymerization of the NMCA monomers. Less than 10 % of the overall weight was lost for polyNMDA and polyNMMA, apparently due to higher crosslinking by the extra olefinic rings present in the side chains. The second loss at around 400-500 ℃ is believed to be caused by decomposition of the polymer backbone. The final loss at around 500-600 ℃ is indicative of further decomposition of the crosslinked fragments and oxidation of the carbon residue. Table 2 summarizes the interesting parameters from the TGA curves for these thermosets taken from the onset of degradation, which is usually taken as the temperature at which 10% degradation occurs (T_{10}), the midpoint temperature of the degradation (T_{50}), and the maximum degradation temperature (T_{max}). As expected, the samples polyNMDA and polyNMMA exhibit the best thermal stability with similar values of

T_{10}, T_{50} and $T_{max.}$ However, lower T_{10}, T_{50} and T_{max} values are observed for polyNMCA due to the incomplete polymerization of the NMCA monomer, because of its high viscosity.

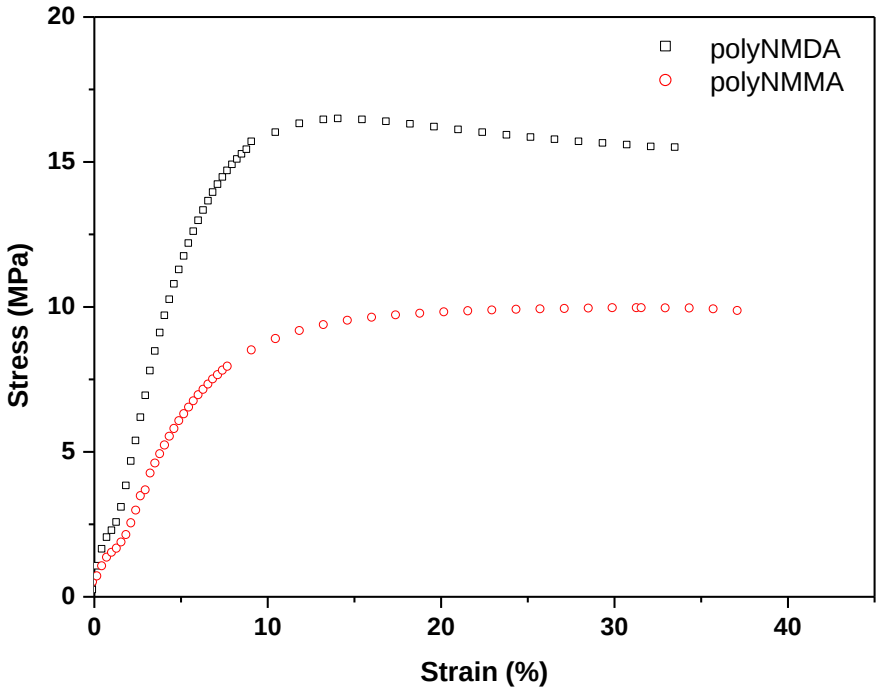

Figure 10. Stress-strain curves for polyNMDA and polyNMMA.

Table 2 also summarizes the mechanical properties for the two most promising thermosets, polyNMDA and polyNMMA. These two samples exhibit Young's moduli ranging from 155 to 310 MPa, tensile strengths ranging from 10-15 MPa, elongation at break values in the range of 35 to 41% and toughness values ranging from 2.9 to 4.1 MPa. It is worth noting that the Young's moduli and tensile strengths of polyNMDA and polyNMMA are comparable to petroleum-based commercial plastics, such as high density polyethylene (HDPE) and poly(norbornene).[29] The stress-strain curves of the polyNMDA and polyNMMA are shown in Figure 10. Both polyNMDA and polyNMMA exhibit behaviors typical of

ductile plastics. Differing from polyNMMA, polyNMDA shows yielding behavior, followed by strain softening. No strain hardening behavior is observed before the specimen breaks. PolyNMDA exhibits higher values of Young's modulus, tensile strength and toughness than polyNMMA. This is expected, since the extra rigid cyclopentane rings obtained after ring-opening of the norbornene ring present in the NMDA side chains should increase the rigidity and toughness of polyNMDA, whereas the linear polymer chains obtained after the ring-opening of the cyclopentene rings in NMMA would not be expected to increase the modulus and toughness all that much.

Conclusions

Four different vegetable oil-based monomers, NMSA, NMDA, NMMA and NMCA, have been synthesized from soybean oil, Dilulin, ML189 and castor oil, respectively, followed by esterification with a bicyclic anhydride, and then homopolymerized using the Grubbs 2nd generation ruthenium catalyst to obtain biorenewable thermosets. The differences in the structures of the side chains and the viscosities of the monomers result in different properties in the final thermosets. Compared with polyNMSA, the polyNMDA and polyNMMA thermosets exhibit lower soluble fractions, and higher thermal stabilities and mechanical properties, because of the successful incorporation of the side chain into the polymer matrix to form effective crosslinking. However, polyNMCA affords a higher soluble fraction, and lower thermal stability, resulting from incomplete polymerization of the highly viscous NMCA monomer. Note that polyNMDA and polyNMMA exhibit tensile stress-strain behaviors of ductile plastics with Young's moduli ranging from 155 to 310 MPa, ultimate tensile strengths ranging from 10 to 15 MPa, and percent elongation at break values ranging from 35 to 41%, affording materials comparable to petroleum-based plastics, like HDPE and

poly(norbornene). This work provides a new way of utilizing renewable resources to prepare environmentally-friendly bioplastics with high performance.

Acknowledgments

We are grateful for financial support from the Center for Crops Utilization Research (CCUR) at Iowa State University and thankful to Professor Michael Kessler from the Department of Materials Science and Engineering at Iowa State University for the use of his thermal analysis equipments. In addition, we thank Dr. Xia Sheng from the Department of Materials Science and Engineering at Iowa State University for his help with the rheometer tests.

References

1) Bozell, J. J. *Clean-Soil Air Water* **2008**, *36*, 641-647.
2) Lu, Y. S.; Larock, R. C. *ChemSusChem* **2009**, *2*, 136-147.
3) Lu, J.; Khot, S.; Wool, R. P. *Polymer* **2005**, *46*, 71-80.
4) Deng, R.; Chen, Y.; Chen, P.; Zhang, L. N.; Liao, B. Polymer Degradation and Stability 2006, 91, 2189-2197.
5) Liu, W. J.; Misra, M.; Askeland, P.; Drzal, L. T.; Mohanty, A. K. Polymer 2005, 46, 2710-2721.
6) Lu, Y. S.; Larock, R. C. *Biomacromolecules* **2007**, *8*, 3108-3114.
7) Lu, Y. S.; Larock, R. C. *Biomacromolecules* **2008**, *9*, 3332-3340.
8) Li, F.; Hanson, M. V.; Larock, R. C. *Polymer* **2001**, *42*, 1567-1579.
9) Kundu, P. P.; Larock, R. C. *Biomacromolecules* **2005**, *6*, 797-806.
10) Li, F. K.; Larock, R. C. *Biomacromolecules* **2003**, *4*, 1018-1025.
11) Li, F. K.; Hasjim, J.; Larock, R. C. *J. Appl. Polym. Sci.* **2003**, *90*, 1830-1838.
12) Li, F.; Marks, D. W.; Larock, R. C.; Otaigbe, J. U. *Polymer* **2000**, *41*, 7925-7939.
13) Rybak, A.; Meier, M. A. R. *ChemSusChem* **2008**, *1*, 542-547.
14) Fokou, P. A.; Meier, M. A. R. *Macromol. Rapid Commun.* **2008**, *29*, 1620-1625.
15) Henna, P. H.; Larock, R. C. *J. Appl. Polym. Sci.* **2009**, *112*, 1788-1797.
16) Henna, P. H.; Larock, R. C. *Macromol. Mat. Eng.* **2007**, *292*, 1201-1209.
17) Bielawski, C. W.; Grubbs, R. H. *Prog. Polym. Sci.* **2007**, *32*, 1-29.
18) Kodali, D. R. U.S. Pat. 6,420,322 (2002).
19) Mauldin, T. C.; Haman, K.; Sheng, X.; Henna, P.; Larock, R. C.; Kessler, M. R. *J. Polym. Sci., Part A: Polym. Chem.* **2008**, *46*, 6851-6860.
20) Jones, A. S.; Rule, J. D.; Moore, J. S.; White, S. R.; Sottos, N. R. *Chem. Mater.* **2006**, *18*, 1312-1317.

21) Andjelkovic, D. D.; Valverde, M.; Henna, P.; Li, F. K.; Larock, R. C. *Polymer* **2005**, *46*, 9674-9685.
22) Xia, Y.; Henna, P. H.; Larock, R. C. *Macromol. Mat. Eng.* **2009**, *294*, 590-598.
23) Kodali, D. R. U.S. Pat. 5,288,805 (1994).
24) Wilson, G. O.; Caruso, M. M.; Reimer, N. T.; White, S. R.; Sottos, N. R.; Moore, J. S. *Chem. Mater.* **2008**, *20*, 3288-3297.
25) Sheng, X.; Lee, J. K.; Kessler, M. R. *Polymer* **2009**, *50*, 1264-1269.
26) Weng, L. H.; Chen, X. M.; Chen, W. L. *Biomacromolecules* **2007**, *8*, 1109-1115.
27) Flory, P. J. *Principles of Polymer Chemistry*; Cornell University Press, Ithaca, 1953.
28) Ward, I. M. *Mechanical Properties of Solid Polymers*; Wiley Interscience, New York, 1971.
29) Mark, J. E. *Polymer Data Handbook*; Oxford University Press, New York, 1999.

CHAPTER 4. CASTOR OIL-BASED THERMOSETS WITH VARIED CROSSLINK DENSITIES PREPARED BY RING-OPENING METATHESIS POLYMERIZATION (ROMP)

A Paper published in Polymer, 51, 2508-2514.

Ying Xia and Richard C. Larock*

Department of Chemistry, Iowa State University, Ames, Iowa 50011

Abstract

Two castor oil-based monomers, (1) norbornenyl-functionalized castor oil (NCO), which has ~0.8 norbornene rings per fatty acid chain and (2) norbornenyl-functionalized castor oil alcohol (NCA), which has ~1.8 norbornene rings per fatty acid chain, have been prepared. Ring-opening metathesis polymerization (ROMP) of different ratios of NCO/NCA using the 2nd generation Grubbs catalyst results in rubbery to rigid biorenewable-based plastics with crosslink densities ranging from 318 to 6028 mol/m^3. Increased crosslink densities result in shorter gelation times, better incorporation of the monomers into the polymer network, and much less soluble materials in the bulk materials. The increased crosslink densities obtained by adding NCA enhance the thermal properties, including the glass transition temperature (T_g) and room temperature storage modulus, which increase from -17.1 ^{o}C to 65.4 ^{o}C and from 2.4 MPa to 831.9 MPa, respectively. The TGA results, where T_{10} increased from 285 ^{o}C to 385 ^{o}C, illustrate that improved thermal stabilities can be obtained for thermosets with higher crosslink densities. The Young's modulus (11-407 MPa), tensile strength (1.6-18 MPa) and toughness (0.14-1.6 MPa) are also improved dramatically

with higher crosslink densities.

Introduction

Bioplastics derived from vegetable oils represent a promising route to green materials, because of the ready availability of the oils and the inherent biodegradability of the products.[1] A variety of biorenewable materials, including thermosetting resins,[2-4] thermoplastics[5] and biocomposites,[6-8] suitable for the replacement of petroleum-based materials have been prepared from vegetable oils and their derivatives. Castor oil's unique structure, where ~90 % of the fatty acid chains bear an hydroxyl group, makes it a very useful vegetable oil in industry.[9] A wide variety of polymers, especially polyurethanes,[10] have been prepared by taking advantage of the hydroxyl groups.

Olefin metathesis, which is a relatively new polymerization method,[11] has been employed to prepare vegetable oil-based polymers. For example, recently, acyclic diene (triene) metathesis polymerization (ADMET/ATMET) has been used to prepare plant oil-based polymers.[12] Novel biorenewable materials have been prepared by ring-opening metathesis polymerization (ROMP) as well. For example, two kinds of ROMP-based systems, norbornenyl anhydride-functionalized castor oil (BCO)/cyclooctene (CO)[13] and Dilulin (a norbornenyl-functionalized linseed oil[14])/dicyclopentadiene (DCPD)[15], have been developed in our group previously. Both systems afford green thermosets and provide a promising new route to bioplastics from biorenewable resources.

However, some improvements need to be made to obtain better ROMP bioplastics. In the BCO/CO system, pure BCO does not undergo facile ROMP because the free carboxylic groups result in strong hydrogen bonding, which hinders coordination between the olefin and the catalyst.[13] In addition, a relatively high loading of the Grubbs catalyst (0.5 wt %) was

required to afford good polymers. For the Dilulin/DCPD system, phase separations were clearly observed due to the difference in ROMP reactivity between DCPD and Dilulin, where approximately two thirds of the fatty acid side chains are not appended with norbornene rings.

To address previously mentioned problems and prepare better ROMP systems, two castor oil-based monomers, (1) norbornenyl-functionalized castor oil (NCO), which has ~0.8 norbornene rings per fatty acid chain and (2) norbornenyl-functionalized castor oil alcohol (NCA), which has ~1.8 norbornene rings per fatty acid chain, have been prepared for ROMP. Mixtures of NCO and NCA in different ratios have been polymerized using only 0.125 wt % of the 2nd generation Grubbs catalyst, resulting in novel castor oil-based rubbery to rigid biorenewable plastics with crosslink densities ranging from 318 to 6028 mol/m^3. The thermal and mechanical analysis results indicate that higher T_gs, higher storage moduli, better thermal stabilities and improved mechanical properties are obtained for the thermosets with higher crosslink densities.

Experimental

Materials. Castor oil, acryloyl chloride, triethylamine and the 2nd generation Grubbs catalyst were purchased from Sigma-Aldrich (Milwaukee, WI). Dicyclopentadiene (DCPD) (>95% pure) was purchased from Alfa Aesar (Ward Hill, MA). Lithium aluminum hydride (LAH) was purchased from Acros (Geel, Belgium). Benzene, ethyl acetate, methylene chloride, $NaHCO_3$ and HCl were obtained from Fisher (Fair Lawn, NJ). Tetrahydrofuran (THF) was distilled over sodium/benzophenone under N_2. Unless otherwise stated, all reagents were used as received without further purification.

Synthesis of Bicyclo[2.2.1]hept-2-ene-5-carbonyl Chloride.[16] Freshly cracked cyclopentadiene (56 g, 0.85 mol) was added dropwise to a solution of acryloyl chloride (70 g,

0.77 mol) in toluene (275 mL) at 0 ^{o}C. The reaction was run at 0 ^{o}C for 3 h and then heated to 100 ^{o}C and held at that temperature for 0.5 h. The toluene was distilled off and the residual liquid was distilled under reduced pressure to yield 95 g (79%) of the product as a clear and colorless oil (83:17 *endo*:*exo*). ^{1}H NMR ($CDCl_3$, δ ppm) at 1.31-1.34 (d), 1.47-1.52 (m), 1.90-1.94 (m), 2.70-2.73 (m), 2.97 (s), 3.27 (s), and 3.43-3.47 (m) are assigned to the non-olefinic protons of both the *endo* and *exo* isomers; 6.02 (m, =CH, *endo*), 6.12 (m, =CH, *exo*), 6.20 (m, =CH, *exo*), 6.25 (m, =CH, *endo*).

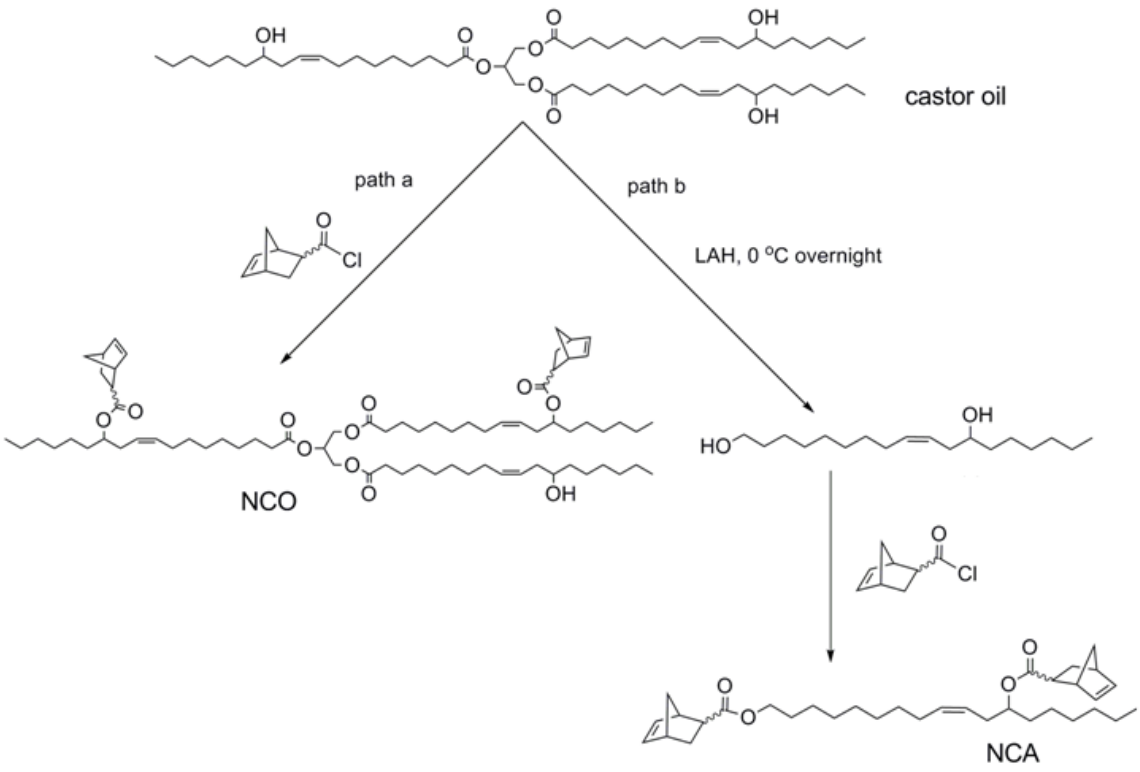

Scheme 1. Preparation of NCO (path a) and NCA (path b) from castor oil.

Synthesis of Norbornenyl-functionalized Castor Oil (NCO). Scheme 1 (path a) illustrates the preparation of NCO. Castor oil (20 g, 0.021 mol) was dissolved in 100 mL of anhydrous

CH_2Cl_2 and cooled to 0 ^oC. A solution of bicyclo[2.2.1]hept-2-ene-5-carbonyl chloride (10.6 g, 0.068 mol) in 100 mL of anhydrous CH_2Cl_2 was added dropwise and then triethylamine (11.4 g, 0.11 mol) was added. The solution was stirred, while allowing it to warm from 0 ^oC to room temperature, and was maintained at that temperature for 48 h. Then the reaction mixture was stirred with 500 mL of aqueous 5 wt % Na_2CO_3 solution overnight to convert the excess bicyclo[2.2.1]hept-2-ene-5-carbonyl chloride to the corresponding water soluble carboxylate salt. After extraction with CH_2Cl_2 and removal of the solvent, a quantitative yield of NCO was obtained as a brown liquid. Figure 1(b) shows the ^1H NMR peak assignments for NCO, which contains ~0.8 norbornene rings per fatty acid chain as determined by ^1H NMR spectral analysis.

Synthesis of Norbornenyl-functionalized Castor Oil Alcohol (NCA). The preparation of NCA is illustrated in Scheme 1 (path b). LAH (12.27 g, 0.32 mol) was added to 100 mL of THF and stirred in a 1000 mL two-neck round bottom flask at 0 ^oC. Castor oil (100 g, 0.11 mol) was dissolved in 600 mL of THF and then added dropwise to the LAH suspension. The reaction was maintained at 0 ^oC overnight. The reaction mixture was poured into ice water, followed by the addition of 1 M HCl, until the solution was clear. Then 300 mL of ethyl acetate was added to carry out the extraction. The organic layer was washed with water to remove glycerol, dried over $MgSO_4$ and filtered. Finally, the clear castor oil alcohol was obtained after removal of the organic solvent under vacuum.

Castor oil alcohol (20 g, 0.071 mol) was dissolved in 100 mL of anhydrous CH_2Cl_2 and cooled to 0 ^oC. A solution of bicyclo[2.2.1]hept-2-ene-5-carbonyl chloride (22.73 g, 0.15 mol) in 100 mL of anhydrous CH_2Cl_2 was added dropwise and then triethylamine (14.68 g, 0.15 mol) was added. The solution was stirred, while allowing it to warm from 0 ^oC to room

temperature, and was maintained for 24 h at that temperature. Then the reaction mixture was stirred with 500 mL of aqueous 5 wt % Na_2CO_3 solution overnight to convert the excess bicyclo[2.2.1]hept-2-ene-5-carbonyl chloride to a water soluble carboxylate salt. After extraction with CH_2Cl_2 and removal of the solvent, a quantitative yield of NCA with a light brown color was obtained. Figure 1(c) shows the ^1H NMR peak assignments for NCO, which contains ~1.8 norbornene rings per fatty acid chain as determined by ^1H NMR spectral analysis.

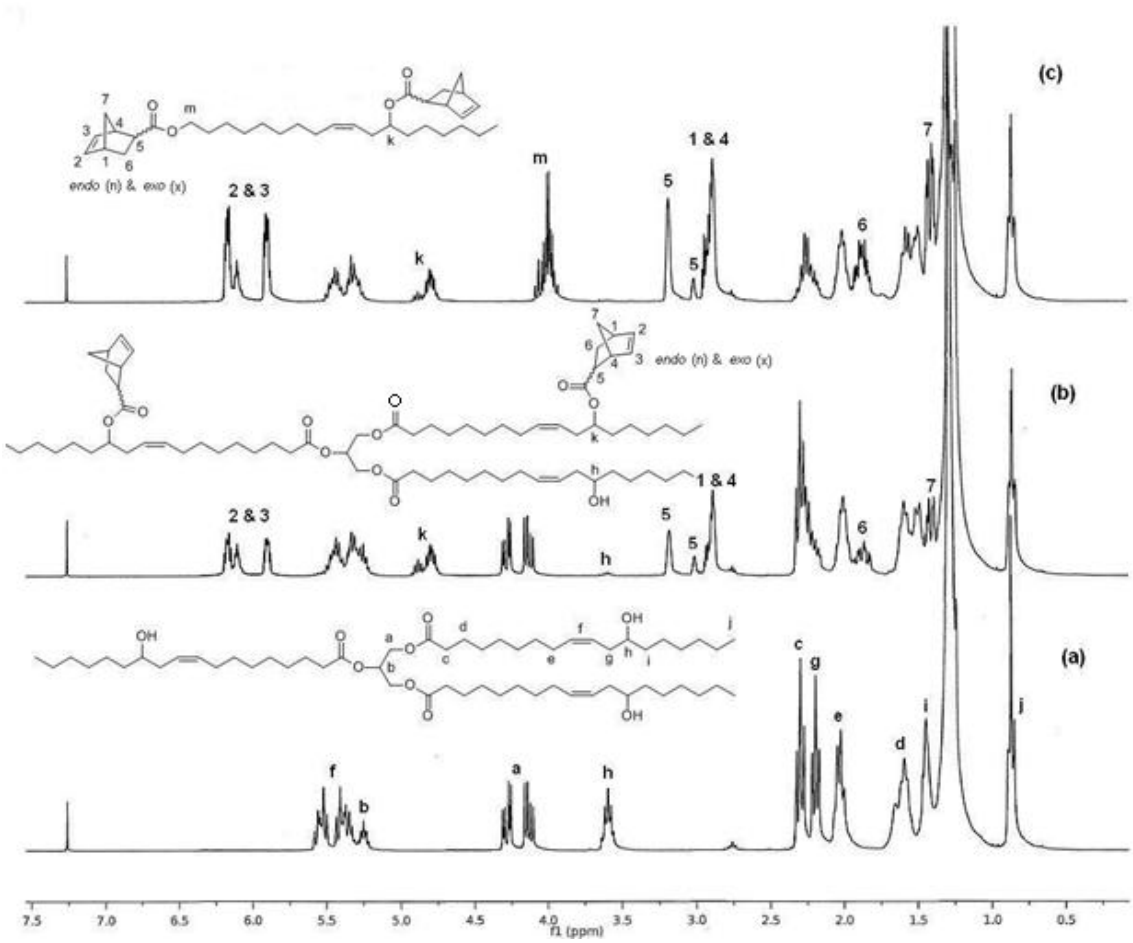

Figure 1. Structures and ^1H NMR spectra of (a) castor oil, (b) norbornenyl-functionalized castor oil (NCO) and (c) norbornenyl-functionalized castor oil alcohol (NCA).

Freeze-drying of the Grubbs Catalyst. To improve the solubility of the Grubbs catalyst in the monomers, freeze-drying of the catalyst was carried out according to a literature procedure.[17] The 2nd generation Grubbs catalyst (250 mg) was dissolved in 5 mL of benzene and the solution was frozen in a liquid nitrogen bath. The frozen sample was then placed in a vacuum oven at room temperature for 5 h to sublime the benzene. This process provided catalyst with a larger surface area.

Polymerization. Freeze-dried Grubbs 2nd generation catalyst (5 mg, 0.125 wt %) was dissolved in the mixture of NCO and NCA (4 g) and stirred with a spatula until all of the catalyst was dissolved and a homogeneous solution was obtained. The solution was poured into a glass mold and cured at 65 ^{o}C for 1 h and 150 ^{o}C for 3 h. The resulting thermosets were transparent, but retain the monomers' original color.

Soxhlet Extractions. A 1.5 g sample of the bulk polymer was extracted with 100 mL of refluxing methylene chloride for 24 h using a Soxhlet extractor. Following extraction, the resulting solution was concentrated under reduced pressure and dried in a vacuum oven at 60 ℃ overnight.

Characterization. ^{1}H NMR spectroscopic analysis of the monomers and the soluble substances extracted from the thermosets by methylene chloride were recorded in $CDCl_3$ using a Varian spectrometer (Palo Alto, CA) at 300 MHz.

The gelation time was determined on an AR2000ex by applying an oscillating strain to the sample and measuring the response stress. All experiments were performed at 50 ^{o}C with the stress control mode at 1 Hz using 25-mm diameter disposable parallel plates and a 0.5 mm gap.

The dynamic mechanical analyses (DMA) was recorded on a TA Instruments Q800

dynamic mechanical analyzer using a film tension mode of 1 Hz. Rectangular samples 0.77 mm thick and 8 mm wide were used for the analysis. The samples were cooled and held isothermally for 3 min at -80 ℃ before the temperature was increased at 3 ℃/min to 200 ℃.

Thermogravimetric analysis (TGA) of the specimens was carried out on a TA Instruments (New Castle, DE) Q50. The samples were scanned from 50 ℃ to 650 ℃ in air at a heating rate of 20 ^{o}C/min.

The mechanical properties of the thermosets were determined using an Instron universal testing machine (model 4502) with a crosshead speed of 50 mm/min. Rectangular specimens of 70 × 8 × 0.8 mm^3 (length × width × thickness) were used. An average value of four replicates of each sample was taken. The toughness of the polymer, which is the fracture energy per unit volume of the sample, was obtained from the area under the corresponding tensile stress-strain curves.

Results and Discussion

Synthesis of the monomers. Castor oil is a vital industrial oil with a typical triglyceride structure containing ~90 % ricinoleic acid chains.[9] A representative structure and ^{1}H NMR spectrum of castor oil is shown in Figure 1(a). The signals at 4.1-4.4 ppm (a) correspond to the methylene protons in the glyceride unit. The vinyl protons (f) in the fatty acid chains are observed at 5.3-5.6 ppm. The tertiary hydrogens adjacent to the hydroxyl group in the fatty acid chain (h) are detected at 3.6 ppm. The detailed peak assignments are listed in Figure 1(a).

The hydroxyl groups of the fatty acid chains make modification of the castor oil quite easy. Esterification of the castor oil by bicyclo[2.2.1]hept-2-ene-5-carbonyl chloride proceeds easily and the norbornenyl-functionalized monomer NCO can be obtained in an excellent yield. Figure 1(b) shows the structure of NCO and the ^{1}H NMR spectral peak assignments.

Compared to castor oil, peak h is substantially reduced in NCO, which means that most of the hydroxyl groups have reacted and a new peak representing the tertiary hydrogen adjacent to the norbornenyl ester is observed at 4.8 ppm. By integrating the peaks k and h, it was found that ~95 % of the hydroxyl groups reacted with bicyclo[2.2.1]hept-2-ene-5-carbonyl chloride and approximately 2.4 norbornene rings were incorporated into the triglyceride (0.8 norbornene rings per fatty acid chain). Besides the peaks corresponding to the castor oil, norbornene hydrogens are found at 5.9-6.2 ppm. The other non-olefinic norbornenyl hydrogens are assigned as well.

To prepare a monomer with more norbornene rings per fatty acid chain, castor oil has been reduced to castor oil alcohol (mainly ricinoleic alcohol), which was then reacted with bicyclo[2.2.1]hept-2-ene-5-carbonyl chloride to prepare NCA (Scheme 1 - path b). Figure 1(c) illustrates the structure and ^{1}H NMR spectra of NCA. Compared to castor oil in Figure 1(a), the peaks a and h disappear, which indicates that castor oil's triglyceride structure was reduced completely and all of the hydroxyl groups were reacted with bicyclo[2.2.1]hept-2-ene-5-carbonyl chloride. A new peak m represents the methylene protons adjacent to the norbornenyl ester. Based on the integration of peaks k and m, it was found that NCA contains approximately 1.8 norbornene rings per fatty acid chain, which is about 2.3 times the number of norbornene rings present in NCO.

ROMP of NCO and NCA. Taking advantage of the high reactivities of the strained norbornene rings appended to NCO and NCA, ROMP readily copolymerizes these two castor oil-based monomers. Scheme 2 illustrates the copolymerization of NCO and NCA. The amount of catalyst used and the cure sequence employed are based on previous research in our group.[15] Thermosets containing 0 to 100 wt % of NCO at 20 wt % intervals were

prepared. Because NCA (~1.8 norbornene rings per fatty acid chain) was copolymerized with NCO (~0.8 norbornene rings per fatty acid chain) in various ratios, thermosets with different crosslink densities can be obtained. Table 1 summarizes the amount of soluble materials obtained from methylene chloride Soxhlet extraction of these thermosets. As one can see from the table, the soluble fraction decreases from 27.7 wt % to 0.8 wt % as the NCA amount increases from 0 to 100 %. This can be explained by the fact that more crosslinked insoluble polymer network is formed with more NCA, which has a larger norbornene ring density.

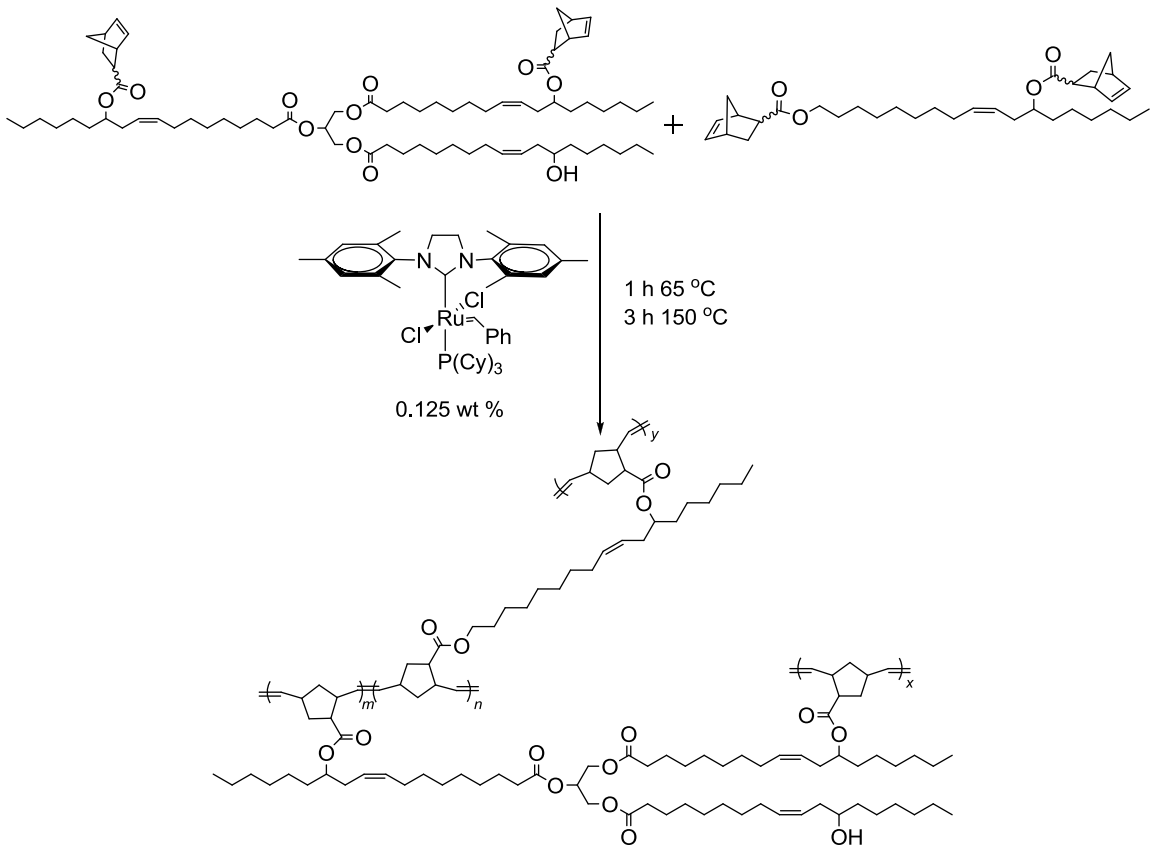

Scheme 2. ROMP of NCO and NCA.

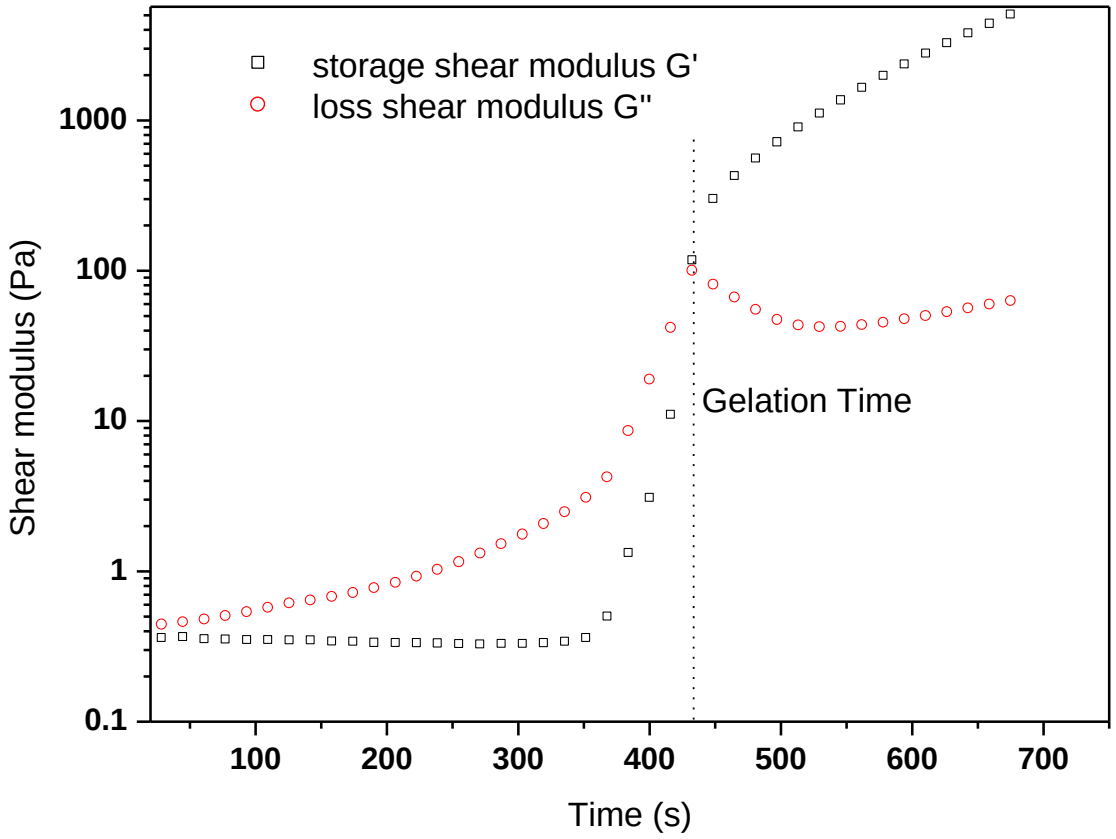

Figure 2. Evolution of the shear moduli during the cure process. Shown here is the NCO20NCA80/catalyst mixture curing at 50 ^{o}C.

The gelation time was determined for all NCO/NCA copolymers using a reported rheology procedure.[18] In general, the viscosity of the monomer/catalyst dramatically increases when gelation occurs. A parallel plate oscillatory rheometer was used to determine the time dependence of the storage shear modulus, *G'*, and the loss shear modulus, *G"*, for the various monomer/catalyst mixtures. All gelation experiments were performed at 50 ^{o}C to make sure appropriate gelation times were obtained for all samples. Figure 2 illustrates the increase in both *G'* and *G"*. The gelation time was obtained when *G'* crosses over *G"*, which indicates the transition of the system from liquid phase dominated to a solid phase dominated

viscoelastic behavior with a three-dimensional (3-D) network formation.[19] Table 1 summarizes the gelation times for all of the samples. As seen from the table, the addition of NCA decreases the gelation time for the NCO/NCA system. NCA is so effective that the gelation time was decreased from 3704 s to 34 s, when the NCA amount increases from 0 to 100 %. As mentioned above, the gelation time represents the moment when a crosslinked 3-D network is formed. The amount of NCA present, which has more crosslink sites per fatty acid chain, accelerates formation of the crosslinked network and decreases the gelation time.

Table 1. Extraction data, gelation times and DMA data for the polymers.

Polymer	Soluble Fraction (%)	Gel Time/s[a]	T_g (°C)[b]	υ_e (mol/m^3)[c]	(Tan δ)$_{max}$	E' at 25 °C (MPa)
NCO100	27.7	3704	-17.1	318	1.21	2.4
NCO80NCA20	14.7	2611	-6.2	740	0.81	5.7
NCO60NCA40	6.7	1617	14.6	1664	0.46	27.8
NCO40NCA60	2.5	1525	27.5	2790	0.42	130.0
NCO20NCA80	1.0	431	49.1	4418	0.32	583.4
NCA100	0.8	34	65.4	6028	0.27	831.9

a) The gelation time was determined at 50 °C. b) Glass transition temperatures represent the maxima of the tan δ curves obtained by DMA analysis. c) Crosslink densities have been calculated at temperatures 50 °C above the T_g.

Thermal Properties. Figure 3 shows the storage modulus (*E'*) and tan δ curves as a function of temperature for different NCO/NCA ratios. Only one peak was observed in the tan δ versus *T* curves for all of the copolymers, which indicates that they are homogeneous copolymers. All thermosets are in the glassy state at low temperatures and *E'* decreases slightly when the temperature increases. Then a rapid decrease in the *E'* value is observed for all of the thermosets in the temperature range of -25 to 100 °C, which is due to the primary relaxation process (α) of the NCO/NCA copolymers obtained, where a maximum is observed

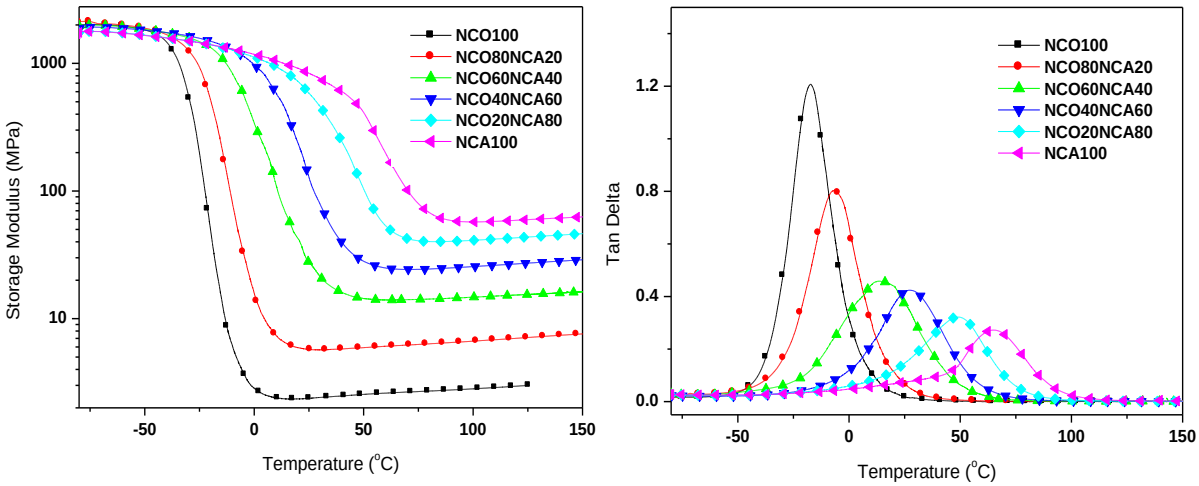

Figure 3. Storage modulus and tan δ curves for all polymers.

in the tan δ versus *T* curve and the temperature there is taken as the glass transition temperature (T_g). At high temperatures after the α relaxation, a plateau was observed in the *E'* versus *T* curves, which is evidence for the existence of the crosslinked network in the NCO/NCA thermosets. The crosslink density (ν_e) of all of the copolymers can be determined from the rubbery moduli using the following equation, according to the kinetic theory of rubber elasticity:[20,21]

$$E' = 3\nu_e RT$$

where E' is the storage modulus at T_g + 50 °C in the rubbery plateau, *R* is the gas constant, and *T* is the absolute temperature at T_g + 50 °C. As one can see from Table 1, the crosslink density increases dramatically from 318 to 6028 mol/m^3, when the NCA amount increases from 0 to 100 %. This indicates that increasing the amount of NCA in the copolymers results in a more crosslinked network, which enhances the thermosets' rubbery modulus. The glass transition temperatures (T_gs), $(\tan\delta)_{max}$ values and room temperature storage moduli (*E'* at 25 °C) for all of the copolymers are also summarized in Table 1. As the crosslink density

increases with an increase in the NCA amount, molecular motions become more restricted and the amount of energy that can be dissipated throughout the polymer specimen decreases dramatically. Therefore, the tan δ peak shifts to a higher temperature and the $(\tan \delta)_{max}$ decreases when the NCA amount increases. Meanwhile, the room temperature storage modulus is enhanced considerably by increasing the NCA content in the thermosets.

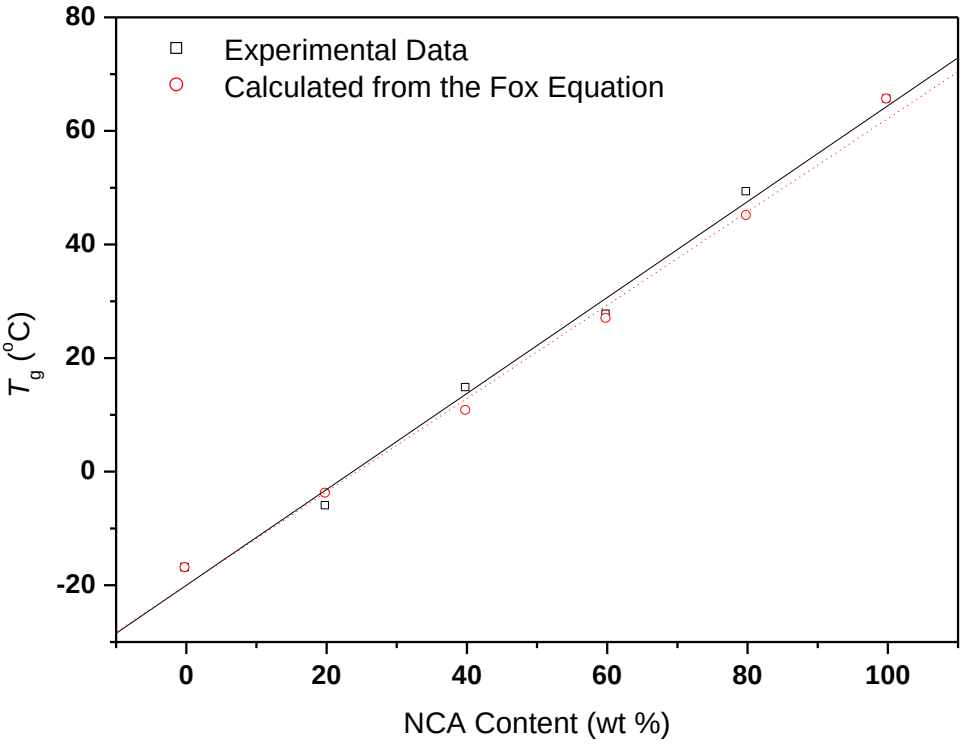

Figure 4. The dependence of glass transition temperature (T_g) of the NCO/NCA copolymers on the NCA content.

The T_gs of all copolymers are in the range of -17.1 to 65.4 °C, which indicates that rubbery to rigid plastics are obtained by changing the NCO/NCA ratio. Figure 4 shows the dependence of the T_gs of the NCO/NCA copolymers on the NCA content. A square indicates the T_gs obtained from experiment and how they increase linearly with an increase in the NCA content. Round dots indicate the T_gs calculated based on the Fox equation:

$$\frac{1}{T_g} = \frac{w_a}{T_{g,a}} + \frac{w_b}{T_{g,b}}$$

where $T_{g,a}$ and $T_{g,b}$ represent the glass transition temperatures of polyNCO and polyNCA and w_a and w_b are their mass fractions. As we can see from Figure 4, the experimental T_gs fit very well with the calculated T_gs. The linear increase of T_gs clearly indicates that the increase in NCA content increases the glass transition temperatures due to better incorporation of the monomers into the copolymer network with resulting higher crosslink densities. Similar results have been reported by Sheng *et al.* previously.[22]

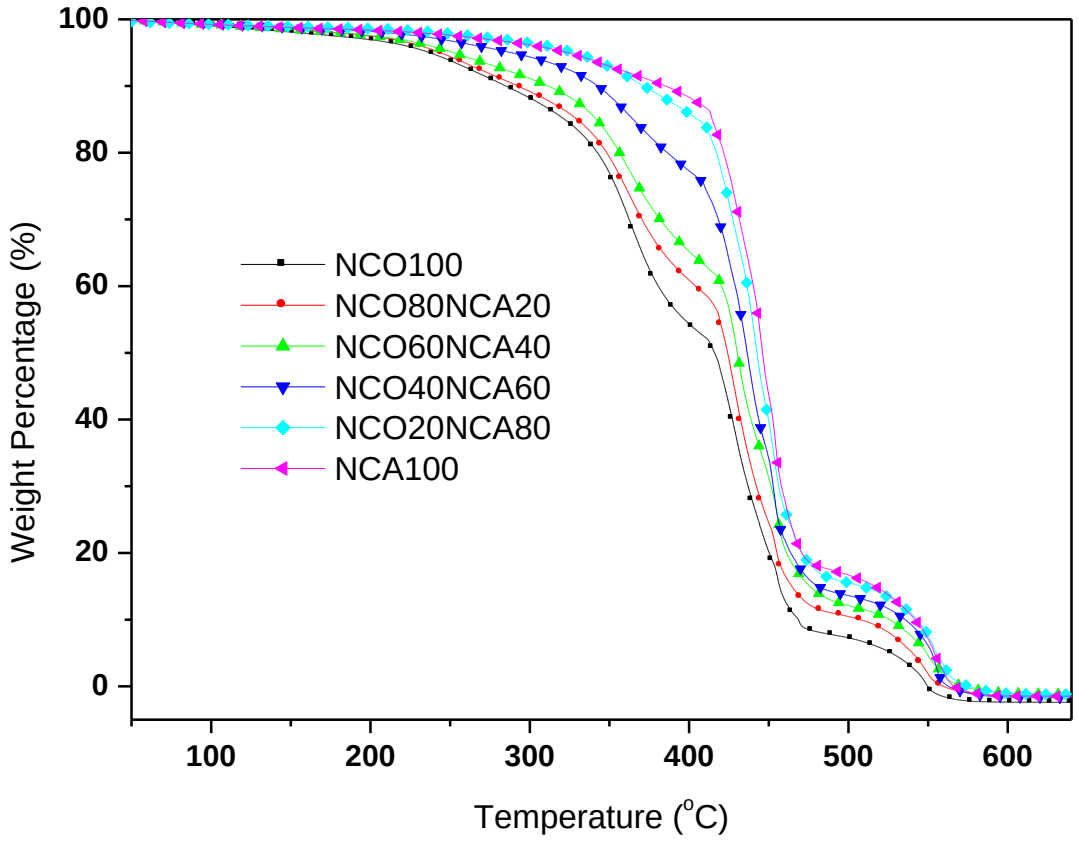

Figure 5. TGA curves for all NCO/NCA copolymers.

The TGA analysis of all copolymers is shown in Figure 5 and all of the corresponding data (T_{10}, T_{50} and T_{max}) are summarized in Table 2. As seen from Figure 5, all thermosets are stable up to 200 ^{o}C and three decomposition stages are clearly seen. The first stage from 200 ^{o}C to 425 ^{o}C corresponds to evaporation and decomposition of the unreacted monomers and other soluble materials in the bulk materials.[23] The weight percentage lost in the first stage decreases for thermosets with higher NCA content, which is due to more effective crosslinking in the polymer. The second stage (425-475 ^{o}C) is the fastest degradation stage. It represents decomposition of the polymer backbone in the bulk thermosets. The last stage (> 475 ^{o}C) corresponds to further oxidation of the crosslinked network and gradual oxidation of the char residue. It can be seen from Table 2 that T_{10}, T_{50} and T_{max} for all of the copolymers increase with an increase in the NCA content. This can be explained by the fact that increased crosslink densities improve the thermal stabilities of the final thermosets.

Table 2. TGA data and mechanical properties for the polymers.

Polymer	TGA data (^{o}C)			Mechanical Properties[d]			
	T_{10}[a]	T_{50}[b]	T_{max}[c]	E (MPa)	σ_b (MPa)	ε_b (%)	Toughness (MPa)
NCO100	285	416	429	-	-	-	-
NCO80NCA20	293	424	429	-	-	-	-
NCO60NCA40	312	430	431	11.0 ±0.4	1.6 ±0.2	16.3 ±2.9	0.14 ±0.04
NCO40NCA60	343	436	437	25.7 ±2.5	4.5 ±0.2	25.2 ±0.5	0.6 ±0.02
NCO20NCA80	372	443	441	166.6 ±9.3	8.9 ±0.7	15.6 ±2.1	0.9 ±0.2
NCA100	385	446	445	407.0 ±37	18.0 ±0.4	13.0 ±3.9	1.6 ±0.6

a) 10% Weight loss temperature. b) 50% Weight loss temperature. c) Temperature of maximum thermal degradation. d) E = Young's modulus, σ_b = tensile strength, and ε_b = elongation at break.

Mechanical Properties. Figure 6 shows the tensile stress-strain behavior of several NCO/NCA copolymers and Table 2 summarizes their Young's moduli, tensile strengths,

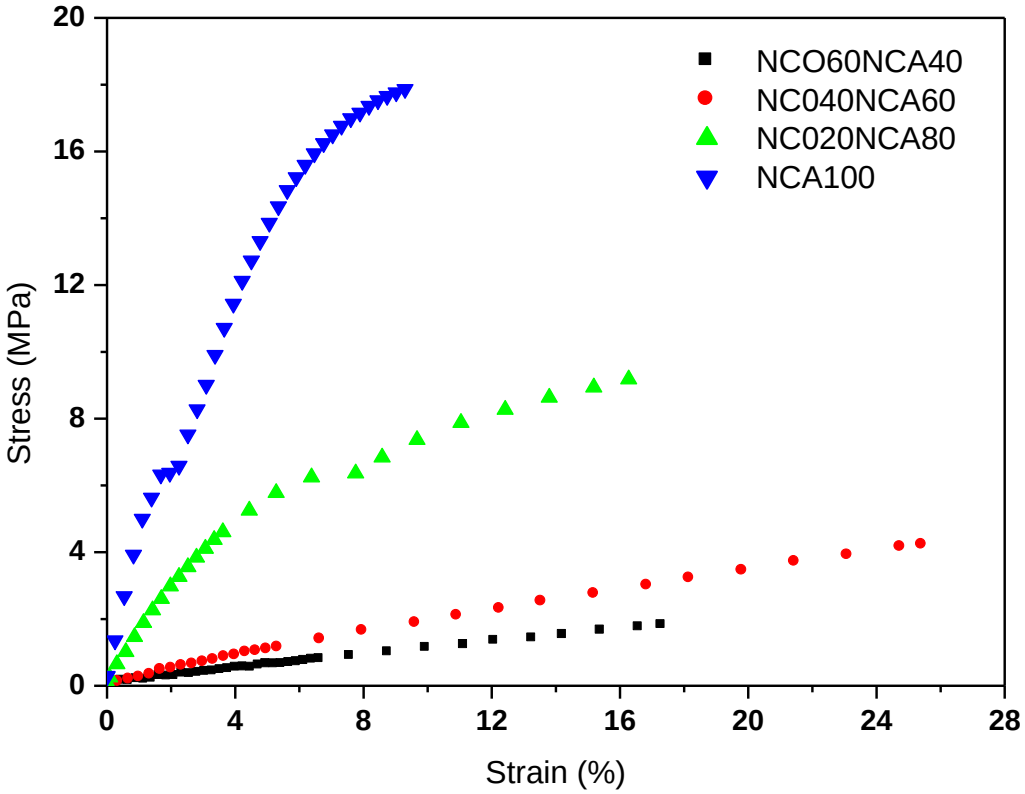

Figure 6. Tensile stress-strain curves for several NCO/NCA copolymers.

elongation at break values, and toughness. PolyNCO100 and polyNCO80NCA20 are too weak to run the tensile tests; so only the other four samples have been investigated. The NCO/NCA copolymers exhibit a variety of stress-strain behaviors depending on the amount of NCA used. PolyNCO60NCA40 and polyNCO40NCA60 exhibit behavior as weak and ductile plastics with Young's moduli of 11.0 and 25.7 MPa, respectively. Much better mechanical properties are observed when the NCA amount is increased to 80 and 100 %; polyNCO20NCA80 and polyNCA100 show Young's moduli of 166.6 and 407 MPa, and ultimate tensile strengths of 8.9 and 18.0 MPa respectively, which are dramatically enhanced compared to the analogous properties for polyNCO60NCA40 and polyNCO40NCA60. The improvements can be explained by both an increase in the crosslink density and the rigidity

of the thermosets. Besides the higher crosslink densities obtained when using more NCA, the number of rigid cyclopentane rings obtained after ring-opening of the norbornene rings increases with an increase in the NCA content. In addition to the Young's moduli and tensile strengths, toughness values have also been obtained from the stress-strain curves by integrating the areas under the stress-strain curves. Tensile toughness is a materials' resistance to fracture when stressed and both the tensile strength and the elongation at break contribute to the tensile toughness. As seen from Table 2, the tensile toughness increases with an increase in the NCA content as well.

Conclusions

Two castor oil-based ROMP monomers, NCO and NCA, which have different numbers of norbornene rings per fatty acid side chain have been prepared and bioplastics with different crosslink densities ranging from 318 to 6028 mol/m^3 have been obtained by varying the initial NCO/NCA ratio during ROMP. The amount of soluble materials obtained by extraction of the NCO/NCA copolymers decreases considerably as the NCA content increases, because of increased crosslinking. The gelation times also dramatically decrease as the NCA content increases. The thermal properties, namely the T_gs and room temperature storage moduli, are improved with an increase in the NCA content. The T_gs increase linearly with the amount of NCA and fit well with the data calculated based on the Fox equation. The TGA data reveals that the thermosets with higher crosslink densities have better thermal stabilities. In addition, the mechanical properties, namely the Young's moduli, tensile strength and toughness, are also improved with an increase in NCA content. These castor oil-based thermosets represent another promising route to environmentally friendly plastics.

Acknowledgments

We are grateful for financial support from the Center for Crops Utilization Research (CCUR) at Iowa State University and thankful to Professor Michael Kessler in the Department of Materials Science and Engineering at Iowa State University for the use of his thermal analysis equipment. In addition, we thank Dr. Yongshang Lu for his thoughtful discussions.

References

1) Lu, Y. S.; Larock, R. C. *ChemSusChem* **2009**, *2*, 136-147.
2) Montero de Espinosa, L.; Ronda, J. C.; Galia, M.; Cadiz, V. *J. Polym. Sci: Part A: Polym. Chem.* **2009**, *47*, 4051-4063.
3) Montero de Espinosa, L.; Ronda, J. C.; Galia, M.; Cadiz, V. *J. Polym. Sci: Part A: Polym. Chem.* **2009**, *47*, 1159-1167.
4) Montero de Espinosa, L.; Ronda, J. C.; Galia, M.; Cadiz, V. *J. Polym. Sci: Part A: Polym. Chem.* **2008**, *46*, 6843-6850.
5) Tian, H. F.; Liu, D. G.; Zhang, L. *J. Appl. Polym. Sci.* **2009**, *111*, 1549-1556.
6) Liu, W. J.; Misra, M.; Askeland, P.; Drzal, L. T.; Mohanty, A. K. *Polymer* **2005**, *46*, 2710-2721.
7) Quirino, R. L.; Larock, R. C. *J. Appl. Polym. Sci.* **2009**, *112*, 2033-2043.
8) Pfister, D. P.; Baker, J. R.; Henna, P. H.; Lu, Y.; Larock, R. C. *J. Appl. Polym. Sci.* **2008**, *108*, 3618-3625.
9) Ogunniyi, D. S. *Bioresour. Tech.* **2006**, *97*, 1086-1091.
10) Sharma, V.; Kundu, P. P. *Prog. Polym. Sci.* **2008**, *33*, 1199-1215.
11) Trnka, T. M.; Grubbs, R. H. *Acc. Chem. Res.* **2001**, *34*, 18-29.
12) Meier, M. A. R. *Macromol. Chem. Phys.* **2009**, *210*, 1073-1079.
13) Henna, P. H.; Larock, R. C. *Macromol. Mater. Eng.* **2007**, *292*, 1201-1209.
14) Kodali, D. R. U.S. Pat. 6420322, 2002.
15) Henna, P.; Larock, R. C. *J. Appl. Polym. Sci.* **2009**, *112*, 1788-1797.
16) Arehart, S. V.; Pugh, C. *J. Am. Chem. Soc.* **1997**, *119*, 3027-3037.
17) Jones, A. S.; Rule, J. D.; Moore, J. S.; White, S. R.; Sottos, N. R. *Chem. Mater.* **2006**, *18*, 1312-1317.
18) Sheng, X.; Lee, J. K.; Kessler, M. R. *Polymer* **2009**, *50*, 1264-1269.
19) Weng, L. H.; Chen, X. M.; Chen, W. L. *Biomacromolecules* **2007**, *8*, 1109-1115.
20) Flory, P. J. *Principles of Polymer Chemistry*; Cornell Univerisity Press: Ithaca, 1953.
21) Ward, I. M. *Mechanical Properties of Solid Polymers*; Wiley Interscience: New York, 1971.
22) Sheng, X.; Kessler, M. R.; Lee, J. K. *J. Therm. Anal. Calorim.* **2007**, *89*, 459-464.
23) Andjelkovic, D. D.; Larock, R. C. *Biomacromolecules* **2006**, *7*, 927-936.

CHAPTER 5. SOYBEAN OIL-ISOSORBIDE-BASED WATERBORNE POLYURETHANE-UREA DISPERSIONS

A Paper published in ChemSusChem, 4, 386-391.

Ying Xia and Richard C. Larock*

Department of Chemistry, Iowa State University, Ames, Iowa 50011

Abstract

A series of soybean oil-based amide diol-isosorbide waterborne polyurethane-urea (PUU) dispersions have been successfully prepared with isosorbide amounts ranging from 0 to 20 wt % of the total diol content. The thermal and mechanical properties of the resulting PUU films have been characterized by dynamic mechanical analysis, differential scanning calorimetry, thermogravimetric analysis, and mechanical testing. The experimental results reveal that the glass transition temperature is increased with an increased amount of isosorbide, and the mechanical properties are improved significantly with the incorporation of isosorbide. For example, the Young's modulus increases from 2.3 to 63 MPa and the ultimate tensile strength increases from 0.7 to 8.2 MPa, when the isosorbide amount is increased from 0 to 20 wt %. The thermal stability decreases slightly with the incorporation of isosorbide. This work provides a new way of utilizing biorenewable materials, like isosorbide and a soybean oil-based amide diol, for the preparation of high performance polyurethane-urea coatings.

Introduction

Polyurethanes (PUs) exhibit a wide range of applications and are one of the most versatile polymers.[1,2] Recently, waterborne polyurethane dispersions (PUDs) have attracted more attention, due to environmental concerns regarding volatile organic chemicals (VOCs) and hazardous air pollutants (HAPs).[3-5] Compared to conventional solvent-borne PUs, waterborne PUDs, which have low viscosity at high molecular weight and good applicability, are one of the most rapidly developing branches of PU chemistry.[6] These PUDs are very useful as adhesives,[7] coatings,[8] and paints[9] with good properties, including excellent adhesion properties and low film-forming temperatures.

Polymers derived from vegetable oils represent a promising route to renewable materials, because of their versatile applications.[10,11] A variety of polymers have been prepared from vegetable oils using free radical,[12] cationic,[13,14] olefin metathesis[15-17] and condensation polymerizations.[18] Vegetable oil-based polyols, obtained from epoxidation followed by ring opening,[19] hydroformylation-reduction,[20] and ozonolysis-reduction,[21] have been introduced to prepare PUs ranging from flexible foams to hard plastics.[22] Vegetable oil-based diisocyanates have also been prepared as an alternative to petroleum-based diisocyanates.[23-25] Recently, waterborne anionic[6] and cationic[26,27] PUDs have been prepared from vegetable oils as well. For example, methoxylated soybean oil polyols (MSOLs) with hydroxyl functionality ranging from 2.4 to 4.0 have been used to prepare waterborne anionic PUDs.[6] An increase in the hydroxyl functionality of the MSOL significantly increases the crosslink density of the PUs, resulting in biorenewable PUs ranging from elastomeric polymers to ductile plastics.[6] Moreover, hybrid latexes have been

obtained by blending vegetable oil-based PUDs with vinyl monomers.[28,29] The hybrid latex films show a significant increase in thermal stability and mechanical properties.

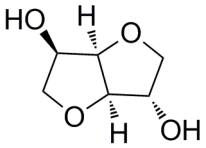

Scheme 1. Structure of isosorbide.

The aminolysis of vegetable oils using diethanolamine has been used to produce fatty amide diols for solution PU and polyester preparations.[30-32] However, very few publications have reported the use of these fatty amide diols for PU dispersions. Isosorbide (Scheme 1) is a diol derived from renewable resources, like cereal-based polysaccharides.[33] With attractive features, like its rigidity and chirality, and its non-toxic nature, isosorbide has been used to prepare polymers with high glass transition temperatures and special optical properties.[33] PUs from isosorbide have been prepared[34-37] and the replacement of 1,4-butanediol by isosorbide has been shown to increase the glass transition temperature and enhance the hydrolytic degradation of the PUs.[37]

Herein, isosorbide has been employed with a soybean oil-based fatty amide diol to prepare waterborne polyurethane-urea (PUU) dispersions for the first time. The effects of the amount of isosorbide on the structure and properties of the resulting cast films have been extensively investigated. The replacement of the soybean oil-based diol with isosorbide increases the glass transition temperature and improves the mechanical properties significantly, indicating a promising future for these environmentally friendly, waterborne dispersions from renewable resources.

Results and Discussion

Structure of the polyurethane-ureas obtained. Isosorbide with a rigid structure has been employed to replace part of the soybean oil-based amide diol to successfully prepare polyurethane/ureas (PUUs). Figure 1 shows the FT-IR spectra for the PUU samples prepared with and without isosorbide. The peaks at 2270 cm^{-1}, assigned to the isocyanate groups,

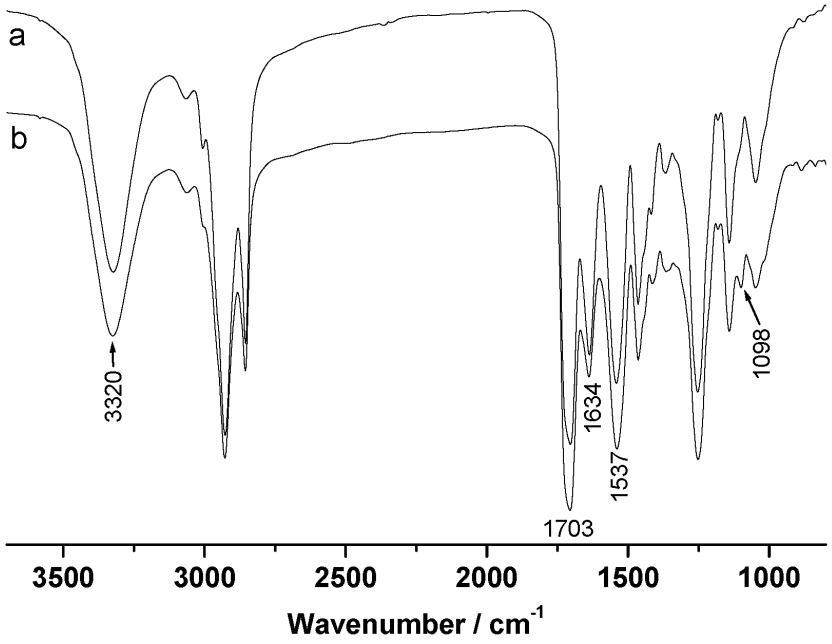

Figure 1. FT-IR spectra of (a) HESA-ISO0, and (b) HESA-ISO20.

disappeared, indicating the complete reaction of the isocyanate groups in the HDI. Hydrogen bonding plays a very important role in PUUs and affects material properties significantly. FT-IR spectroscopy can be used to investigate the hydrogen bonding in the PUUs and help understand the phase structure. In these PUUs, the hydrogen bonds are mainly formed between N-H bonds and the urethane/urea carbonyl. As seen in Figure 1, a single stretching peak located around 3320 cm^{-1} corresponds to a hydrogen-bonded N-H stretching

vibration.[38] The hydrogen-bonded carbonyl groups from the urethane are observed at 1706 cm^{-1}.[39] The carbonyl stretch around 1707 cm^{-1} can be attributed to hydrogen bonding in disordered regions, that is urethane/urea linkages "dissolved" in soft segment phases.[40] The stronger hydrogen bonding in the ordered/crystalline regions of the urethane carbonyl groups occurs at a lower frequency, ranging from 1684 to 1702 cm^{-1}. This is not observed in the HESA-ISO PUUs, indicating the amorphous nature of these PUUs.[40] In addition, urea carbonyls are observed at 1634 cm^{-1}. Compared to HESA-ISO0, a small peak appears at 1098 cm^{-1} in all isosorbide PUUs, corresponding to the ether linkage in the isosorbide, which indicates that the isosorbide is successfully incorporated into the PUUs.

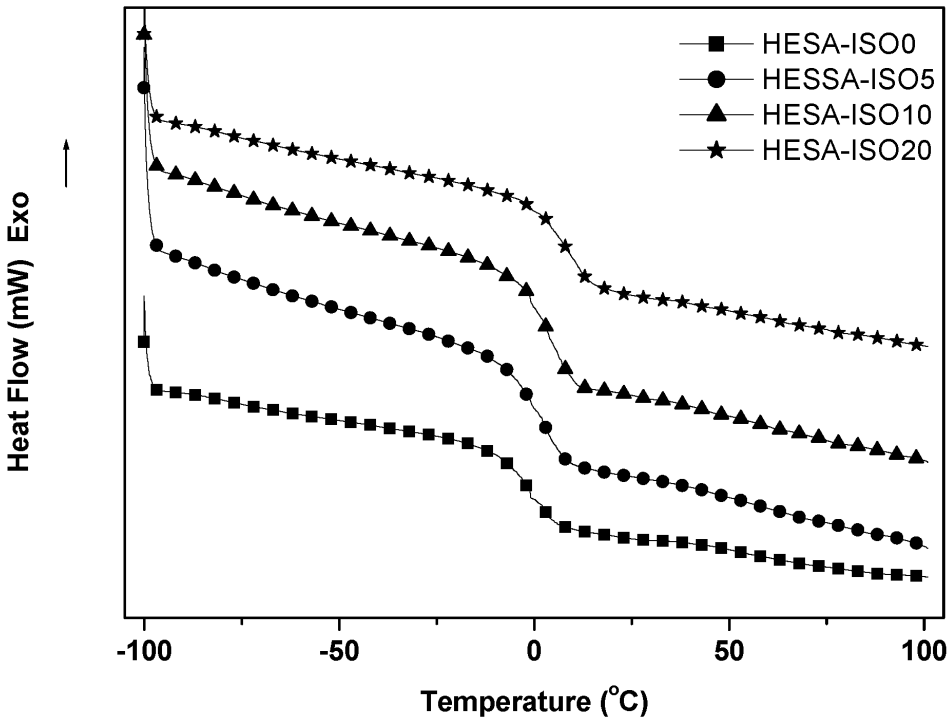

Figure 2. DSC thermograms of the PUU films.

Thermal Properties. The DSC thermograms of the PUU films with different amounts of isosorbide are shown in Figure 2. No crystallization transition is observed in the DSC curves, indicating the amorphous nature of these PUUs, which is in good agreement with the IR results. All of the samples show only one glass transition temperature (T_g), increasing from -1.6 to 9.7 ^oC as the amount of isosorbide is increased from 0 to 20 wt % (Table 1). The increase in T_g can be explained by incorporation of the isosorbide with a rigid bicyclic structure. The incorporation of isosorbide also increases the hard segment (HS) content of the PUUs from 52.7 to 67.4 wt % (Table 1), which also results in increased T_gs.

Table 1. DMA, DSC and TGA data for the HESA-ISO polymers.

Polymer	HS (wt %)[a]	T_g (^oC)[b]	T_g (^oC)[c]	E' at 25 ^oC (MPa)	TGA data (^oC)			
					T_{10}[d]	T_{50}[e]	T_{max1}[f]	T_{max2}[g]
HESA-ISO0	52.7	44.7	-1.6	205	215	306	221	463
HESA-ISO5	56.8	45.8	3.2	456	216	301	224	465
HESA-ISO10	60.6	54.3	3.9	828	212	295	221	446
HESA-ISO20	67.4	64.6	9.7	1203	210	292	225	440

[a] Hard segment (HS) content = [mass (ISO + DMPA + EDA + HDI + TEA)] / [mass (HESA + ISO + DMPA + EDA + HDI + TEA)].
[b] Glass transition temperature obtained from DMA.
[c] Glass transition temperature obtained from DSC.
[d] 10% Weight loss temperature.
[e] 50% Weight loss temperature.
[f] Temperature of maximum thermal degradation of the urethane/urea bonds.
[g] Temperature of maximum thermal degradation of the soybean fatty acid chains.

The dynamic mechanical properties of these PUU films have been investigated by DMA, since it is more useful than DSC for investigating the mobility of the soft segments through relaxation at the molecular level. Figure 3 shows the storage moduli (E') and tan δ values of the PUU films as a function of temperature. All of the films are glassy below 10 ^oC, and their storage moduli decrease slowly with an increase in the temperature. A dramatic

drop was observed in the *E*' values later on, due to the primary relaxation process of the PUU films. Besides the primary relaxation, another relaxation was observed at around -60 ^{o}C in the tan δ curves, which corresponds to relaxation of the free soybean oil fatty acid chains.[41] The *E*' at room temperature and the T_gs obtained from the maximum of the tan δ curves are summarized in Table 1. The *E*' at room temperature increases from 205 to 1203 MPa as the isosorbide content is increased from 0 to 20 wt %, a direct result of incorporating the rigid bicyclic skeleton of isosorbide. The T_gs increase from 44.7 to 64.6 ^{o}C, due to the presence of the rigid diol and an increase in the hard segment content.

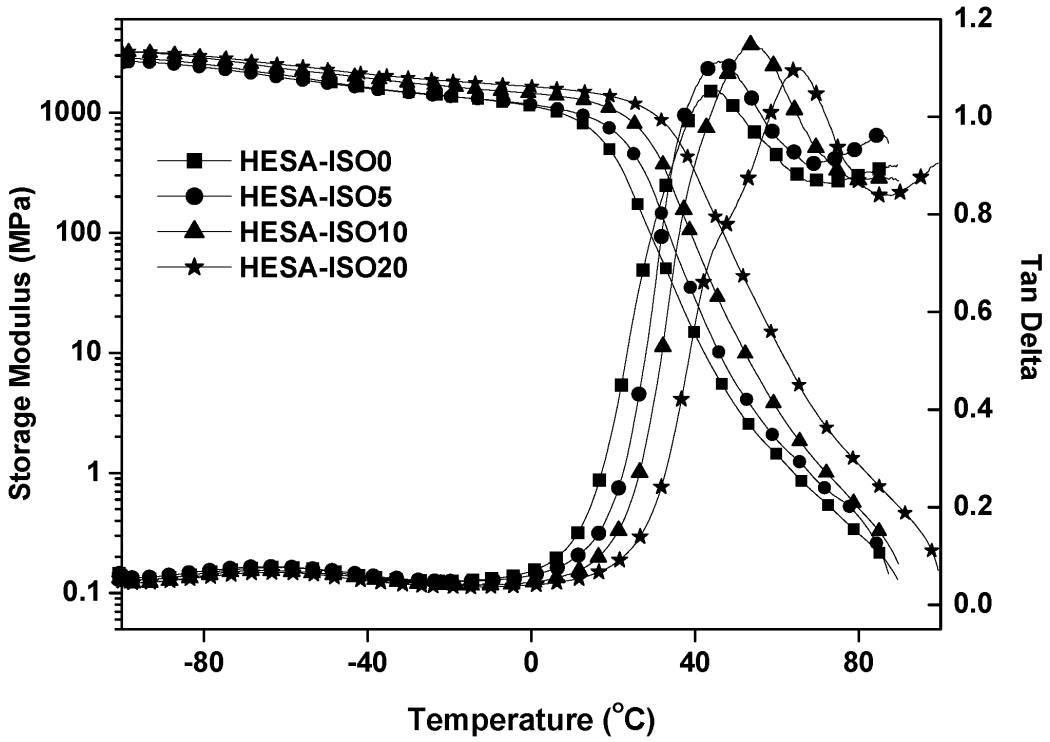

Figure 3. The storage modulus and loss factor (tan δ) as a function of the temperature for PUU films with different amounts of ISO.

The T_gs of the PUU films obtained by DMA and DSC as a function of the amount of isosorbide in the HESA/ISO mixture have been plotted in Figure 4. We have found

previously that the T_gs increase linearly with the hydroxyl content of the soybean oil-based polyols in related PU films.[42,43] Herein, the T_gs increase linearly with the amount of rigid isosorbide, offering r values of 0.981 and 0.978 for the data obtained by DMA and DSC, respectively. The T_gs obtained from DMA are higher than those obtained from DSC, due to the different nature of these two methods. DSC measures the heat capacity change from frozen to unfrozen chains, while DMA measures changes in the mechanical response of the polymer chains.[44]

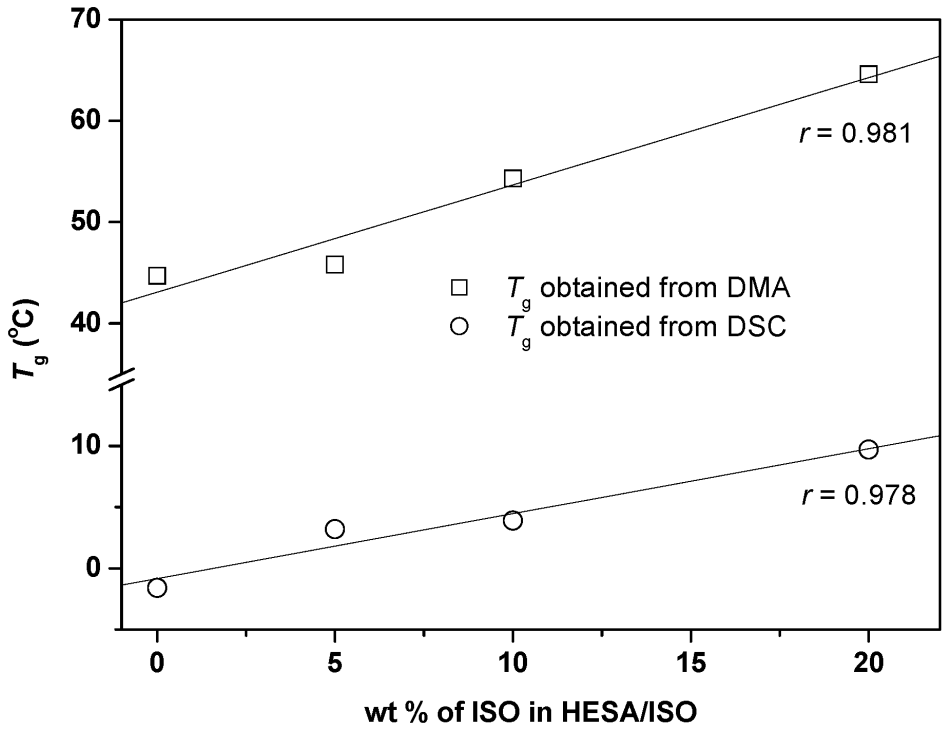

Figure 4. Dependence of the T_g of the films on the wt % of ISO in HESA/ISO.

TGA curves for all of the PUU films are shown in Figure 5. The thermal decomposition of a urethane or a urea involves dissociation into an isocyanate and an alcohol or an amine, as well as the formation of carbon dioxide, olefins, secondary amines, and

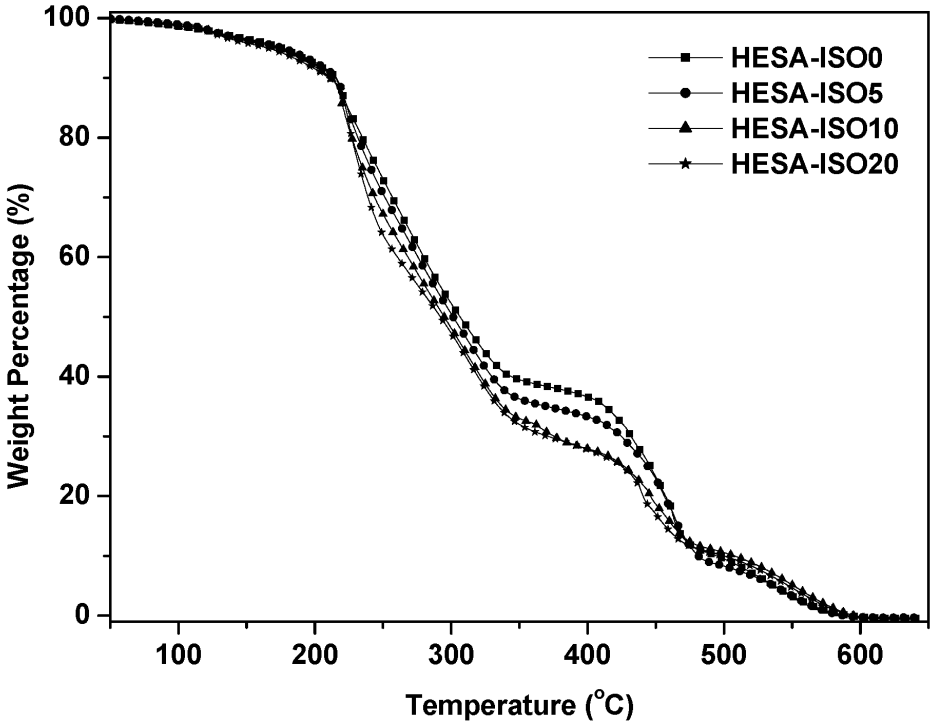

Figure 5. TGA curves for all of the PUU films.

transesterification.[45] Two main decomposition stages are observed for all of the HESA/ISO samples (Figure 5). The weight loss below 350 °C is due to degradation of the urethane/urea groups, and the degradation process above 350 °C is mainly attributed to the isosorbide/soybean fatty acid chain scission. The temperature of maximum thermal degradation for these two stages and the temperature of 10% and 50% weight loss (T_{10} and T_{50}) are summarized in Table 1. The decrease for both T_{10} and T_{50} indicates that the thermal stabilities of the PUU films decrease with the replacement of HESA by isosorbide, which is in good agreement with Marin *et al.*'s work.[37] Furthermore, isosorbide (168 g/mol) has a lower molecular weight compared to HESA (366 g/mol). Thus, replacement of the HESA by isosorbide decreases the total weight percentage of the diol and increases the thermally labile urethane/urea weight percentage in the PUUs, which also contributes to the decrease

observed in the thermal stabilities. The T_{max1} is ascribed to the maximum degradation of the urethane/urea groups and this is nearly the same for all of the PUU films. The T_{max2}, which represents the maximum degradation of the isosorbide/soybean oil fatty acid chains, decreases with more isosorbide, probably because isosorbide is more thermally unstable than the soybean oil-based derivative.[37]

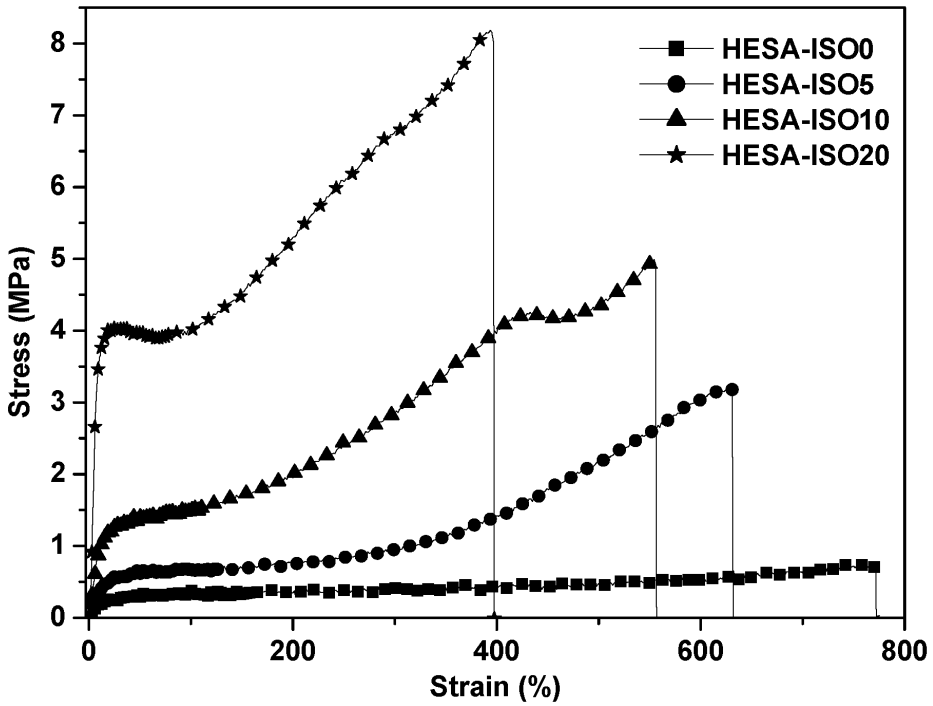

Figure 6. Stress-strain curves for all of the PUU films.

Mechanical Properties. Figure 6 shows the tensile stress-strain curves for all PUU films and Table 2 summarizes their Young's moduli, tensile strengths, elongation at break values, and toughness. All samples behave as elastomeric polymers with elongation at break values higher than 400%, which indicates that these samples can effectively sustain the stretch when stressed. For samples HESA-ISO10 and HESA-ISO20, a second yielding point was

observed, which can be explained by competitive deformation of the HESA-enriched phase and the isosorbide-enriched phase, with the two phases having different activation energies.[23,46] Replacement of the HESA by isosorbide improves the mechanical properties significantly. For example, the Young's modulus and tensile strength increase from 2.34 to 63.0 MPa and 0.69 to 8.15 MPa, respectively, when the isosorbide amount is increased from 0 to 20 wt % of the total diol. The improvements can be explained by an increase in the hard segment content and incorporation of the rigid bicyclic structure of the isosorbide. The elongation at break decreases from 794 to 406 %, as expected, when the amount of isosorbide is increased from 0 to 20 wt %. Tensile toughness is a materials' resistance to fracture and can be measured by integrating the areas under the stress-strain curves. The toughness of the PUU films is increased from 3.76 to 21.2 MPa with an increase in the isosorbide content from 0 to 20 wt %. The above results indicate that stronger and tougher PUU films can be made with the incorporation of isosorbide.

Table 2. Mechanical properties for the HESA-ISO polymers.

Polymer	Mechanical Properties[a]			
	E (MPa)	σ_b (MPa)	ε_b (%)	Toughness (MPa)
HESA-ISO0	2.34 ± 0.3	0.69 ± 0.09	794 ± 21	3.76 ± 0.29
HESA-ISO5	4.12 ± 0.3	3.23 ± 0.13	663 ± 38	9.49 ± 0.90
HESA-ISO10	10.7 ± 0.2	4.78 ± 0.30	557 ± 1.0	14.8 ± 1.1
HESA-ISO20	63.0 ± 3.0	8.15 ± 0.05	406 ± 13	21.2 ± 0.18

a) *E* = Young's modulus, σ_b = tensile strength, and ε = elongation at break.

Conclusions

Up to 20 wt % of isosorbide and a soybean oil-based amide diol have been successfully incorporated into waterborne polyurethane-urea (PUU) dispersions. The effect of the amount of isosorbide on the thermal and mechanical properties of the resulting PUU films has been extensively studied. The experimental results reveal that the glass transition temperature is increased with increasing amounts of isosorbide, and the mechanical properties are improved significantly with the incorporation of isosorbide. However, the thermal stability decreases slightly with the incorporation of isosorbide. These soybean oil amide diol-isosorbide-based PUUs represent a promising new route to biorenewable coatings.

Experimental

Materials. Wesson soybean oil was purchased at the local supermarket and used directly without further purification. Diethanolamine, sodium methoxide, hexamethylene diisocyanate (HDI), *D*-isosorbide (ISO) and dimethylol propionic acid (DMPA) were purchased from Aldrich Chemical Company (Milwaukee, WI). Ethylenediamine, triethylamine (TEA), magnesium sulfate, methyl ethyl ketone (MEK), and ethyl acetate were purchased from Fisher Scientific Company (Fair Lawn, NJ). All materials were used as received without further purification.

Synthesis of the *N, N-bis*(2-hydroxyethyl)soybean amide (HESA).[47] Diethanolamine (31.5 g, 0.3 mol) was placed in a round-bottomed flask fitted with a stirrer and dropping funnel. Sodium methoxide (0.19 g, 0.0035 mol) was added and the mixture was stirred at 115 ^{o}C until the sodium methoxide dissolved. Then soybean oil (43.6 g, 0.05 mol) was added dropwise over 30 min. The reaction was heated for 1.5 h. After cooling, the mixture was dissolved in ethyl acetate and washed with 15 wt % aq. NaCl solution. After drying the

organic layer over magnesium sulfate, the ethyl acetate was distilled off to obtain 52.3 g of HESA (95%) possessing a yellow orange color: ^{1}H NMR ($CDCl_3$, δ ppm) at 5.31 (m, CH=CH), 3.72-3.76 (dt, C<u>H</u>$_2$-OH), 3.45-3.49 (dt, O=C-N-CH_2), 2.73 (m, -C=C-CH_2-C=C-), 2.35 (t, CH_2-C=O), 2.00 (m, CH_2-C=C), 1.57 (m, CH_2-C-C=O), 1.22-1.28 (m, CH_2), 0.85-0.94 (t, CH_3).

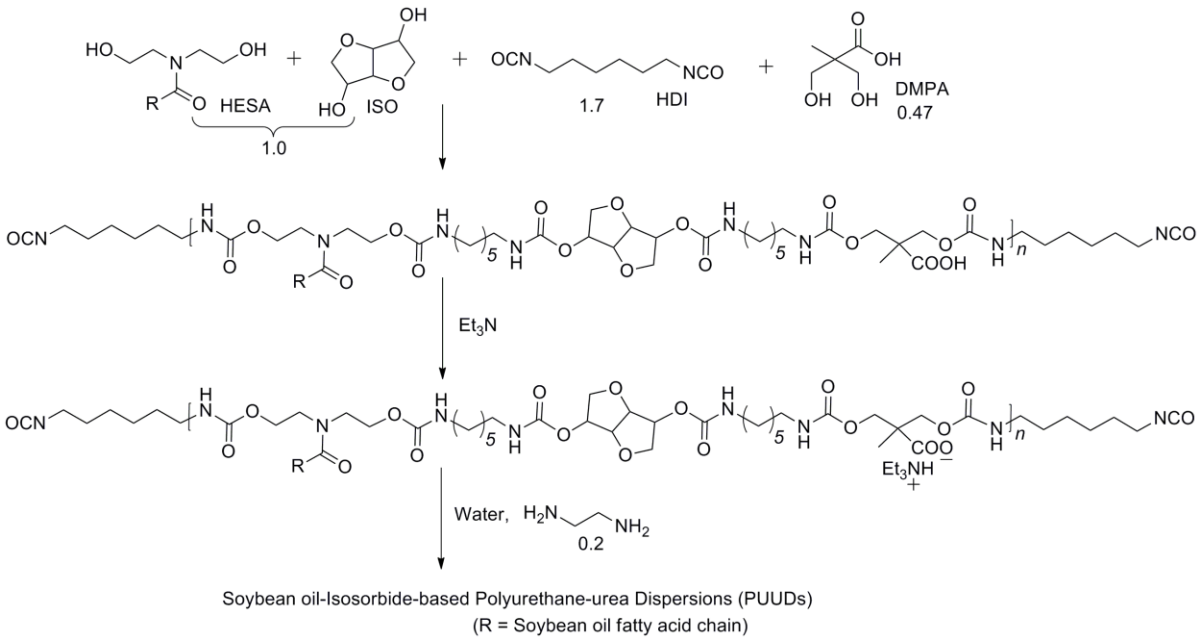

Scheme 2. Synthesis of HESA/ISO-based polyurethane-urea dispersions.

Synthesis of the HESA/ISO-based polyurethane-urea dispersions (PUUDs). Scheme 2 depicts the approach used to prepare the HESA/ISO-based PUUDs. The HESA, ISO, HDI (3.91 g) and DMPA (0.86 g) were added to a four-necked flask equipped with a mechanical stirrer, nitrogen inlet, condenser, and thermometer. The mole ratio between the NCO groups of the HDI, the OH groups of the HESA and ISO, the OH groups of the DMPA, and the NH_2 groups of the ethylenediamine is 1.7 : 1.0 : 0.47 : 0.2. The amount of ISO in the

HESA/ISO mixture has been varied from 0 to 5, 10, and 20 wt %. The reaction was carried out at 78 ^{o}C for 1 h and then 24 g of MEK was added to reduce the viscosity of the mixture. The reaction was kept for another 2 h at 78 ^{o}C. After allowing the reaction mixture to cool to room temperature, the mixture was neutralized by TEA (1.2 equiv. per mole of DMPA) and stirred for 30 min. Then water (90 g) and ethylenediamine (0.16 g) were added, followed by vigorous stirring for 30 min, to form a dispersion. After removal of the MEK under a vacuum, HESA/ISO-based PUUDs were obtained; the corresponding films were obtained by drying the PUUDs at ambient temperatures in a glass mold. The nomenclature for the samples is as follows: a PUUD prepared from 10 wt % of ISO in the total mass of HESA/ISO is designated as HESA-ISO10.

Characterization. The ^{1}H NMR spectra were recorded in $CDCl_3$ using a Varian spectrometer (Palo Alto, CA) at 400 MHz. The FT-IR spectra of the films were recorded on a Bruker IFS-66V spectrometer (Billerica, MA).

The dynamic mechanical analyses (DMA) were carried out on a TA Instruments Q800 dynamic mechanical analyzer using a film tension mode of 1 Hz. Rectangular samples 0.5 mm thick and 8 mm wide were used for the analysis. The samples were cooled and held isothermally for 3 min at -100 ℃ before the temperature was increased at 5 ℃/min to 150 ℃.

Differential scanning calorimetry (DSC) was performed on a thermal analyzer (TA instrument Q2000). The samples were equilibrated at -100 ^{o}C, and then heated to 100 ^{o}C at 20 ^{o}C/min. The glass transition temperatures (T_g) of the samples were determined from the midpoint temperature in the heat capacity change of the DSC scan. Samples of ~5 mg were cut from the films and used for analysis.

A thermogravimeter (TA instrument TGA Q50) was used to measure the weight loss of the films obtained under an air atmosphere. The samples were heated from 100 to 650 ^{o}C at a heating rate of 20 ^{o}C/min. Generally, approximately 10 mg samples were used for the thermogravimetric analysis.

The mechanical properties of the PUU films were determined using an Instron universal testing machine (model 4502) with a crosshead speed of 50 mm/min. Rectangular specimens of $70 \times 10 \times 0.5$ mm^3 (length $\times$ width $\times$ thickness) were used. An average value of at least three replicates of each sample was taken. The toughness of the polymer, which is the fracture energy per unit volume of the sample, was obtained from the area under the corresponding tensile stress-strain curves.

Acknowledgements

We gratefully acknowledge financial support from the Consortium for Plant Biotechnology Research (CPBR) and Archer Daniels Midland (ADM) Company. We also thank Professor Michael Kessler in the Department of Materials Science and Engineering at Iowa State University for the use of his thermal analysis equipment. In addition, we thank Dr. Yongshang Lu for his thoughtful discussions.

References

1. M. Lonescu, *Chemistry and Technology of Polyols for Polyurethane*, Rapra Technology Limited, Shawbury, Shrewsbury, Shropshire, UK, **2005**.
2. G. T. Howard, *Inter. Biodeter. Biodegrad.* **2002**, *49*, 245-252.
3. K. L. Noble, *Prog. Org. Coat.* **1997**, *32*, 131-136.
4. Y. U. Ahn, S. K. Lee, H. M. Jeong, B. K. Kim, *Prog. Org. Coat.* **2007**, *60*, 17-23.
5. D. H. Jung, M. A. Jeong, H. M. Jeong, B. K. Kim, *Coll. Polym. Sci.* **2010**, *288*, 1465-1470.

6. Y. S. Lu, R. C. Larock, *Biomacromolecules* **2008**, *9*, 3332-3340.
7. M. M. Rahman, W. K. Lee, *J. Appl. Polym. Sci.* **2009**, *114*, 3767-3773.
8. Q. B. Meng, S. I. Lee, C. Nah, Y. S. Lee, *Prog. Org. Coat.* **2009**, *66*, 382-386.
9. A. C. Aznar, O. R. Pardini, J. I. Amalvy, *Prog. Org. Coat.* **2006**, *55*, 43-49.
10. Y. Xia, R. C. Larock, *Green Chem.* **2010**, *12*, 1893-1909.
11. M. Haq, R. Burgueno, A. K. Mohanty, M. Misra, *Comp. Sci. Technol.* **2008**, *68*, 3344-3351.
12. P. H. Henna, D. D. Andjelkovic, P. P. Kundu, R. C. Larock, *J. Appl. Polym. Sci.* **2007**, *104*, 979-985.
13. D. D. Andjelkovic, R. C. Larock, *Biomacromolecules* **2006**, *7*, 927-936.
14. Y. Xia, P. H. Henna, R. C. Larock, *Macromol. Mater. Eng.* **2009**, *294*, 590-598.
15. P. Henna, R. C. Larock, *J. Appl. Polym. Sci.* **2009**, *112*, 1788-1797.
16. Y. Xia, Y. Lu, R. C. Larock, *Polymer* **2010**, *51*, 53-61.
17. Y. Xia, R. C. Larock, *Polymer* **2010**, *51*, 2508-2514.
18. X. D. Cao, Y. Z. Tao, L. A. Lucia, L. N. Zhang, *J. Appl. Polym. Sci.* **2010**, *116*, 1299-1305.
19. A. Guo, Y. J. Cho, Z. S. Petrovic, *J. Polym. Sci. Part A: Polym. Chem.* **2000**, *38*, 3900-3910.
20. Z. S. Petrovic, I. Cvetkovic, D. Hong, X. M. Wan, W. Zhang, T. W. Abraham, J. Malsam, *Eur. J. Lipid Sci. Technol.* **2010**, *112*, 97-102.
21. Z. S. Petrovic, W. Zhang, I. Javni, *Biomacromolecules* **2005**, *6*, 713-719.
22. Z. S. Petrovic, *Polym. Rev.* **2008**, *48*, 109-155.
23. L. Hojabri, X. H. Kong, S. S. Narine, *Biomacromolecules* **2010**, *11*, 911-918.
24. L. Hojabri, X. H. Kong, S. S. Narine, *J. Polym. Sci. Part A: Polym. Chem.* **2010**, *48*, 3302-3310.
25. L. Hojabri, X. H. Kong, S. S. Narine, *Biomacromolecules* **2009**, *10*, 884-891.
26. Y. Lu, R. C. Larock, *Prog. Org. Coat.* **2010**, *69*, 31-37.
27. Y. Lu, Richard C. Larock, *ChemSusChem* **2010**, *3*, 329-333.
28. Y. S. Lu, R. C. Larock, *Biomacromolecules* **2007**, *8*, 3108-3114.
29. Y. Lu, Y. Xia, R. C. Larock, *Prog. Org. Coat.* **2010**, submitted.
30. S. Ahmad, S. M. Ashraf, E. Sharmin, M. Alam, *J. Macromol. Sci. Pure Appl. Chem.* **2005**, *A42*, 751-764.
31. S. Dutta, N. Karak, *Prog. Org. Coat.* **2005**, *53*, 147-152.
32. S. Yadav, F. Zafar, A. Hasnat, S. Ahmad, *Prog. Org. Coat.* **2009**, *64*, 27-32.
33. F. Fenouillot, A. Rousseau, G. Colomines, R. Saint-Loup, J. P. Pascault, *Prog. Polym. Sci.* **2010**, *35*, 578-622.
34. F. Bachmann, J. Reimer, M. Ruppenstein, J. Thiem, *Macromol. Rapid Commun.* **1998**, *19*, 21-26.
35. M. Beldi, R. Medimagh, S. Chatti, S. Marque, D. Prim, A. Loupy, F. Delolme, *Eur. Polym. J.* **2007**, *43*, 3415-3433.
36. C. H. Lee, H. Takagi, H. Okamoto, M. Kato, A. Usuki, *J. Polym. Sci. Part A: Polym. Chem.* **2009**, *47*, 6025-6031.
37. R. Marin, S. Munoz-Guerra, *J. Appl. Polym. Sci.* **2009**, *114*, 3723-3736.
38. V. W. Srichatrapimuk, S. L. Cooper, *J. Macromol. Sci. Phys.* **1978**, *B15*, 267-311.

39. S. K. Pollack, D. Y. Shen, S. L. Hsu, Q. Wang, H. D. Stidham, *Macromolecules* **1989**, *22*, 551-557.
40. L. S. Teo, C. Y. Chen, J. F. Kuo, *Macromolecules* **1997**, *30*, 1793-1799.
41. X. Kong, S. S. Narine, *Biomacromolecules* **2007**, *8*, 2203-2209.
42. Z. S. Petrovic, L. T. Yang, A. Zlatanic, W. Zhang, I. Javni, *J. Appl. Polym. Sci.* **2007**, *105*, 2717-2727.
43. T. W. Pechar, G. L. Wilkes, B. Zhou, N. Luo, *J. Appl. Polym. Sci.* **2007**, *106*, 2350-2362.
44. Y. S. Lu, L. H. Weng, X. D. Cao, *Carbohydr. Polym.* **2006**, *63*, 198-204.
45. J. M. Cervantes-Uc, J. I. M. Espinosa, J. V. Cauich-Rodriguez, A. Avila-Ortega, H. Vazquez-Torres, A. Marcos-Fernandez, J. S. Roman, *Polym. Degrad. Stab.* **2009**, *94*, 1666-1677.
46. G. F. Shan, W. Yang, M. B. Yang, B. H. Xie, J. M. Feng, Q. Fu, *Polymer* **2007**, *48*, 2958-2968.
47. L. E. Gast, W. J. Schneide, J. C. Cowan, *J. Am. Oil Chem. Soc.* **1966**, *43*, 418-421.

CHAPTER 6. CASTOR OIL-BASED WATERBORNE POLYURETHANE DISPERSIONS CURED WITH AN AZIRIDINE-BASED CROSSLINKER

A Paper published in Macromolecular Materials and Engineering, 296, 703-709.

Ying Xia and Richard C. Larock*

Department of Chemistry, Iowa State University, Ames, Iowa 50011

Abstract

Castor oil-based anionic polyurethane (PU) dispersions have been post-cured by a multi-aziridine-based crosslinker CX-100 with the percent of aziridine to carboxylic acid groups ranging from 0% to 100% in 25% intervals. The carboxylate groups present in the PU dispersion react with the aziridine groups to further crosslink the PU films, which is evidenced by the fact that the amount of ethanol absorbed by the film and the amount of the film dissolved in ethanol both decrease with more CX-100. The thermal and mechanical properties of the resulting films have been extensively investigated by dynamic mechanical analysis, differential scanning calorimetry, thermogravimetric analysis, and tensile tests. The mechanical properties are dramatically improved with the crosslinker CX-100. For example, the Young's modulus and tensile strength increase from 14.5 to 125 MPa and 13.1 to 18.1 MPa, respectively, when the percent of aziridine increases from 0% to 100%. The onset decomposition temperature of the films, T_5, increases from 162 to 209 ^oC, indicating a significant increase in the thermal stability as the amount of aziridine is increased. This work provides an effective way of curing biorenewable anionic polyurethane dispersions to prepare high performance, environmentally-friendly coatings.

Introduction

Biorenewable vegetable oil-based polymeric materials have received much attention during the last decade, due to environmental concerns and finite petroleum resources.[1,2] A variety of polymerization methods, including free radical,[3] cationic,[4] olefin metathesis,[5] and condensation polymerization,[6] have been employed to prepare these polymers. Vegetable oil-based polyols have been used to prepare polyurethanes (PUs) with a wide range of thermal and mechanical properties, which appear promising as replacements for petroleum-based PUs.[7] Vegetable oil-based diisocyanates have also been prepared as possible replacements for petroleum-based diisocyanates in PUs.[8,9]

Waterborne anionic and cationic polyurethane dispersions (PUDs) have been prepared with a wide range of applications, including adhesives,[10] coatings,[11] and paints.[12] They exhibit excellent adhesion properties and possess low film-forming temperatures. Compared to conventional solvent-based PUs, waterborne PUDs are environmentally-friendly with low volatile organic chemicals (VOCs) and low hazardous air pollutants (HAPs).[13] Vegetable oil-based anionic and cationic PUDs have been successfully prepared in our group by incorporating dimethylol propionic acid (DMPA)[14,15] and N-methyl diethanolamine (MDEA),[16,17] respectively. The PU films obtained range from elastomeric polymers to ductile plastics, depending on the hydroxyl content of the vegetable oil-based polyols and their hard segment content. These materials should find wide applications as high performance coatings.

For anionic PUDs prepared with DMPA, the carboxylate groups in the PU provide surface charged PU particles, which stabilize the PU dispersion in the water phase. These aqueous PUDs have a disadvantage in that the PU films exhibit high hydrophilic properties

due to the presence of the hydrophilic carboxylate groups, resulting in poor water or solvent resistance.[18] Therefore, postcuring reactions[19-23] and polymer hybridization[15] have been used to improve the molecular weight and the crosslink density. Among these solutions, reacting the carboxylate groups in the PUDs with an aziridinyl curing agent, when the pH drops below 6.0, or air drying[24] represent perhaps the most convenient solutions. These aziridinyl cured PU films demonstrate dramatically improved thermal and mechanical properties.[21]

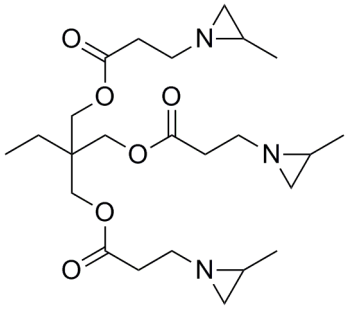

Scheme 1. Structure of CX-100.

Herein, a triaziridinyl curing agent CX-100 (Scheme 1) has been blended with castor oil-based anionic PUDs to obtain self-curable PU dispersions. The aziridine groups react with the carboxylate groups present in the PU at ambient temperature to eliminate the hydrophilic carboxylate groups and further crosslink the PU network. In this way, solvent resistance, and the thermal and mechanical properties of the castor oil-based PU films are increased significantly. This work provides a new way to prepare biorenewable, high performance coating materials.

Experimental

Materials. Castor oil, isophorone diisocyanate (IPDI), dimethylol propionic acid (DMPA), and dibutyltin dilaurate (DBTDL) were purchased from Aldrich Chemical Company (Milwaukee, WI). Triethylamine (TEA) and methyl ethyl ketone (MEK) were purchased from Fisher Scientific Company (Fair Lawn, NJ). The aziridine-based crosslinker CX-100 [trimethylolpropane tris-(1-(2-methyl)aziridino)propionate] (Scheme 1) was obtained from DSM NeoResins (Waalwijk, The Netherlands). All materials were used as received without further purification.

Synthesis of the castor oil-based polyurethane dispersions (PUDs). Scheme 2 shows the approach used to prepare the castor oil-based PUDs. The castor oil (20.00 g), IPDI (12.46 g), DMPA (3.72 g) and 1 drop of DBTDL as catalyst were added to a four-necked flask equipped with a mechanical stirrer, nitrogen inlet, condenser, and thermometer. The mole ratio between the NCO groups of the IPDI, the OH groups of the castor oil, and the OH groups of the DMPA is 2.0 : 1.0 : 0.99. The reaction was carried out at 78 ^{o}C for 1 h and then 100 mL of MEK was added to reduce the viscosity and prevent gelation. The reaction was kept for another 2 h at 78 ^{o}C. After cooling down to room temperature, the PU solution was neutralized by TEA (1.2 equiv. per DMPA) and stirred for 30 min. Then water (300 mL) was added, followed by 30 min of vigorous stirring to effect dispersion. After removal of the MEK under vacuum, castor oil-based PUDs were obtained with a solid content of ~10 wt %.

Preparation of the CX-100 cured PU films. The desired amount of CX-100 was added dropwise to the castor oil-based PUDs, followed by stirring for 30 min. Then the dispersion was poured into a glass mold to dry at ambient temperature. The films were further cured at 50 ^{o}C for 24 h and conditioned at 25 % humidity before testing.

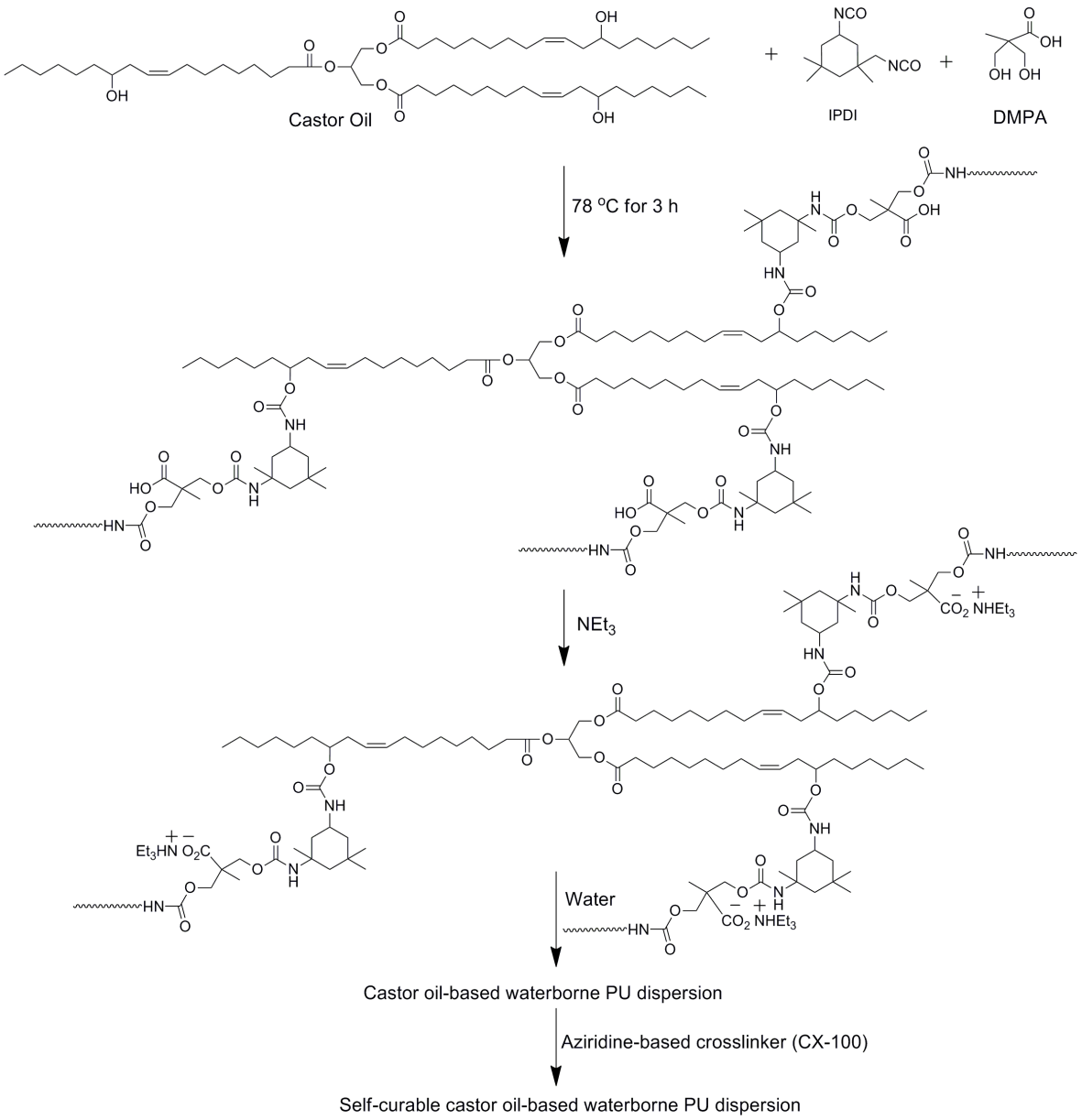

Scheme 2. Synthesis of the castor oil-based PU dispersions cured by CX-100.

The amounts of CX-100 used [0, 2.8, 5.6, 8.4, and 11.2 parts per hundred rubber (phr)] are summarized in Table 1, where the CX-100 has reacted with 0, 25, 50, 75 and 100 % of the carboxylates in the castor oil-based PU, respectively. The nomenclature for the resulting

samples is as follows: a CX-100-cured PU film, where the percent of the aziridine to the carboxylic acid groups is 75%, is designated as PU-AZ75.

Table 1. DMA, DSC, and TGA data for the PU-AZ films

Polymer	AZ/ COOH	CX-100 amount (phr)	Gel Content (wt %)	T_g (^oC)[a]	T_g (^oC)[b]	TGA data (^oC)		
						T_5[c] / ^oC	T_{50}[d] / ^oC	T_{max}[e] / ^oC
PU-AZ0	0	0	84	41.3	13.3	162	333	314
PU-AZ25	0.25	2.8	86	44.7	16.5	183	337	318
PU-AZ50	0.50	5.6	87	47.7	17.0	189	332	317
PU-AZ75	0.75	8.4	88	51.8	16.2	198	327	318
PU-AZ100	1.00	11.2	89	51.7	16.4	209	337	342

a) Glass transition temperature obtained from DMA.
b) Glass transition temperature obtained from DSC.
c) 5% Weight loss temperature.
d) 50% Weight loss temperature.
e) Temperature of maximum thermal degradation.

Characterization. Ethanol uptake and ethanol absorption have been measured as follows.[22] Dry PU films of 20 × 20 mm were conditioned by drying at 50 ^oC for 24 h, cooled in a desiccator and weighed (W_0). The films were then immersed in a 95 % ethanol bath for 48 h. The towel-dried sample weight (W_1) and reconditioned sample (dried at 50 ^oC for 24 h and cooled in a desiccator) weight (W_2) were obtained. The percentage of ethanol absorption (W_a) and weight loss of the polymer films in ethanol (W_d) have been calculated according to the following equations:

$$W_a\% = \frac{W_1 - W_2}{W_2} \times 100\%$$

$$W_d\% = \frac{W_0 - W_2}{W_0} \times 100\%$$

where W_a and W_d are the amount of ethanol absorbed by the PU film and the amount of PU film dissolved in ethanol, respectively.

The dynamic mechanical properties of the films were determined using a TA Instruments DMA Q800 dynamic mechanical analyzer with a film tension mode of 1 Hz. Rectangular samples 0.5 mm thick and 8 mm wide were used for the analysis. The samples were cooled and held isothermally for 3 min at -80 ℃ before the temperature was increased at 5 ℃/min to 150 ℃. The glass transition temperatures (T_gs) of the samples were obtained from the peak of the tan δ curves.

Differential scanning calorimetry (DSC) was performed on a thermal analyzer (TA instrument Q2000). The samples were heated at a rate of 20 ^{o}C/min from 25 to 100 ^{o}C to erase the thermal history, equilibrated at -70 ^{o}C and then heated to 150 ^{o}C at a heating rate of 20 ^{o}C/min. The T_gs of the samples was determined from the midpoint temperature in the heat capacity change of the second DSC scan. Samples of ~5 mg were cut from the films and used for analysis.

Thermogravimetric analysis (TGA) of the films was carried out on a TA instrument Q50 (New Castle, DE). The samples were heated from 50 to 650 ^{o}C at a heating rate of 20 ^{o}C/min in air. Generally, approximately 10 mg samples were used for the thermogravimetric analysis.

The tensile properties of the PU films were determined using an Instron universal testing machine (model 4502) with a crosshead speed of 100 mm/min. Rectangular specimens of 80 × 10 mm^2 (length × width) were used. An average value of at least four replicates of each sample was taken. The toughness of the polymer, which is the fracture energy per unit volume of the sample, was obtained from the area under the corresponding tensile stress-strain curves.

Results and Discussion

Structure and Ethanol Uptake. The castor oil-based anionic PU dispersions contain carboxylate groups, which act as an internal emulsifier to stabilize the dispersions. These carboxylate groups can react with aziridine groups very quickly to open the aziridine ring and form an ester group and a secondary amine (Scheme 3). The crosslinking reaction between the aziridine and the carboxylate can occur at ambient conditions with a reasonable rate, and no heat or catalyst is needed to complete the cure process.[25] Thus, the multi-aziridine rings in the crosslinker CX-100 can react with the carboxylate groups in the PU to form a more highly crosslinked network, providing a very efficient way to crosslink the castor oil-based anionic PU dispersions, and improve the thermal and mechanical properties of the films.

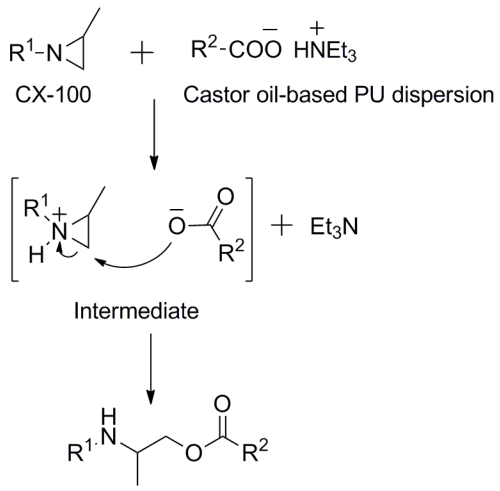

Scheme 3. Reaction between the PU dispersion and CX-100.

The amount of ethanol swelling and the gel content indicate the degree of crosslinking of a polymer. Figure 1 shows the ethanol uptake results. The amounts of ethanol absorbed and the amounts of film dissolved in ethanol decrease from 155.9 to 73.9 % and

16.3 % to 10.8 %, respectively, when the percent aziridine is increased from 0 % to 100 %, which indicates that post-cure between the CX-100 and the anionic PU dispersions has occurred and the crosslink densities of the films have increased. Similar results have been reported by Lai et al.[22] The amount of crosslinked polymer formed (gel content) increases from 84 to 89 wt % (Table 1), as a result of the increased crosslink density.

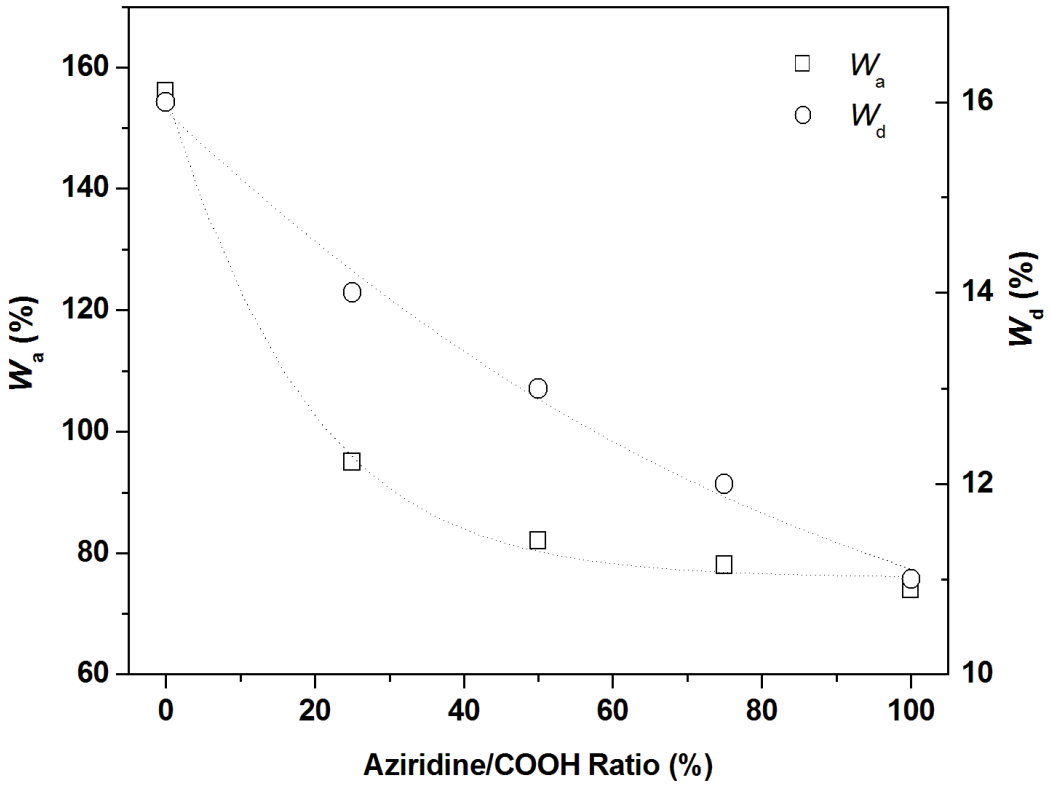

Figure 1. Ethanol uptake results for the films: the amount of ethanol absorbed by the film (W_a); the amount of film dissolved in ethanol (W_d).

Thermal Properties. The storage modulus (E') and tan δ curves as a function of temperature for films with different CX-100 loadings are shown in Figure 2. All of the films are in the glassy state below room temperature and E' decreases slightly with an increase in temperature. Then a rapid decrease in E' occurs above 25 ^{o}C for all of the films and a peak

maximum is observed in the tan δ versus T curves (α relaxation), which is taken as the glass transition temperature (T_g). All of the films show only one tan δ peak, indicating the homogeneous nature of the aziridine-cured PU system. Both the storage moduli at room temperature and high temperature are enhanced, which is evidence that the aziridine-curing process increases the crosslink densities and improves the mechanical properties. Moreover, a rubbery storage modulus plateau is observed for PU-AZ100 at high temperatures, indicating the enhanced crosslinking for the PUs with CX-100. Furthermore, the decreased height of the tan δ peak with higher amounts of CX-100 indicates increased crosslink densities for the films.[26] The T_gs obtained from DMA are summarized in Table 1. The T_gs increase from 41.3 ^oC to 51.7 ^oC, when the percent aziridine increases from 0% to 100%. This can be explained by the polymer chain motion being restricted at higher crosslink densities.

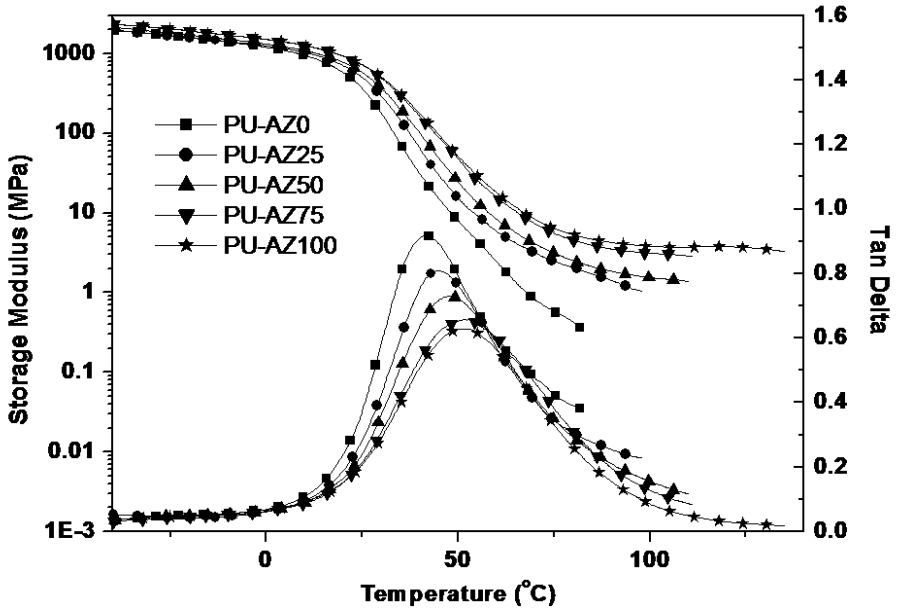

Figure 2. The storage modulus and loss factor (tan δ) as a function of temperature for the PU-AZ films.

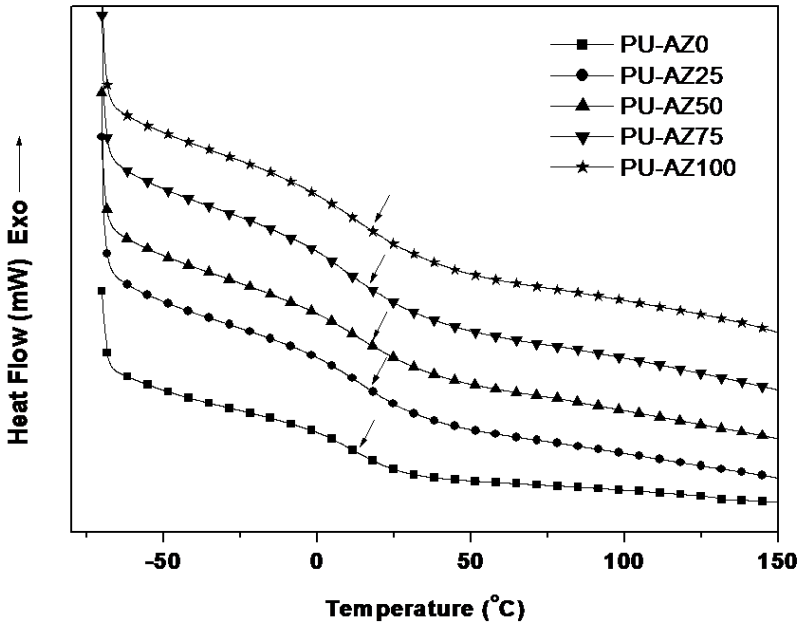

Figure 3. DSC scans for the PU-AZ films.

The DSC thermograms of the PU films are depicted in Figure 3. All of the curves show one glass transition with no melting or crystallization transition, indicating the amorphous nature of these PUs. The T_g values are summarized in Table 1. Compared to the neat PU film, PU films cured with CX-100 have higher glass transition temperatures, which result from the increased crosslink densities. However, the PU films with a variety of CX-100 loadings have pretty similar T_gs, presumably because the soft chains from the CX-100 compensate for the increased crosslink densities. A similar phenomenon has been observed in the DMA results from PU-AZ75 and PU-AZ100. The T_gs obtained from DMA are approximately 30 ^oC higher than the T_gs obtained from DSC. This results from the different nature of these two methods. DMA measures the change in the mechanical response of the polymer chains, while DSC measures the change in heat capacity from frozen to unfrozen chains.[14]

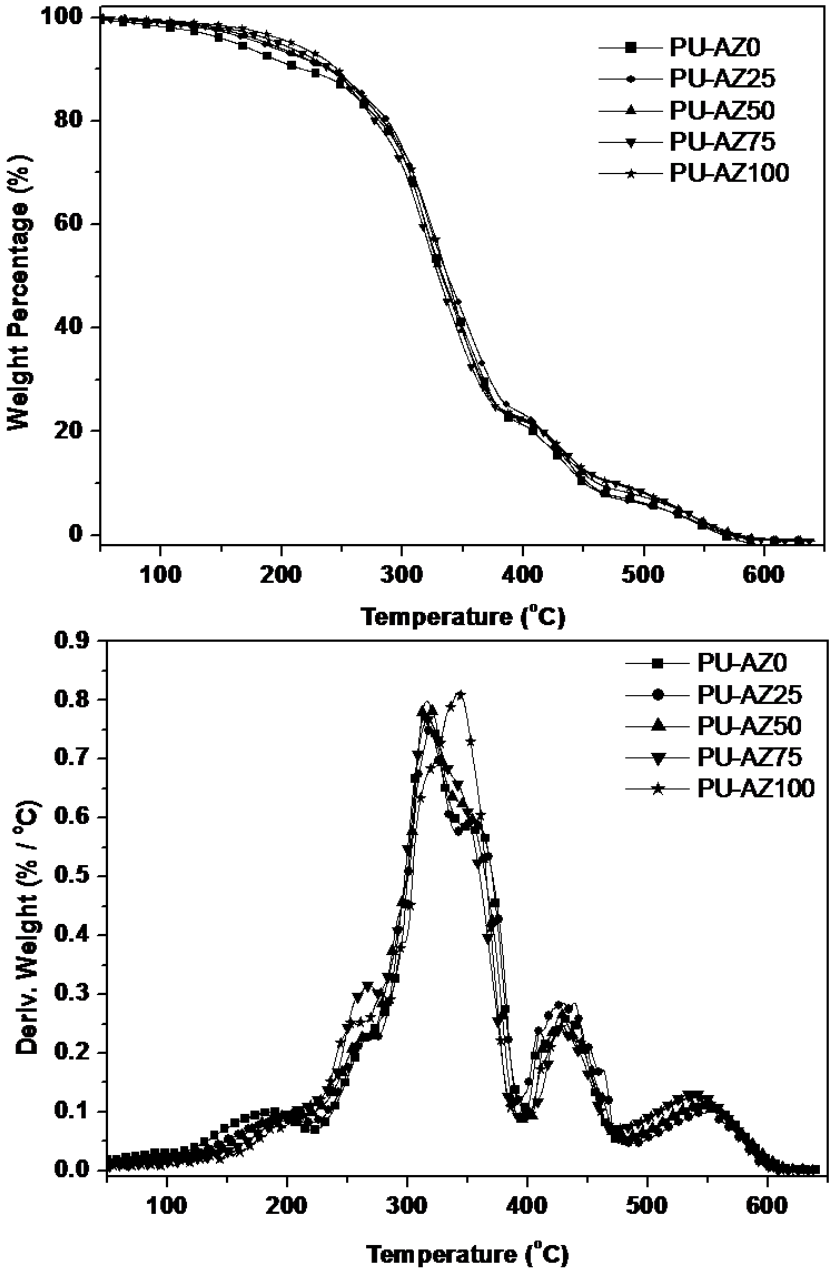

Figure 4. TGA curves and their derivative curves for the PU-AZ films.

The TGA curves for all of the PU-AZ films with different CX-100 loadings are shown in Figure 4, and the T_5, T_{50}, and T_{max} data are summarized in Table 1. PUs are generally thought to have a relatively low thermal stability, due to the labile urethane bonds,

which usually decompose below 300 ^{o}C through dissociation of the urethane bonds to form isocyanates, alcohols, primary amines, secondary amines, olefins, and carbon dioxide.[27] According to Figure 4, three thermal degradation processes for the PU films are observed. Degradation in the range 150-300 ^{o}C is attributed to decomposition of the urethane bonds. The fastest degradation process between 300 to 450 ^{o}C results from chain scission of the castor oil. The last degradation step above 450 ^{o}C corresponds to further thermo-oxidation of the PU films in air. The onset decomposition temperatures of the PU films are recorded as T_5, where 5 wt % mass of the films is lost. As summarized in Table 1, T_5 increases from 162 to 209 ^{o}C as the CX-100 amount increases from 0 to 11.2 phr. This significantly increased thermal stability of the PU films can be ascribed to the increased crosslink density imparted by the aziridine-based crosslinker CX-100. However, T_{50}, the temperature at which the PU films lose 50 wt % of their mass, does not change that much as the CX-100 amount increases, which can perhaps be explained by the fact that the secondary amines formed by reacting the carboxylate groups with the aziridine decompose together with the amines formed from dissociation of the urethane groups. The maximum degradation temperatures (T_{max}) can be obtained from the TGA derivative curves and are summarized in Table 1. Increased crosslink densities increase the T_{max} and PU-AZ100, which has all of the carboxylate groups reacted with aziridine groups, has a much higher T_{max} compared to PU-AZ0. This is in good agreement with the thermal stabilities of the PU-AZ films, which are significantly improved with the increased crosslink densities.

Mechanical Properties. Figure 5 shows the tensile stress-strain behavior of all of the PU-AZ films with CX-100 amounts ranging from 0 to 11.2 phr, and Table 2 summarizes the Young's moduli, tensile strengths, elongation at break values, and toughness of the PU-AZ films. All

of the PU-AZ films show characteristics of ductile polymers. With an increase in the percent aziridine from 0 % to 100 %, the Young's moduli and tensile strengths dramatically increase from 14.5 MPa to 125 MPa, and 13.1 MPa to 18.1 MPa, respectively, due to the multi-aziridine-containing crosslinker CX-100 crosslinking the polyurethane chains more effectively. On the other hand, the elongation at break values decrease from 336.1 % to 173.1 % with the increase in crosslink density, as expected.

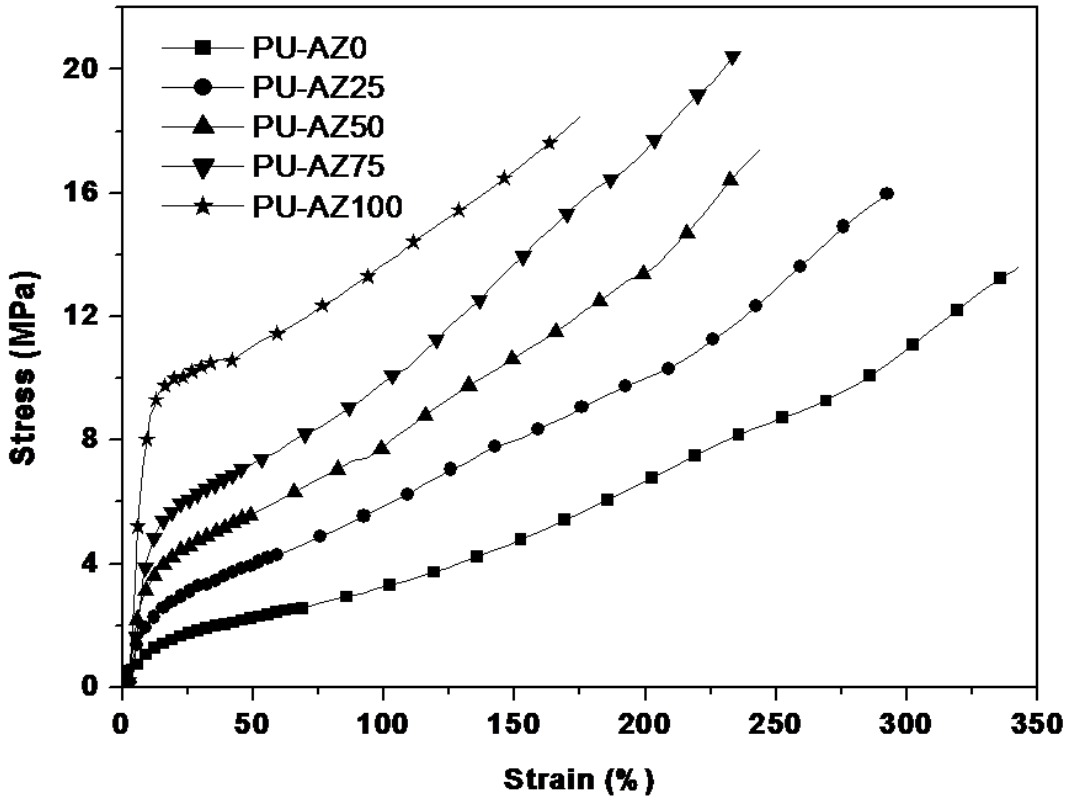

Figure 5. Stress-strain curves for the PU-AZ films.

Besides the Young's modulus and strength, the toughness, which is a material's resistance to fracture when stressed, is also obtained from Figure 5 by integrating the area below the stress-strain curve. Ductile materials are tough, while brittle materials have low

toughness.[28] Both the tensile strength and the elongation at break contribute to the overall toughness value. As seen in Table 2, the toughness first increases from 20.7 MPa to 29.2 MPa with an increase in the percent of aziridine from 0 % to 75 %, and then the toughness drops to 21.7 MPa with a 100 % percent aziridine. Generally, an increased crosslink density increases the tensile strength, but lowers the elongation at break.[28] This results in a change in the toughness for these PU-AZ films. Compared to the previously prepared methoxylated soybean oil polyols (MSOLs),[14,16] the homogeneous distribution of hydroxyl groups in castor oil results in PU films with higher toughness, which mainly results from the high elongation at break values.

Table 2. Tensile properties for the PU-AZ films

Polymer	Mechanical Properties[a]			
	E (MPa)	σ_b (MPa)	ε_b (%)	Toughness (MPa)
PU-AZ0	14.5 ± 2.4	13.1 ± 0.7	336.1 ± 6.5	20.7 ± 0.5
PU-AZ25	21.9 ± 5.6	16.3 ± 0.5	278.2 ± 15.1	22.9 ± 1.0
PU-AZ50	43.5 ± 5.3	17.7 ± 0.5	246.2 ± 2.3	23.6 ± 1.2
PU-AZ75	48.4 ± 7.1	21.7 ± 1.2	241.4 ± 11.2	29.2 ± 2.4
PU-AZ100	125.0 ± 20.3	18.1 ± 0.5	173.1 ± 4.2	21.7 ± 1.3

a) *E* = Young's modulus, σ_b = tensile strength, and ε_b = elongation at break.

Conclusions

Castor oil-based anionic PU dispersions have been post-cured by a multi-aziridine-based crosslinker CX-100 to prepare coatings with higher thermal and mechanical properties. The crosslink densities of the resulting films increase with more CX-100, which is evidenced by their ethanol uptake. The T_gs of the resulting films increase with an increase in the amount of the crosslinker, but do not change a lot at higher CX-100 loadings, which results from the

flexible CX-100 chains compensating for the increased crosslink density. The mechanical properties are dramatically improved with the crosslinker CX-100. For example, the Young's modulus and tensile strength increase from 14.5 MPa to 125 MPa and 13.1 MPa to 18.1 MPa, respectively, when the percent aziridine increases from 0 % to 100 %. The onset decomposition temperatures of the resulting films, T_5, increase from 162 ^oC to 209 ^oC, indicating a significantly increase in the thermal stability of the resulting films. This work provides an effective and promising way of curing biorenewable anionic polyurethane dispersions for environmentally-friendly, high performance coatings. Moreover, future work on using fatty acid-derived aziridine crosslinkers[29] is under consideration.

Acknowledgements

We gratefully acknowledge financial support from the Consortium for Plant Biotechnology Research (CPBR) and Archer Daniels Midland (ADM) Company. We also thank Professor Michael Kessler in the Department of Materials Science and Engineering at Iowa State University for the use of his thermal analysis equipment. In addition, we thank Dr. Yongshang Lu for his thoughtful discussions.

References

1. J. J. Bozell, *Science*, **2010**, *329*, 522.
2. Y. Xia, R. C. Larock, *Green Chem.*, **2010**, *12*, 1893.
3. P. H. Henna, D. D. Andjelkovic, P. P. Kundu, R. C. Larock, *J. Appl. Polym. Sci.*, **2007**, *104*, 979.
4. Y. Xia, P. H. Henna, R. C. Larock, *Macromol. Mater. Eng.*, **2009**, *294*, 590.
5. M. A. R. Meier, *Macromol. Chem. Phys.*, **2009**, *210*, 1073.
6. G. Lligadas, J. C. Ronda, M. Galià, V. Cádiz, *Biomacromolecules*, **2010**, *11*, 2825.
7. Z. S. Petrovic, *Polym. Rev.*, **2008**, *48*, 109.
8. L. Hojabri, X. H. Kong, S. S. Narine, *Biomacromolecules*, **2010**, *11*, 911.
9. L. Hojabri, X. H. Kong, S. S. Narine, *Biomacromolecules*, **2009**, *10*, 884.
10. M. M. Rahman, W. K. Lee, *J. Appl. Polym. Sci.*, **2009**, *114*, 3767.

11. Q. B. Meng, S. I. Lee, C. Nah, Y. S. Lee, *Prog. Org. Coat.*, **2009**, *66*, 382.
12. A. C. Aznar, O. R. Pardini, J. I. Amalvy, *Prog. Org. Coat.*, **2006**, *55*, 43.
13. K. L. Noble, *Prog. Org. Coat.*, **1997**, *32*, 131.
14. Y. S. Lu, R. C. Larock, *Biomacromolecules*, **2008**, *9*, 3332.
15. Y. S. Lu, R. C. Larock, *Biomacromolecules*, **2007**, *8*, 3108.
16. Y. Lu, R. C. Larock, *Prog. Org. Coat.*, **2010**, *69*, 31.
17. Y. Lu, Richard C. Larock, *ChemSusChem*, **2010**, *3*, 329.
18. S. C. Wang, P. C. Chen, J. T. Yeh, K. N. Chen, *React. Funct. Polym.*, **2007**, *67*, 299.
19. J. Z. Lai, P. J. Chen, J. T. Yeh, K. N. Chen, *J. Appl. Polym. Sci.*, **2005**, *97*, 550.
20. J. Z. Lai, H. J. Ling, J. T. Yeh, K. N. Chen, *J. Appl. Polym. Sci.*, **2004**, *94*, 845.
21. J. Z. Lai, Y. C. Chang, J. T. Yeh, K. N. Chen, *J. Appl. Polym. Sci.*, **2004**, *91*, 1997.
22. J. Z. Lai, H. J. Ling, G. N. Chen, J. T. Yeh, K. N. Chen, *J. Appl. Polym. Sci.*, **2003**, *90*, 3578.
23. G. D. Chen, S. X. Zhou, G. X. Gu, L. M. Wu, *Colloid. Surf. A: Physicochem. Eng. Asp.*, **2007**, *296*, 29.
24. G. N. Chen, K. N. Chen, *J. Appl. Polym. Sci.*, **1997**, *63*, 1609.
25. P. G. Liu, Q. F. Zhang, L. H. He, Q. J. Xie, H. Y. Ding, *J. Appl. Polym. Sci.*, **2009**, *113*, 2628.
26. Y. Xia, R. C. Larock, *Polymer*, **2010**, *51*, 2508.
27. Z. S. Petrovic, L. T. Yang, A. Zlatanic, W. Zhang, I. Javni, *J. Appl. Polym. Sci.*, **2007**, *105*, 2717.
28. F. K. Li, R. C. Larock, *J. Polym. Sci. Part B: Polym. Phys.*, **2001**, *39*, 60.
29. S. Furmeier, J. O. Metzger, *Eur. J. Org. Chem.*, **2003**, *4*, 649.

CHAPTER 7. PREPARATION AND PROPERTIES OF AQUEOUS CASTOR OIL-BASED POLYURETHANE-SILICA NANOCOMPOSITE DISPERSIONS THROUGH A SOL-GEL PROCESS

A Paper published in Macromolecular Rapid Communications, 32, 1331-1337.

Ying Xia and Richard C. Larock*

Department of Chemistry, Iowa State University, Ames, Iowa 50011

Abstract

Waterborne castor oil-based polyurethane-silica nanocomposites with the polymer matrix and silica nanoparticles chemically bonded have been successfully prepared through a sol-gel process. The formation of silica nanoparticles in water not only reinforces the resulting coatings, but also increases the crosslink density of the nanocomposites. The ^{29}Si solid state NMR spectrum indicates the formation of silica and the TEM indicates that the nanoparticles are embedded in the polymers, resembling a core-shell structure. The silica nanoparticles in the polymer matrix play an important role in improving both the mechanical properties and the thermal stabilities of the resulting nanocomposites. This work provides an effective and promising way to prepare biorenewable, high performance nanocomposite coatings.

Introduction

Polymers from renewable resources have received much attention during the past decade, due to finite petroleum resources and environmental concerns.[1] Vegetable oils represent one of the most promising routes to biorenewable polymers due to their ready

availability and many versatile applications.[2] Polyurethanes (PUs), one of the most versatile classes of polymers, have been prepared from vegetable oils[3] through vegetable oil-based polyols[4] or vegetable oil-based diisocyanates.[5] Recently, vegetable oil-based anionic and cationic waterborne polyurethane dispersions have also successfully been prepared in our group by employing dimethylolpropionic acid (DMPA)[6] and *N*-methyldiethanolamine (MDEA),[7] respectively, in the polyurethane backbone, followed by neutralization with triethylamine or acetic acid. Compared to conventional solvent-based PUs, waterborne PUs have many advantages, including low viscosity at high molecular weight, good applicability, and the fact that they are environmentally-friendly due to low hazardous air pollutants (HAPs) and low volatile organic chemicals (VOCs).[8]

Organic-inorganic nanocomposites have been developed to combine the desirable properties of polymers, such as toughness and elasticity, with those of inorganic fillers, including rigidity, high thermal stability, and chemical resistance.[9] The interface interaction between the polymer network and the filler is dominant in the nanocomposites' properties. The interaction is either physical and weak, such as hydrogen bonding, or strong, such as chemical covalent bonding. The strong interaction is preferred, because it can decrease the extent of phase separation or increase the compatibility of the polymer filler interaction.[10] Silica nanoparticles, which can be introduced into the polymer systems by blending, a sol-gel process, or *in situ* polymerization,[10] have been widely used to improve the thermal stability, and mechanical and electrical properties of nanocomposites.[11] The sol-gel process, involving the hydrolysis and polycondensation reactions of silicon alkoxides, has been used as an effective and simple way to prepare waterborne polyurethane-silica nanocomposite dispersions.[12] Recently, linseed oil-based polyols containing silica nanoparticles prepared

by a sol-gel process have been further reacted with toluene-2,4-diisocyanate to obtain silica embedded PUs with better thermal stability and antibacterial properties.[13]

In this study, alkoxysilane-containing polyurethanes have been prepared by reacting different and excess amounts of 3-aminopropyl triethoxysilane (APTES) with isocyanate-capped castor oil-based polyurethane prepolymers, and these have been dispersed in water to form silica nanoparticles by a sol-gel process. The castor oil-based polyurethane is chemically bonded with the silica nanoparticles and the crosslink density of the nanocomposites is increased substantially. The increased crosslink density and reinforcement by the silica result in improved thermal stability and enhanced mechanical properties. The nanocomposites obtained may find applications in high-performance organic-inorganic hybrid coatings.

Experimental

Materials. Castor oil, isophorone diisocyanate (IPDI), dimethylol propionic acid (DMPA), 3-aminopropyl triethoxysilane (APTES), and dibutyltin dilaurate (DBTDL) were purchased from Aldrich Chemical Company (Milwaukee, WI). Triethylamine (TEA) and methyl ethyl ketone (MEK) were purchased from Fisher Scientific Company (Fair Lawn, NJ). All materials were used as received without further purification.

Synthesis of the castor oil-based polyurethane-silica (PU-silica) nanocomposites. Scheme 1 shows the method used to prepare the castor oil-based PU-silica nanocomposites. The castor oil (10.00 g), IPDI (6.23 g), DMPA (1.69 g) and 1 drop of DBTDL as catalyst were added to a four-necked flask equipped with a mechanical stirrer, nitrogen inlet, condenser, and thermometer. The mole ratio of the NCO groups of the IPDI, the OH groups

of the castor oil, and the OH groups of the DMPA was 2.0 : 1.0 : 0.9. The reaction was carried out at 78 ^{o}C for 1 h and then 50 mL of MEK was added to reduce the viscosity and

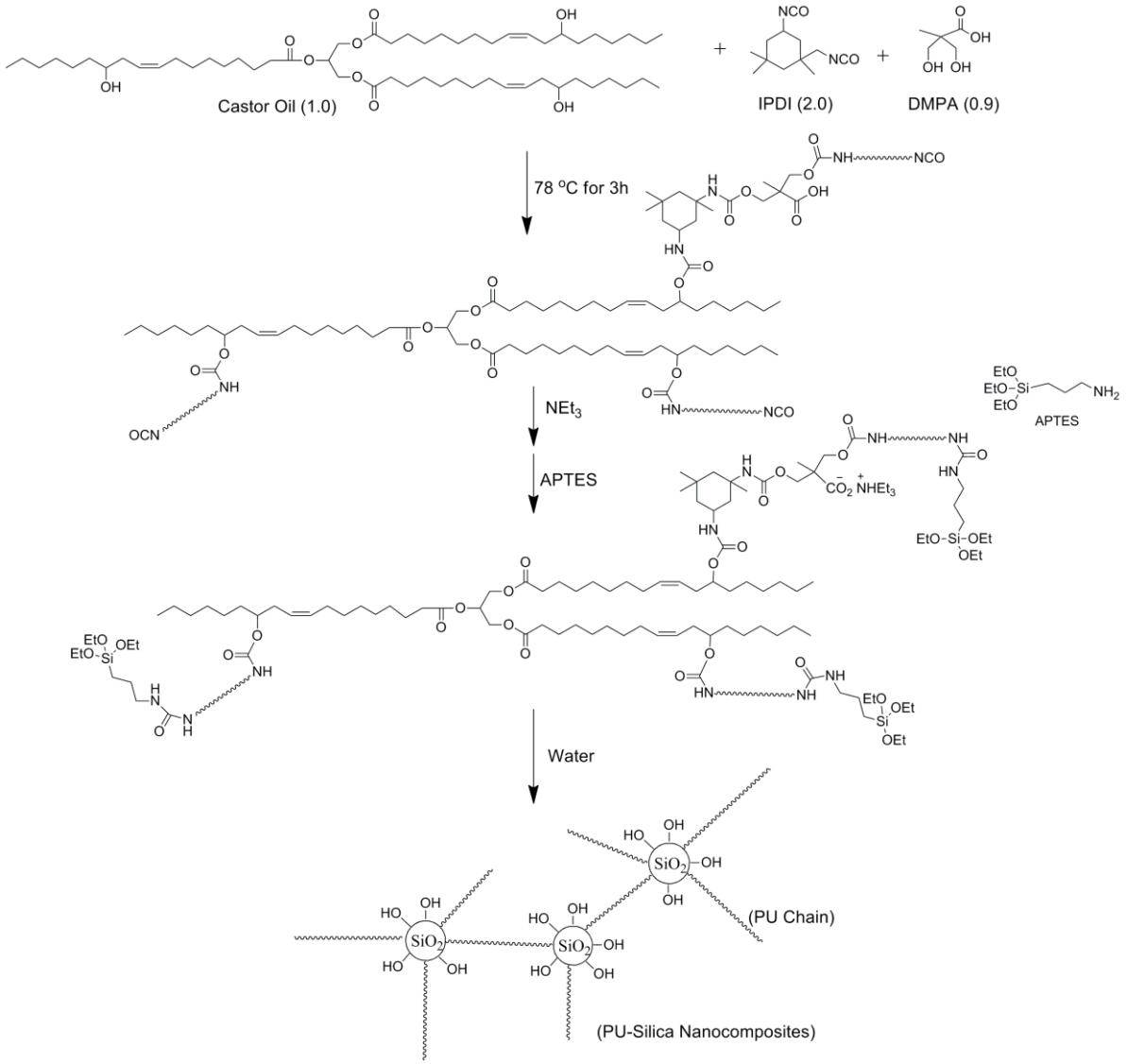

Scheme 1. Synthesis of castor oil-based PU-silica nanocomposites.

prevent gelation. The reaction was kept for another 2 h at 78 ^{o}C. After allowing the reaction mixture to cool down to room temperature, TEA (3 equiv. per DMPA) was added to the polyurethane solution and stirred for 30 min to neutralize all the carboxylic acid groups and to provide basic conditions for the following sol-gel process.[12a] The APTES was added and

allowed to react with the excess amount of NCO groups at room temperature for 1 h. Finally, water (150 mL) was added, followed by 1 h of vigorous stirring to effect dispersion and form silica nanoparticles through a sol-gel process. After removal of the MEK under vacuum, aqueous castor oil-based PU-silica nanocomposite dispersions were formed with a solids content of ~10 wt %.

Differing amounts of APTES were added to obtain PU-silica nanocomposites with different amounts of silica. Specifically, 0.75 g, 1.5 g, and 3.0 g of APTES were added to the polyurethane prepolymer solutions to react with all of the NCO groups and form PU-silica nanocomposites with silicon amounts of 0.5, 1, and 2 wt %, respectively. The nomenclature used for the resulting nanocomposites is as follows: a nanocomposite containing 1 wt % of silicon element is designated as PU-Si1. For comparison, the sample without APTES was also prepared, and the residual isocyanate reacted with water to form amines, which can then react with the remaining isocyanate to form a polyurea. This comparison sample is designated as PU-Si0.

The nanocomposite dispersions were poured into a glass mold to dry at ambient temperature and then allowed to dry at 50 ^{o}C for 24 h to obtain transparent films.

Characterization. Solid state ^{29}Si NMR spectral analysis of the nanocomposites was performed using a Bruker Avance 600 spectrometer (Bruker America, Billerica).

The morphology of the particles in the dispersion was observed on a transmission electron microscope (JEOL 1200EX). The dispersions were diluted to ~0.5 wt %, and then 3 μL of the dispersion was deposited onto a carbon film grid. After drying, the samples were characterized.

The dynamic mechanical behavior of the nanocomposite films was determined using a TA Instruments DMA Q800 dynamic mechanical analyzer with a film tension mode of 1 Hz and a heating rate of 5 ℃/min in the temperature range from -80 ℃ to 150 ℃. Rectangular samples 0.5 mm thick and 8 mm wide were used for the analysis. The glass transition temperatures (T_gs) of the samples were obtained from the peak of the tan δ curves.

Differential scanning calorimetry (DSC) was carried out on a thermal analyzer (TA Instruments Q2000). The samples were heated at a rate of 20 ^{o}C/min from room temperature to 100 ^{o}C to erase the thermal history, equilibrated at -70 ^{o}C, and then heated to 150 ^{o}C at a heating rate of 20 ^{o}C/min. The T_gs of the samples was determined from the midpoint in the heat capacity change in the second DSC scan. Samples of ~5 mg were cut from the films and used for analysis.

Thermogravimetric analysis (TGA) of the films was carried out on a TA Instruments Q50 (New Castle, DE). The samples were heated at a heating rate of 20 ^{o}C/min from 50 to 650 ^{o}C in air. Generally, approximately 5 mg samples were cut from the films for the thermogravimetric analysis.

The tensile properties of the PU-silica films were determined using an Instron universal testing machine (model 4502) with a crosshead speed of 100 mm/min. Rectangular specimens of 80 × 10 mm^2 (length × width) were used. An average value of at least four replicates of each sample was taken. The toughness of the polymer was obtained from the area under the corresponding tensile stress-strain curves.

Results and Discussion

Structure and Morphology. The amino groups in the APTES were allowed to react with the remaining isocyanate groups to form alkoxysilane-containing polyurethane prepolymers, and

then silica nanoparticles were formed by hydrolysis of the silicon ethoxy groups in water and silanol polycondensation. In this way, the polyurethane chains are chemically bonded to the silica nanoparticles, to increase the crosslink density and reinforce the thermal/mechanical properties of the coatings.

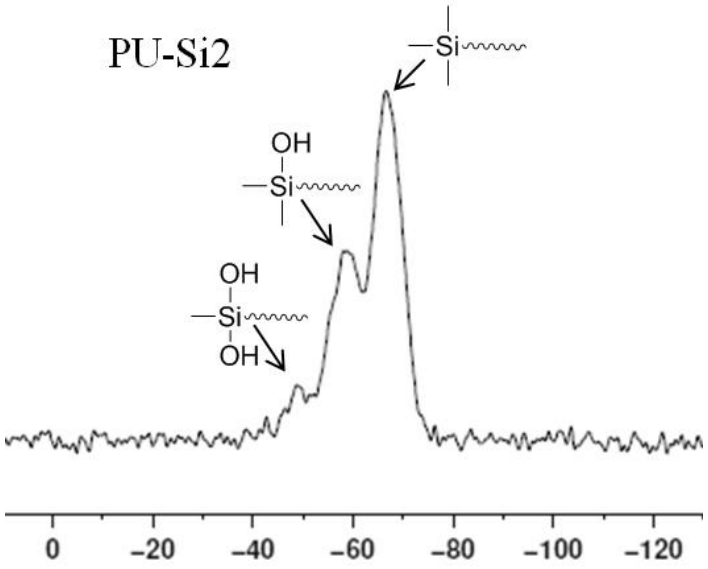

Figure 1. Solid state ^{29}Si NMR spectrum of PU-Si2.

Figure 1 shows the solid state ^{29}Si NMR spectra of PU-Si2. Unmodified silica usually has a chemical shift around -100 ppm and the silica prepared from methyltriethoxysilane (MTES) has a chemical shift around -60 ppm.[14] PU-Si2 has a chemical shift similar to the silica prepared from MTES, indicating the successful formation of silica nanoparticles from the APTES. Specifically, three peaks are observed as shown in Figure 1. The right peak results from the full condensation of the silanols. The middle peak represents the silicon with one unreacted hydroxyl group, and the left peak is assigned to a silicon bearing two hydroxyl

groups.[12a, 15] The strong right peak indicates that the degree of silanol condensation is high, suggesting silica clusters are formed.

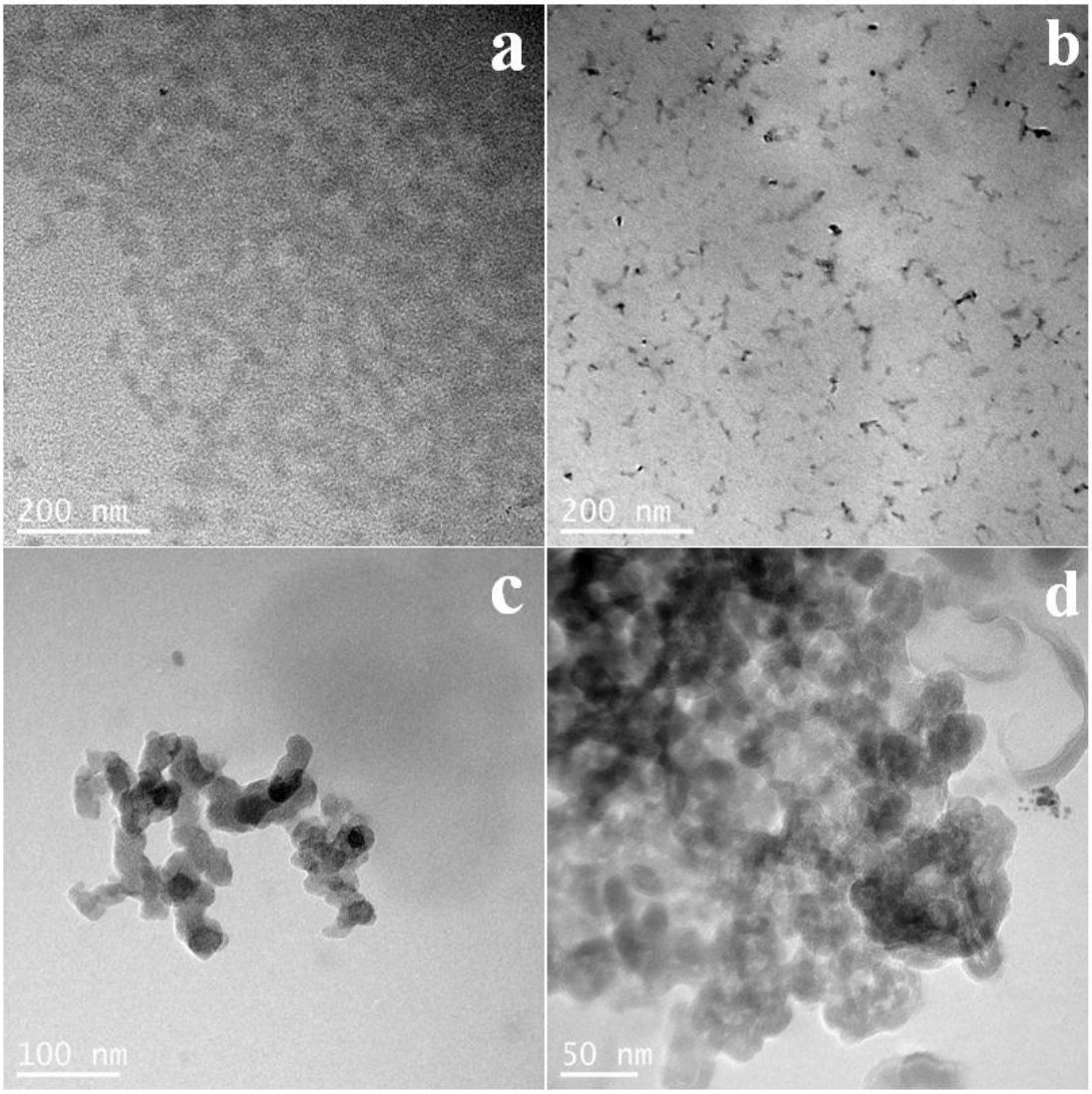

Figure 2. TEM images of (a) PU-Si0, (b) PU-Si0.5, (c) PU-Si1, and (d) PU-Si2.

The TEM morphology of the PU-silica nanocomposite dispersions is shown in Figure 2. Pure polyurethane particles in Figure 2a have a gray color. The black dots in the other three figures indicate the formation of silica nanoparticles. As the amount of the APTES is

increased, larger silica particles are formed, due to increasing amounts of the APTES feedstock and the tendency of the silica nanoparticles to aggregate at higher APTES concentrations.[12b] Figure 2 also shows that the silica nanoparticles are mainly embedded in the polyurethane polymers, which can be explained by the hydrophilic carboxylate groups on the polyurethane chains forming on the outside of the particle after adding water, and the silicon alkoxides being located in the core and thus forming silica nanoparticles later. Similar core-shell structures formed through a sol-gel process have been reported recently.[12b]

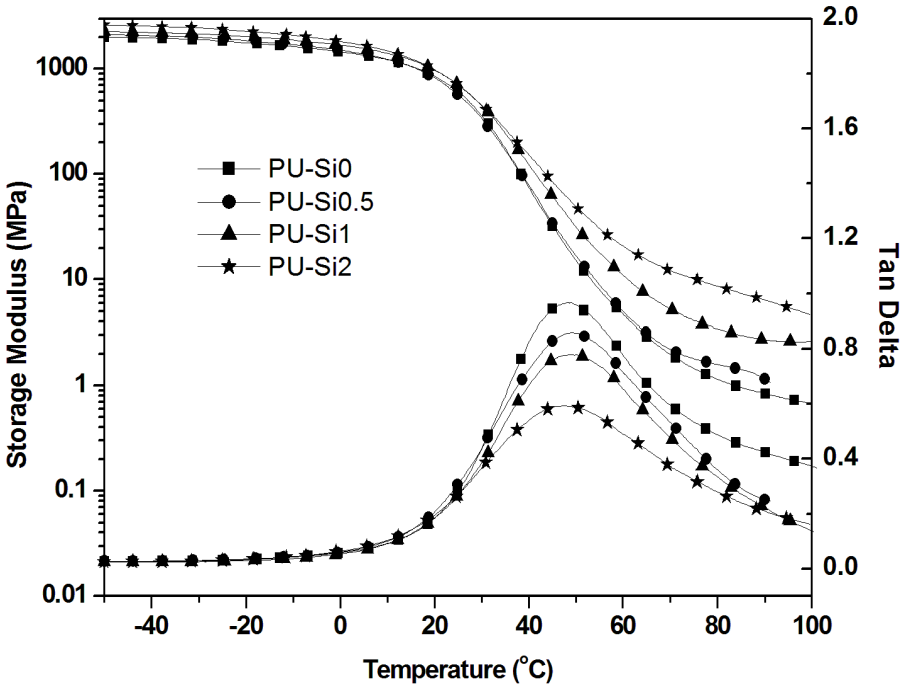

Figure 3. The storage modulus and loss factor (tan δ) as a function of temperature for the PU-Si nanocomposites.

Thermal Properties. The storage modulus (*E'*) and tan δ curves as a function of temperature for nanocomposite films with different silica loadings are shown in Figure 3. All of the films are glassy below room temperature and the storage modulus decreases slightly with an

increase in the temperature. The storage modulus decreases rapidly above 20 °C for all of the samples and a peak maximum is observed in the tan δ curves (α relaxation), which is taken as the glass transition temperature (T_g). The crosslink density (υ_e) of all of the films can be calculated from the rubbery moduli at 40 °C above T_g using the following equation, according to rubber elasticity theory:[16]

$$E' = 3\upsilon_e RT$$

where E' is the storage modulus at 40 °C above T_g, R is the gas constant, and T is the absolute temperature. As summarized in Table 1, the crosslink densities of the nanocomposites increase from 90 to 766 mol/m^3 when the silicon content increases from 0 wt % to 2 wt %. This can be explained by the fact that the silicon alkoxides connected to the polyurethane chains aggregate through a sol-gel process to form silica nanoparticles, thus acting as crosslinks in the nanocomposites. With an increase in the silica loading, more crosslinks are formed and the crosslink density of the films increases.

Table 1. DMA, DSC, and TGA for the PU-Si nanocomposites

Polymer	T_g (°C)[a]	υ_e (mol/m^3)[b]	(Tan δ)$_{max}$	T_g (°C)[c]	ΔC_p [J/(g•°C)][d]	TGA data (°C)		
						T_{10}[e] / °C	T_{50}[f] / °C	T_{max}[g] / °C
PU-Si0	50.9	90	0.95	18.0	0.250 ± 0.004	257	344	321
PU-Si0.5	49.4	131	0.86	18.8	0.238 ± 0.005	258	346	331
PU-Si1	49.1	304	0.78	20.9	0.174 ± 0.002	266	353	337
PU-Si2	47.5	766	0.59	20.2	0.163 ± 0.008	268	364	341

a) Glass transition temperature obtained from DMA.
b) Crosslink densities have been calculated at temperatures 40 °C above the T_g.
c) Glass transition temperatures obtained from DSC.
d) Heat capacity change at T_g .
e) 10% Weight loss temperature.
f) 50% Weight loss temperature.
g) Temperature of maximum thermal degradation.

The T_gs obtained from DMA are also summarized in Table 1. The T_gs decrease slightly from 50.9 ^oC to 47.5 ^oC, when the silica content increases. Generally, increased crosslink density results in higher glass transitions. However, the free volume in the nanocomposites increases due to poor wetting[17] and repulsive forces between the silica nanoparticles and the carboxylate groups in the PU chains.[18] The free volume is also increased due to the silica-induced disruption of packing of the hard segments in the polyurethane polymers.[19] The above-mentioned increased free volume compensates for the increased crosslink density, resulting in the slightly decreased T_gs for the nanocomposites. Figure 3 also indicates that all of the samples have only one tan δ peak, indicating the homogeneous nature of the nanocomposites. Furthermore, the decreased height of the tan δ peaks with higher loadings of silica indicates the increased crosslink densities for the films.[20]

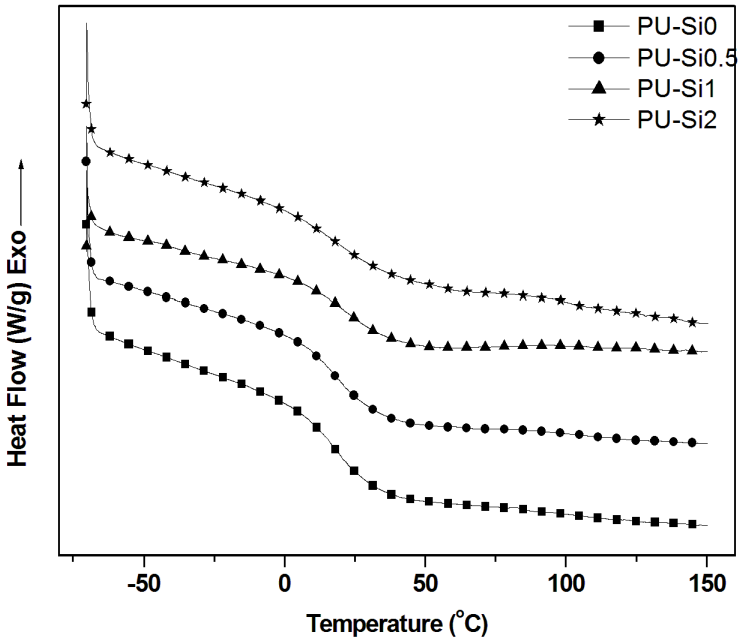

Figure 4. DSC scans for the PU-Si nanocomposites.

Figure 4 shows the DSC thermograms of the PU-Si nanocomposites. The T_gs obtained from DSC are summarized in Table 1. Compared to the sample without silica, all of the nanocomposites have higher T_gs due to increased crosslinking. Specifically, the T_g increases from 18.0 to 20.9 ^oC when the silicon loading increases from 0 to 1.5 wt %, and then drops to 20.2 ^oC in the nanocomposite PU-Si2, due to competition between the increased crosslinking and the increased free volume of the nanocomposites as mentioned earlier. The T_gs obtained from DMA are approximately 30 ^oC higher than the T_gs obtained from DSC. This is because DMA measures the change in mechanical response of the polymer chains, whereas DSC measures the heat capacity change from frozen to unfrozen chains.[6b] The heat capacity change (ΔC_p) at T_g calculated from DSC is summarized in Table 1. The decreased ΔC_p at T_g results from the increased crosslink density[21] and the increased steric hindrance caused by the silica nanoparticles.[22]

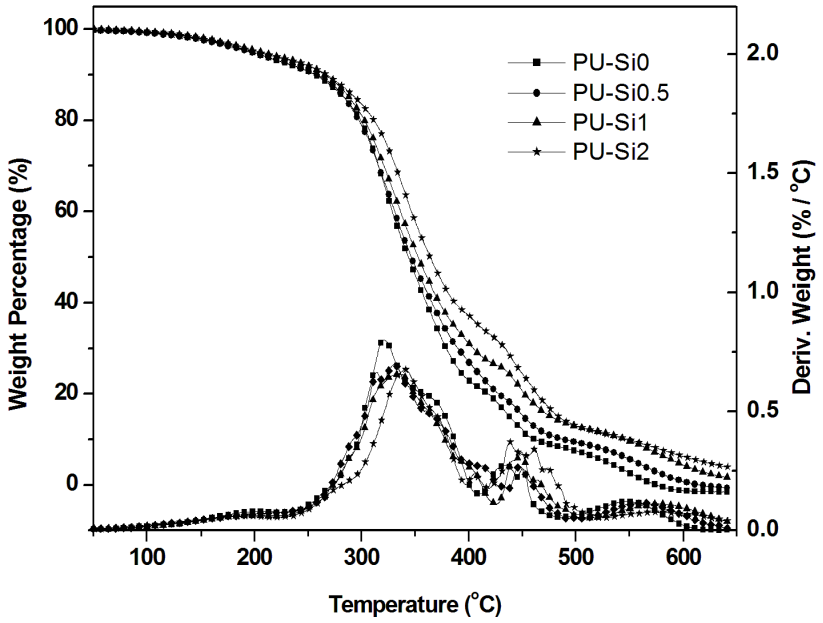

Figure 5. TGA curves and their derivative curves for the PU-Si nanocomposites.

Figure 5 shows the TGA curves and their derivative curves for all of the PU-Si nanocomposite films with different silica loadings, and the T_{10}, T_{50}, and T_{max} data are summarized in Table 1. Generally, PUs have a relatively low thermal stability, due to the labile urethane bonds, which usually decompose below 300 ^{o}C, depending upon the isocyanates and polyols employed. In the present study, degradation of all of the samples in the temperature range 150 to 300 ^{o}C can be attributed to dissociation of the urethane bonds to form isocyanates, alcohols, primary and secondary amines, olefins, and carbon dioxide.[23] The following fast degradation process between 300 to 500 ^{o}C is attributed to castor oil chain scission. The last degradation step above 500 ^{o}C corresponds to further thermo-oxidative degradation of the nanocomposites. The onset decomposition temperatures of the nanocomposite films are recorded as T_{10}, where 10 wt % mass of the films is lost. As summarized in Table 1, T_{10} increases from 257 ^{o}C to 268 ^{o}C as the amount of silicon increases from 0 to 2 wt %. Furthermore, T_{50} and T_{max} (the maximum degradation temperatures) both increase with increased silica loadings, indicating an improved thermal stability. The increased thermal stability can be ascribed to the increased crosslink density imparted by silica nanoparticle formation. The incorporation of silica also reduces the amount of more combustible organic components and produces silicaceous residue barrier layers that inhibit heat and mass transfer, which also contribute to the increased thermal stability.[24]

Mechanical Properties. Table 2 summarizes the Young's moduli, tensile strengths, elongation at break values, and toughness of all of the PU-Si nanocomposites with silicon content ranging from 0 to 2 wt %; and their tensile stress-strain behaviors are shown in Figure 6. All of the samples behave as ductile polymers. Compared to the neat polymer PU-

Si0, the Young's modulus is increased to 116.0 MPa from 32.3 MPa when the silicon content increases from 0 to 2 wt %. At the same time, the tensile strength is increased to 20.0 MPa from 15.1 MPa. Both of these enhancements can be ascribed to the increased crosslink density and the reinforcement of the silica filler. The silica nanoparticles also play an important role in strengthening the nanocomposites by effectively transferring the stress between the silica and the polymer matrix.[25] On the other hand, the elongation at break values decrease from 379 % to 91 % with the increase in the crosslink density, as expected.

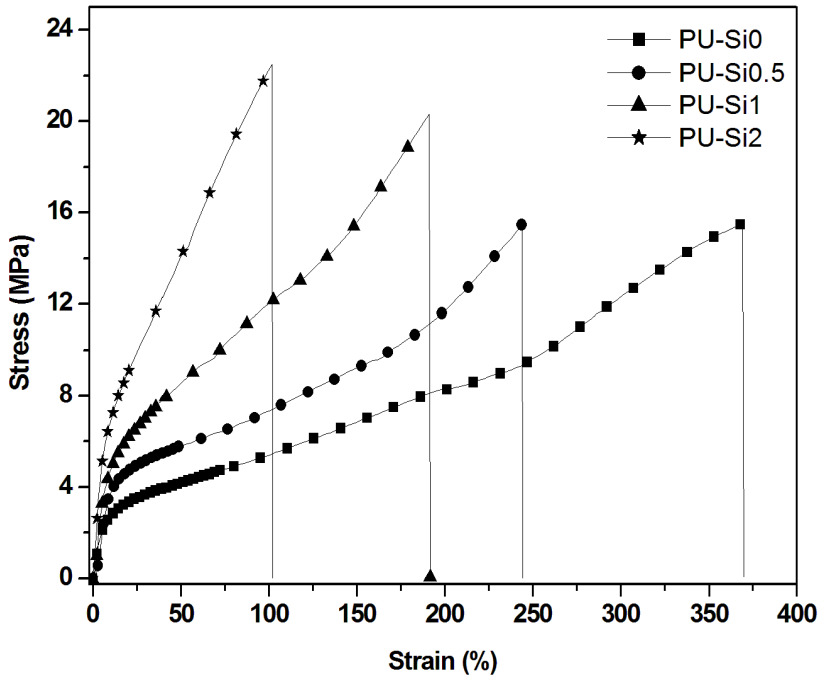

Figure 6. Stress-strain curves for the PU-Si nanocomposites.

Besides the Young's modulus and the tensile strength, the toughness, which is a measurement of the material's resistance to fracture when stressed, is also calculated from Figure 6 by integrating the area below the stress-strain curve. Both the tensile strength and

the elongation at break value contribute to the overall toughness value. As seen in Table 2, the toughness decreases from 31.1 MPa to 11.2 MPa in going from 0 % to 2 wt % silicon. Although the tensile strength is enhanced with the increased crosslink density, the large drop in elongation at break values results in the decreased toughness.

Table 2. Tensile properties for the PU-Si nanocomposites

Polymer	Mechanical Properties[a]			
	E (MPa)	σ_b (MPa)	ε_b (%)	Toughness (MPa)
PU-Si0	32.3 ± 4.8	15.1 ± 0.8	379 ± 37	31.1 ± 4.3
PU-Si0.5	54.1 ± 13.7	16.1 ± 0.9	256 ± 20	22.7 ± 2.9
PU-Si1	65.7 ± 8.1	20.5 ± 1.1	192 ± 3	22.2 ± 1.0
PU-Si2	116.0 ± 6.3	20.0 ± 2.3	91 ± 11	11.2 ± 2.6

a) *E* = Young's modulus, σ_b = tensile strength, and ε = elongation at break.

Conclusions

Castor oil-based polyurethane-silica nanocomposites have been successfully prepared through a sol-gel process. The polymer chains are chemically connected to the silica nanoparticles and the incorporation of silica not only works as a reinforcement filler, but also increases the crosslink density of the nanocomposites, which is evidenced by the lower tan δ height and the large drop in the heat capacity change at T_g. The ^{29}Si solid state NMR spectra indicate the formation of silica and the TEM shows the nanoparticles are embedded in the polymers, similar to a core-shell structure. The silica nanoparticles in the polymer matrix play an important role in improving the thermal stabilities and mechanical properties of the resulting nanocomposites. For example, the Young's modulus and tensile strength increase from 32.3 MPa to 116 MPa and 15.1 MPa to 20.0 MPa, respectively, when the silicon

content increases from 0 % to 2 wt %, and the nanocomposites' onset decomposition temperatures, T_{10}, increase from 257 ^{o}C to 268 ^{o}C. This work provides an effective and promising way to prepare biorenewable, high performance nanocomposite coatings, where the polymer matrix and filler are chemically bonded.

Acknowledgements

We gratefully acknowledge financial support from the Consortium for Plant Biotechnology Research (CPBR) and Archer Daniels Midland (ADM) Company. We also thank Professor Michael Kessler in the Department of Materials Science and Engineering at Iowa State University for the use of his thermal analysis equipment and Ms. Tracey M. Pepper of the Microscopy and NanoImaging Facility at Iowa State University for her assistance with the TEM analysis. In addition, we thank Dr. Yongshang Lu for his thoughtful discussions.

References

1. Y. Xia, R. C. Larock, *Green Chem.* **2010**, *12*, 1893.
2. (2a) Y. S. Lu, R. C. Larock, *ChemSusChem* **2009**, *2*, 136; (2b) M. A. R. Meier, *Macromol. Chem. Phys.* **2009**, *210*, 1073.
3. G. Lligadas, J. C. Ronda, M. Galià, V. Cádiz, *Biomacromolecules* **2010**, *11*, 2825.
4. (4a) Z. S. Petrovic, A. Guo, I. Javni, I. Cvetkovic, D. P. Hong, *Polym. Int.* **2008**, *57*, 275; (4b) M. Ionescu, Z. S. Petrovic, X. M. Wan, *J. Polym. Environ.* **2007**, *15*, 237.
5. (5a) L. Hojabri, X. H. Kong, S. S. Narine, *Biomacromolecules* **2010**, *11*, 911; (5b) L. Hojabri, X. Kong, S. S. Narine, *Biomacromolecules* **2009**, *10*, 884.
6. (6a) Y. Xia, R. C. Larock, *ChemSusChem* **2011**, *4*, 386; (6b) Y. S. Lu, R. C. Larock, *Biomacromolecules* **2008**, *9*, 3332; (6c) Y. S. Lu, R. C. Larock, *Biomacromolecules* **2007**, *8*, 3108.
7. (7a) Y. Lu, R. C. Larock, *Prog. Org. Coat.* **2010**, *69*, 31; (7b) Y. Lu, Richard C. Larock, *ChemSusChem* **2010**, *3*, 329.
8. K. L. Noble, *Prog. Org. Coat.* **1997**, *32*, 131.
9. D. K. Chattopadhyay, A. D. Zakula, D. C. Webster, *Prog. Org. Coat.* **2009**, *64*, 128.
10. H. Zou, S. S. Wu, J. Shen, *Chem. Rev.* **2008**, *108*, 3893.
11. G. D. Chen, S. X. Zhou, G. X. Gu, H. H. Yang, L. M. Wu, *J. Colloid Interf. Sci.* **2005**, *281*, 339.

12. (12a) J. M. Yeh, C. T. Yao, C. F. Hsieh, H. C. Yang, C. P. Wu, *Eur. Polym. J.* **2008**, *44*, 2777; (12b) H. Sardon, L. Irusta, M. J. Fernández-Berridi, M. Lansalot, E. Bourgeat-Lami, *Polymer* **2010**, *51*, 5051.
13. D. Akram, S. Ahmad, E. Sharmin, *Macromol. Chem. Phys.* **2010**, *211*, 412.
14. G. D. Chen, S. X. Zhou, G. X. Gu, L. M. Wu, *Macromol. Chem. Phys.* **2005**, *206*, 885.
15. C. H. Yang, F. J. Liu, Y. P. Liu, W. T. Liao, *J. Colloid Interf. Sci.* **2006**, *302*, 123.
16. (16a) P. J. Flory, *Principles of Polymer Chemistry*, Cornell Univerisity Press, Ithaca, **1953**; (16b) I. M. Ward, *Mechanical Properties of Solid Polymers*, Wiley Interscience, New York, **1971**.
17. (17a) D. R. Paul, L. M. Robeson, *Polymer* **2008**, *49*, 3187; (17b) P. Rittigstein, J. M. Torkelson, *J. Polym. Sci. Part B* **2006**, *44*, 2935.
18. L. Bistricic, G. Baranovic, M. Leskovac, E. G. Bajsic, *Eur. Polym. J.* **2010**, *46*, 1975.
19. T. C. Merkel, B. D. Freeman, R. J. Spontak, Z. He, I. Pinnau, P. Meakin, A. J. Hill, *Science* **2002**, *296*, 519.
20. Y. Xia, R. C. Larock, *Polymer* **2010**, *51*, 2508.
21. H. J. Chung, K. S. Woo, S. T. Lim, *Carbohydrate Polym.* **2004**, *55*, 9.
22. W. J. Seo, Y. T. Sung, S. J. Han, Y. H. Kim, O. H. Ryu, H. S. Lee, W. N. Kim, *J. Appl. Polym. Sci.* **2006**, *101*, 2879.
23. Z. S. Petrovic, L. T. Yang, A. Zlatanic, W. Zhang, I. Javni, *J. Appl. Polym. Sci.* **2007**, *105*, 2717.
24. D. K. Chattopadhyay, D. C. Webster, *Prog. Polym. Sci.* **2009**, *34*, 1068.
25. H. C. Kuan, H. Y. Su, C. C. M. Ma, *J. Mater. Sci.* **2005**, *40*, 6063.

CHAPTER 8. GENERAL CONCLUSIONS

This dissertation discusses the synthesis and characterization of novel biorenewable vegetable oil-based polymeric materials, including thermosets and environmentally-friendly waterborne polyurethane dispersions. The thermosets prepared by cationic polymerization and ring-opening metathesis polymerization (ROMP) display a wide range of thermophysical and mechanical properties from soft and flexible rubbers to hard and rigid plastics, which show promise as alternatives to petroleum-based plastics. The vegetable oil-based polyurethane dispersions may find applications as protective and decorative coatings in many industries.

In Chapter 2, homogeneous thermosets containing 57-97 wt% of biorenewable materials have been prepared by the cationic copolymerization of modified linseed oils (Dilulin or ML189) and dicyclopentadiene (DCPD), due to similar reactivity between the modified linseed oils and DCPD. The room temperature storage moduli increases significantly with an increased amount of DCPD, and the T_gs of the resulting copolymers increase linearly with an increase in the DCPD amount as well. All of the thermosets are thermally stable up to 150 ^{o}C in air.

In Chapter 3, biorenewable thermosets have been successfully synthesized by the ROMP of norbornenyl-functionalized fatty alcohols derived from soybean oil (NMSA), Dilulin (NMDA), ML189 (NMMA) and castor oil (NMCA), using the Grubbs 2nd generation ruthenium catalyst. PolyNMDA and polyNMMA exhibit lower soluble fractions, higher thermal stabilities and better mechanical properties due to successful incorporation of the side fatty acid chains into the polymer matrix. PolyNMCA affords the highest soluble

fraction and lowest thermal stability, due to incomplete polymerization of the highly viscous monomer.

In Chapter 4, two castor oil-based monomers, NCO and NCA, which have approximately 0.8 and 1.8 norbornenyl groups per fatty acid chain, respectively, have been developed by reacting castor oil and its fatty alcohol with norbornene carbonyl chloride. The ROMP of NCO/NCA in different ratios results in rubbery to rigid transparent plastics with crosslink densities ranging from 318 to 6028 mol/m^3. The increased crosslink densities reinforce the thermophysical properties, mechanical properties, and thermal stabilities of the final thermosets.

In Chapter 5, up to 20 wt% of bicyclic rigid isosorbide has been mixed with a soybean oil-based amide diol to prepare waterborne polyurethane-urea (PUU) dispersions. Incorporation of the rigid isosorbide increases the T_gs and improves the mechanical properties significantly. However, the thermal stability decreases slightly with incorporation of the isosorbide, due to the thermally unstable isosorbide.

In Chapter 6, castor oil-based anionic polyurethane dispersions have been post-cured by means of a multiaziridine-based crosslinker CX-100 to eliminate hydrophilic carboxylate groups and to further crosslink the polyurethane network. The T_gs of the post-cured films increase with an increase in the amount of the crosslinker and the mechanical properties are dramatically improved with the crosslinker CX-100. The onset decomposition temperatures of the resulting films, T_5, increase from 162 to 209 ^oC, showing a large increase in their thermal stabilities.

In Chapter 7, castor oil-based polyurethane-silica nanocomposite dispersions have been successfully prepared through a sol-gel process. The polymer chains are chemically

bonded to the silica nanoparticles and the incorporation of silica not only works as a reinforcement filler, but also increases the crosslink densities of the nanocomposites, which improve both the mechanical properties and the thermal stabilities of the resulting coating materials.

The vegetable oil-based biorenewable polymeric materials have attractive properties and look to have a promising future. However, many challenging problems still exist and the development of better vegetable oil-based materials appears certain. The cure time for the thermosets could be reduced to make them suitable for industrial applications. For polymers prepared from ROMP, replacement of the expensive and unrecyclable Grubbs catalysts with less expensive catalysts would significantly reduce the cost of the resulting materials. Furthermore, novel vegetable oil-based monomers can be prepared to not only afford polymers with high performance, but also increase the renewable source content in the final resins. Moreover, controlled polymer architectures can be built based on vegetable oil-based monomers by employing living polymerization methods to expand the applications of these bio-based polymers, especially in high-end uses. Finally, a variety of fillers can be incorporated with these biorenewable resins for the preparation of high-performance composites, which have wide applications in many industries.

The vegetable oil-based polyurethane dispersions (PUDs) can also be explored further. Nanofillers, such as carbon tubes and silver nanoparticles, can be added into the PUDs to improve the thermal and mechanical properties of the resulting coatings. Antimicrobial reagents can also be incorporated physically or chemically into the coating systems to prepare functional coatings, which can find medical applications. Furthermore, the soft

segment/hard segment ratio in the polyurethanes can be tuned to prepare not only coatings, but also pressure sensitive adhesives (PSAs) and paints.

In conclusion, vegetable oil-based thermosets and polyurethane coating materials, which show promise as alternatives to petroleum-based plastics, have been successfully synthesized and characterized in this dissertation. With the continually increasing demand for renewable materials and the many advantages of vegetable oils, including ready availability, inherent biodegradability, and relatively inexpensive costs, a wider variety of vegetable oil-based polymeric materials will no doubt be developed in the future and used for various applications.

ACKNOWLEDGEMENTS

I would like to express my sincere gratitude to my advisor Distinguished Professor Richard C. Larock for the continuous support of my Ph.D. studies and research, for his inspiration, encouragement, patience and immense knowledge. He is truly a great professor and a nice person.

I want to thank Professor Michael R. Kessler, who is always willing to help and has allowed me to use his thermal analysis equipments. My sincere thanks also go to my Program of Study committee, Professors Malika Jeffries-EL, Klaus Schmidt-Rohr, and Yan Zhao, for their valuable time and insightful comments.

I thank all of my fellow labmates for their friendship. In particular, I thank Dr. Yongshang Lu, Dr. Phillip Henna, Dr. Marlen Valverde, Dr. Dan Pfister, Rafael Quirino, and Tom Garrison for their helpful and stimulating discussions. I especially want to thank Dr. Yongshang Lu for his excellent guidance when facing challenges in my research and Dr. Phillip Henna for helping me out during my early efforts at research.

I need to thank my parents, Yongjiu Xia and Xiuhua Shen, for doing their best to provide me with everything they could. Last, but not least, I want to thank my wife, Nan Xiao, for her selfless love, encouragement, and support throughout the years.